FACULTÉ DES ÉTUDES SUPÉRIEURES ET POSTOCTORALES

uOttawa

L'Université canadienne
Canada's university

FACULTY OF GRADUATE AND POSDOCTORAL STUDIES

Simon Hind
AUTEUR DE LA THÈSE / AUTHOR OF THESIS

M.A.Sc. (Mechanical Engineering)
GRADE / DEGREE

Department of Mechanical Engineering
FACULTÉ, ÉCOLE, DÉPARTEMENT / FACULTY, SCHOOL, DEPARTMENT

Predicting and Measuring Thermal Conductivity in Carbon/Epoxy Unidirectional Tape and Textile Reinforced Composites

TITRE DE LA THÈSE / TITLE OF THESIS

François Robitaille
DIRECTEUR (DIRECTRICE) DE LA THÈSE / THESIS SUPERVISOR

CO-DIRECTEUR (CO-DIRECTRICE) DE LA THÈSE / THESIS CO-SUPERVISOR

Jeremy Laliberté

Michael Munro

Gary W. Slater
Le Doyen de la Faculté des études supérieures et postdoctorales / Dean of the Faculty of Graduate and Postdoctoral Studies

PREDICTING AND MEASURING THERMAL CONDUCTIVITY IN CARBON/EPOXY UNIDIRECTIONAL TAPE AND TEXTILE REINFORCED COMPOSITES

Simon Hind

A thesis submitted to the Faculty of Graduate and Postdoctoral Studies
in partial fulfillment of the requirements for the degree of
MASTER OF APPLIED SCIENCE
in Mechanical Engineering

Ottawa-Carleton Institute for Mechanical and Aerospace Engineering
University of Ottawa
Ottawa, Canada

Library and Archives
Canada

Published Heritage
Branch

395 Wellington Street
Ottawa ON K1A 0N4
Canada

Bibliothèque et
Archives Canada

Direction du
Patrimoine de l'édition

395, rue Wellington
Ottawa ON K1A 0N4
Canada

Your file Votre référence
ISBN: 978-0-494-65983-0
Our file Notre référence
ISBN: 978-0-494-65983-0

NOTICE:

The author has granted a non-exclusive license allowing Library and Archives Canada to reproduce, publish, archive, preserve, conserve, communicate to the public by telecommunication or on the Internet, loan, distribute and sell theses worldwide, for commercial or non-commercial purposes, in microform, paper, electronic and/or any other formats.

The author retains copyright ownership and moral rights in this thesis. Neither the thesis nor substantial extracts from it may be printed or otherwise reproduced without the author's permission.

AVIS:

L'auteur a accordé une licence non exclusive permettant à la Bibliothèque et Archives Canada de reproduire, publier, archiver, sauvegarder, conserver, transmettre au public par télécommunication ou par l'Internet, prêter, distribuer et vendre des thèses partout dans le monde, à des fins commerciales ou autres, sur support microforme, papier, électronique et/ou autres formats.

L'auteur conserve la propriété du droit d'auteur et des droits moraux qui protège cette thèse. Ni la thèse ni des extraits substantiels de celle-ci ne doivent être imprimés ou autrement reproduits sans son autorisation.

In compliance with the Canadian Privacy Act some supporting forms may have been removed from this thesis.

While these forms may be included in the document page count, their removal does not represent any loss of content from the thesis.

Conformément à la loi canadienne sur la protection de la vie privée, quelques formulaires secondaires ont été enlevés de cette thèse.

Bien que ces formulaires aient inclus dans la pagination, il n'y aura aucun contenu manquant.

Canada

Abstract

The directional thermal conductivity of composite parts and moulds has a strong effect on out-of autoclave manufacturing operations. Limited thermal conductivity and variability data is available for composites made from carbon fibres that are widely used in mould and aircraft construction. A summary of experimental measurements and directional thermal conductivity models for carbon/epoxy composite materials is presented. Experimental data were collected for AS4 fibre unidirectional tape prepreg and T300 fibre unidirectional non-woven and plain weave textile reinforced composites. Lamination sequences included $[0°]_n$, $[0°/90°]_n$, $[0°/90°/0°]_n$, $[0°/60°/-60°]_n$ and $[0°/+45°/-45°/90°]_n$. Manufacturing methods included hybrid hand-layup and autoclave curing. Variability is quantified in all cases. Techniques for the predictive modeling of directional thermal conductivity are assessed. Classical lamination theory and models of conductivity for homogeneous assemblies of aligned fibres were used to determine thermal conductivity of tape prepreg and thermal properties of textile yarns. Unit cell simulations of textile based composites were performed to quantify the effect of changes in reinforcement geometry and configuration on directional thermal conductivity. A series of steady-state finite element models were developed for non-woven composites, unidirectional and cross-ply, and for plain weave textiles [0°/90°], $[0°/90°/0°]_n$ and [0°/+45°/-45°/90°]. Recommendations for the applicability of different modeling methods for the determination of thermal conductivity in composite materials are presented.

Acknowledgements

I owe a huge debt of gratitude to my thesis supervisor Dr. Francois Robitaille. Without his technical guidance and encouragement this thesis would not have been possible. His support and enthusiasm have been ever present from the formative stages to the final version of this thesis.

I would also like to acknowledge the National Research Council Institute for Aerospace Research for materials, equipment and financial support.

Table of Contents

List of Figures

List of Tables

Nomenclature

$2h$	laminate thickness
θ	angle between fibre and measurement direction
θ_i	angle of ith ply
a	yarn aspect ratio – width to height
dT	temperature difference between two points
dz	distance between two points
gh	horizontal gap between yarns
gv	vertical gap between yarns
k_1	thermal conductivity of unidirectional lamina in axial direction
k_2	thermal conductivity of unidirectional lamina in transverse direction
k_c	composite thermal conductivity
k_{cd}	directional composite thermal conductivity
k_{ci}	in-plane composite thermal conductivity
k_{fa}	axial fibre conductivity
k_{ft}	transverse fibre conductivity
k_m	resin thermal conductivity
k_x	0° axial in-plane composite thermal conductivity
k_y	90° transverse in-plane composite thermal conductivity
k_{45}	45° in-plane composite thermal conductivity
k_{ya}	axial yarn conductivity
k_{yt}	transverse yarn conductivity
k_z	transverse composite thermal conductivity

n	ellipse shape power
q_z''	heat flux
t_i	thickness of ith ply
V_{fy}	yarn fibre volume fraction
V_f	fibre volume fraction
yh	yarn height
yw	yarn width
x and y	orthogonal directions

Glossary

ASTM	American Society for Testing and Materials
C/E	carbon/epoxy
CFD	computational fluid dynamics
CFRP	carbon fibre reinforced plastic
CLT	classical lamination theory
CTE	coefficient of thermal expansion
CVD	chemical vapour deposition
FE	finite element
IAR	Institute for Aerospace Research
MSC	MacNeil-Schwendler Corporation
NRC	National Research Council
PAN	polyacrylonitrile
PMC	polymer matrix composite
ROM-A	axial rule of mixtures
ROM-T	transverse rule of mixtures
UD	unidirectional

1 Introduction

The National Research Council of Canada – Institute for Aerospace Research (NRC – IAR) has developed conductive heating technology used for controlling temperatures in resin infusion and other polymer matrix composite (PMC) manufacturing processes [1]. PMC parts are often manufactured in PMC moulds, Figure 1.1; using the same material for the mould and part largely resolves issues related to mismatch in coefficients of thermal expansion (CTE).

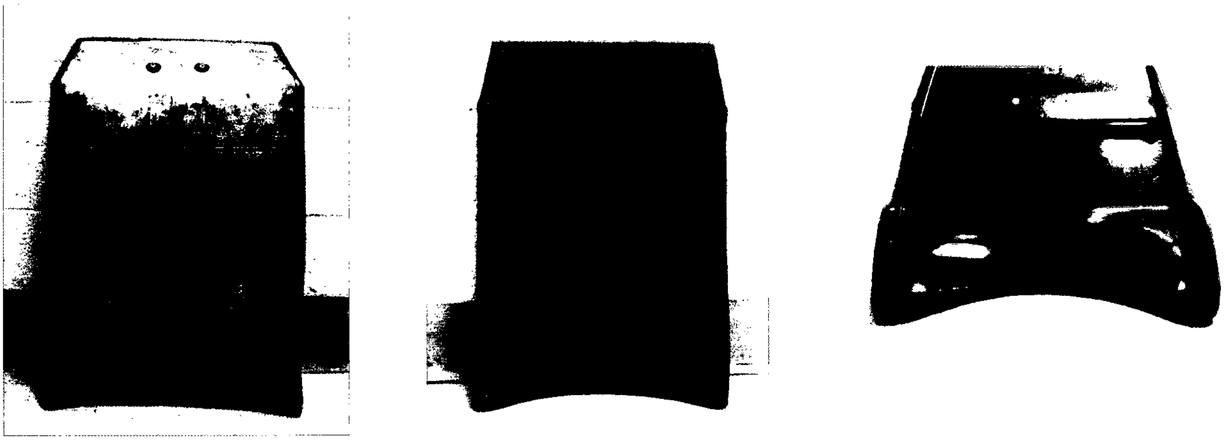

Figure 1.1: C/E PMC mould used for manufacturing C/E PMC parts; outer face with bonded conductive copper plate (left), inner face (centre and right)

Accurate heating of aerospace PMC materials such as carbon/epoxy (C/E) laminates is challenging because of their low thermal conductivity k_c. Experience shows that the directional thermal conductivity k_{cd} of PMC moulds has a strong effect on equipment operation. When manufacturing PMC parts, non-uniform heat flux must be projected on the inner surface of the mould in order to generate the uniform temperature required for adequate and certifiable cure. To determine the optimum configuration of heating systems, predictive simulations of heat transfer in PMC manufacturing require accurate values of the directional in-plane k_{ci} and through-thickness thermal conductivity k_z for materials. However, limited thermal conductivity data and associated variability is available for PMCs made from reinforcements of different types. Data is notably scarce in the case of PMCs made from polyacrylonitrile (PAN)-based carbon fibres, which are primarily used for their structural properties in aircraft parts and mould construction.

Practical difficulties associated with measuring thermal conductivity in composites stem from the need to test along multiple directions and to quantify variability. Any change in the reinforcement or matrix materials, lamination sequence, fibre volume fraction V_f or construction technique can lead to significant changes in conductivity and require extensive testing with associated delays and costs. Most published thermal conductivity data measured directly on fibres consists of axial fibre conductivity values k_{fa} for exotic graphite fibres produced by chemical vapour deposition (CVD) and used at cryogenic temperatures [2-4]. More often, axial and transverse fibre conductivities k_{fa} and k_{ft} are back-calculated from measurements taken on a reference unidirectional composite sample, and then used for predicting the conductivity of other composites made of the same fibres using various closed-form analytical, semi-analytical or empirical models [5]. The axial rule of mixtures model (ROM-A) relating the axial conductivities of fibres and homogeneous unidirectional composites, such as laminates made from tape prepreg, is widely used [6]. Diverse models relating the transverse conductivities of fibres and homogeneous unidirectional composites have been proposed. In this case, values of transverse conductivity calculated for the fibres from measurements made on the PMC depend on the model used. Any measurement error present in the reference composite data is multiplied when the fibre thermal conductivity is determined because of error in V_f and fibre orientation. It is multiplied again when the conductivity of the PMC part or mould of interest is predicted, for the same reason. The problem is especially acute in the case of the transverse conductivity as this varies strongly with V_f. Error is further increased when data characterising the homogeneous elements within textile-reinforced PMCs, such as impregnated yarns, are used in predicting the conductivity of heterogeneous PMCs made from such yarns; this case arises when a woven reinforcement is used, Figure 1.2. Here the increase in error results from geometric uncertainty over precise yarn configuration.

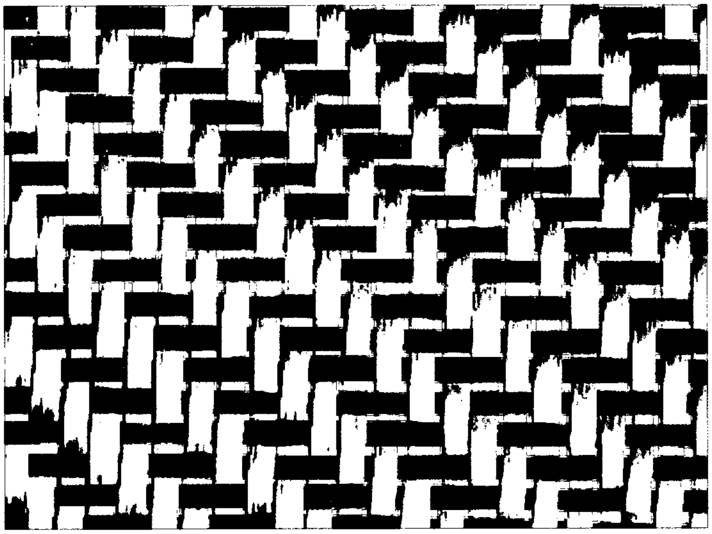

Figure 1.2: C/E PMC made from a textile-based, woven reinforcement; individual yarns and inter-yarn gaps are visible

Geometrical models of weaves have been used in predicting the conductivity of PMCs made from woven reinforcements [7-10]. However, the relation between the accuracy of the geometrical and the accuracy of the predicted thermal conductivity values was not addressed.

More importantly, the relation between geometrical accuracy and the resulting accuracy of predicted conductivity values was not compared to error in experimental conductivity values. This comparison is useful in assessing the relevance of techniques available for predicting the thermal conductivity of composites for different types of reinforcements.

Chapter 2 features a literature review presenting relevant thermal conductivity data available for carbon fibres in the axial and transverse directions k_{fa} and k_{ft}, and for C/E PMCs in the in-plane k_{ci}, axial in-plane k_x, transverse in-plane k_y and transverse through-thickness directions k_z. Closed-form models available for predicting various thermal conductivities for PMCs are also reviewed, and their applicability to yarns (k_{ya} and k_{yt}), laminated prepreg PMCs and textile-reinforced PMCs is discussed. Models specifically developed for the case of heterogeneous textile-reinforced PMCs, which feature input information about the configuration of the yarns, are also reviewed; available models are largely computational.

Chapter 3 features experimental material. The Hukseflux THASYS and THISYS apparatus used for measuring in-plane and through-thickness transverse conductivities are described along with modifications made to the samples enabling the measurement of directional in-plane thermal conductivities. Three material systems are described: material 1 is a C/E unidirectional tape prepreg, material 2 is a C/E plain weave textile-reinforced prepreg, and material 3 is a unidirectional carbon fabric infused with a liquid epoxy resin. All materials feature carbon fibres that are widely used in mould and aircraft construction. Fourteen laminates featuring different laminated sequences were manufactured in autoclave or under press; values of the directional in-plane k_{ci} and through-thickness transverse thermal conductivity k_z were measured and analysed. More than 750 thermal conductivity measurements are reported. Variability is quantified in all cases and the effects of lamination sequence and orientation are also documented.

Chapter 4 reports on modelling work. Homogeneous laminates of tape prepreg material 1 were analysed using closed-form models and the classical laminate theory (CLT). The closed-form models were also used in calculating axial and transverse thermal conductivities of homogeneous yarns k_{ya} and k_{yt}, used in simulations of heat transfer through PMC unit cells of non-interlaced materials and woven materials corresponding to materials 3 and 2 respectively. Nine series of finite element models were built in increasing order of complexity. In each case the modelling evolved in stages, from early trials to models approaching actual reinforcement geometry; many meshes featured inter-yarn gaps with dimensions equivalent to approximately three fibre diameters. The effect of selected geometric parameters on composite thermal conductivity k_c was evaluated and compared with the general variability of experimental values. From this the value of different modelling approached is discussed. More than 80 finite element models were built and used in simulations.

A general conclusion appears in chapter 5.

2 Literature Review

This review opens on a presentation of thermal conductivity data for carbon fibres as available from the scientific literature and commercial suppliers. The capabilities, hypotheses and validation of analytical models for the prediction of thermal conductivity in PMCs are discussed next; these models are primarily applicable to homogeneous PMC materials where the reinforcement is devoid of a textile structure, such as tape prepregs or the yarns within textile reinforcements. This is followed by a brief review of elements of the classical laminate theory (CLT) applicable to the work presented in this thesis. The chapter closes on a presentation of computational models of the thermal conductivity of textile-reinforced PMCs, and a discussion of results obtained from these models.

2.1 Fibre Properties

Values of axial thermal conductivity k_{fa} quoted for carbon fibres at room temperature range from 7 W/mK to 950 W/mK; a value of 8 W/mK is quoted for T300 fibres [11]. Extensive data was published for fibres made by CVD or from mesophase pitch, graphitized at high temperatures and tested at low temperatures [2, 3]. Nearly ideal molecular structures in such fibres lead high conductivity values up to 1,100 W/mK [2, 4].

Published values of fibre the axial thermal conductivity k_{fa} appeared in the 1960s. Johnson and Watt [12, 13] discussed the relation between graphitisation temperature T_g, fibre structure and axial thermal conductivity k_{fa} of PAN fibres. A value of k_{fa} = 59.4 W/mK at room temperature was reported. Lee and Taylor [14] made repeated measurements of k_{fa} for

Morganite II and Thornel 50S fibres at temperature T = 300K, directly and from unidirectional composites. Averages of reported values are 12.2 W/mK and 58.7 W/mK; variability due to sample non-uniformity was estimated at 12% to 15%. Other values from 22 W/mK to 102 W/mK were cited from conference proceedings and private communications. Data scatter was mentioned, with reported values of k_{fa} varying from around 60 W/mK in this and another publication, to 90 W/mK elsewhere.

In the 1980s a strong effect of T in the cryogenic range on k_{fa} was observed. Piraux *et al.* [15] investigated a CVD fibre graphitised at T_g = 3000°C in 1984. Reported k_{fa} values went from 4 W/mK at T = 5K to 1050 W/mK at T = 300K, peaking close to 1200 W/mK around peak temperature T_p = 150K. For these fibres k_{fa} was seen to decrease with T at room temperature. The authors stated that the high level of structural perfection of fibres processed at such high T_g lead to k_{fa} values nearly 2 orders of magnitude larger than those seen with commercial PAN fibres. The same authors measured k_{fa} for commercial P100 pitch fibres [16] going from 0.02 W/mK at T = 3K to 500 W/mK at T = 300K, stabilising at room temperature; hence the effect of T at room temperature was markedly weaker for these fibres. A value of k_{fa} = 175 W/mK at room temperature was also reported for GY70 PAN fibres graphitised at T_g = 3000°C. It should be noted that whilst lower k_{fa} value were linked fibres having a less perfect structure, fibres such as P100 and GY70 were then at the higher end of the spectrum of commercial fibres in terms of modulus.

Heremans and Beetz [17] clearly demonstrated the effect of the graphitisation temperature T_g on k_{fa} by testing fibres processed at 1130°C and after heat treatment at 3000°C. The heat treatment strongly increased k_{fa} measured between 10K and 370K. The temperature of peak conductivity T_p was reduced; whilst prior to heat treatment k_{fa} increased with T at room temperature, it decreased after heat treatment. In 1985 Heremans *et al.* [18] reviewed the effects of graphitisation temperature T_g and measurement temperature T on k_{fa} in PAN fibres below room temperature. The authors also observed that high-modulus fibres tend to be more conductive at these temperatures [14]. Additional measurements performed on CVD, pitch and PAN fibres below room temperature confirmed the trends mentioned above, with widely spread values of k_{fa} strongly affected by T_g and T. In 1991 Nysten *et al.* [19] measured k_{fa} between $T = 3K$ and $T = 300K$ for 6 pitch fibres graphitised at increasing temperatures. They also noted a strong effect of T. At room temperature k_{fa} went from 37 W/mK for fibre E55 graphitised at lower T_g to 525 W/mK for fibres E130 graphitised at higher T_g. The authors proposed models of k_{fa} based on quantized lattice vibrations, that predicted measured values accurately below room temperature.

The relation between k_{fa} and fibre structure was further clarified at the turn of the 21st century [20, 21]. Aligned structures found in circular mesophase pitch fibres graphitised at T_g = 3000°C were replicated at T_g = 2400°C by careful spinning of ribbon-shaped fibres. Comparable values of k_{fa} were achieved from a more economical process. The importance of the structure of the spun fibre prior to graphitisation was seen as minor differences in spinning temperature were found to alter k_{fa} of the graphitised fibres.

Lavin *et al.* [22] proposed a correlation between k_{fa} and electrical resistivity, which is easier to measure. It should be noted [23] that whilst this is true for single fibres the same is not equally true with composites. Conductivity values going from 0.03 W/mK to 100 W/mK between T = 5K and T = 280K were reported. However, [20] features two correlations for the same fibres, highlighting k_{fa} data scatter. Differences in k_{fa} up to 25% were seen for the same fibres when 2 direct measurement methods were used [20, 21]. Variability of k_{fa} data was estimated at 15% in [24] and at 10% for a photo-thermal method [25]. Scatter larger than 50% in some cases was reported in [26] when different measurement methods were used.

Cleary the direct measurement of k_{fa} is challenging, as is the preparation and quantification of samples. Furthermore, conductivity values of commercial fibres can be affected strongly by the measurement temperature T. Direct measurement of thermal conductivity of carbon fibres is ongoing. In 2005 Rochais *et al.* [27] demonstrated a photoreflectance microscopy method allowing, for the first time, the direct evaluation of both axial and transverse conductivities of PAN fibres up to 1000°C. An anisotropy ratio of 5 was obtained from diffusivity values for the unidentified fibre.

Most k_{fa} data cited above were measured at cryogenic to room temperatures for CVD or high-modulus fibres. The following data was obtained at or near room temperature, which is more practically relevant to the work presented in this thesis. Yamane *et al.* [28] measured values from 5 W/mK to 175 W/mK for PAN-based fibres including T300. All fibres showed increasing k_{fa} with T at room temperature but the effect of temperature was limited between 300K and 773K. Scott *et al.* [5] also reported limited temperature effect on the transverse conductivity of composites made from PAN-based AS4 fibres between 30°C to 140°C. Reported values of k_{fa} for fibre T300 at room temperature average at 8.4 W/mK [29-33], with

5.90 W/mK and 6.35 W/mK also quoted [28, 34]. A k_{fa} value of 9.5 ± 1.1 W/mK was reported for fibre AS4 at room temperature [35]; 8.4 W/mK was also used [10]. Orthotropy ratios reported for PAN fibres and unidirectional composites vary from 5 to 10 [9, 10, 36]. A ratio of 10 is cited for fibre T300 in [8, 32, 33]; ratios of 4 to 5 are also cited [34]. A ratio of 10 was used for fibre AS4 [10]. Reported room temperature values of epoxy conductivity k_m average at 0.20 W/mK [7, 8, 10, 29, 36, 37].

Figures 2.1 and 2.2 present axial thermal conductivity data for carbon fibres, plotted against the axial fibre modulus and electrical resistivity respectively. The data presented in these figures is publicly available from manufacturers of commercial PAN and pitch fibres [38, 39, 40]. A single mid-range value was collated for each grade when ranges were provided. The values are assumed to be valid at room temperature when this is not stated. As reported above, the axial thermal conductivity of carbon fibres varies widely across two orders of magnitude. Clear trends emerge whereby the axial conductivity increases along with the axial modulus, and it decreases with increasing electrical resistivity. No correlation was identified between axial thermal conductivity and axial tensile strength. Whilst low modulus carbon fibres generally have high strength and vice-versa, this does not always hold for economical grades of commercial fibres; the trend clearly lies with modulus, and not strength. The axial thermal conductivity, axial modulus and electrical resistivity are related through the fibre structure, which varies with graphitisation temperature and duration. Transverse thermal conductivity data that would allow the production of similar curves are not available. Such data is very scarce. Estimated transverse conductivity data was available from one fibre; this is not reported here.

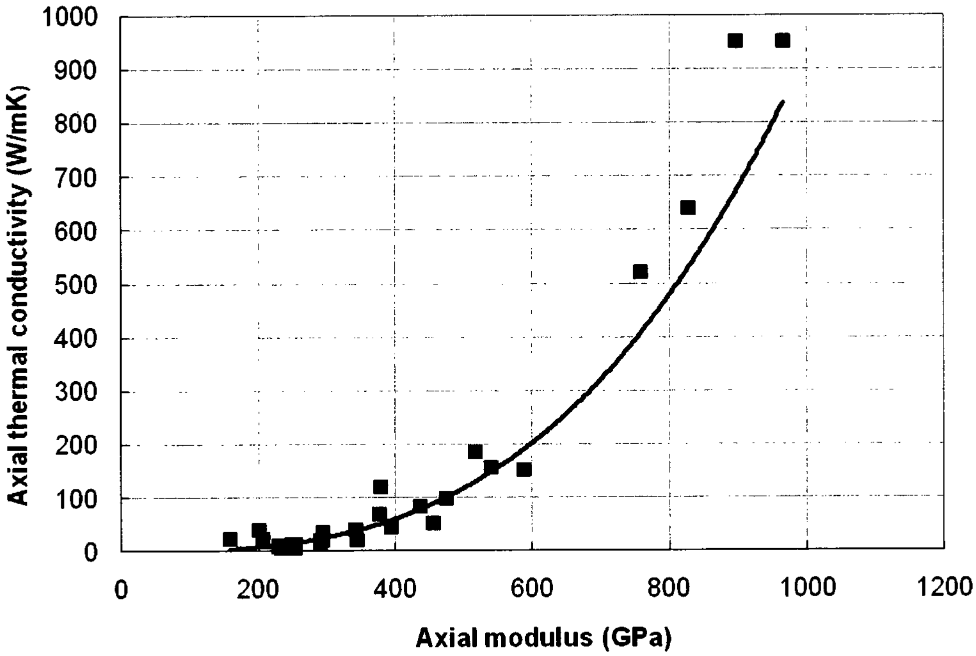

Figure 2.1: Axial thermal conductivity of carbon fibres as a function of their axial modulus

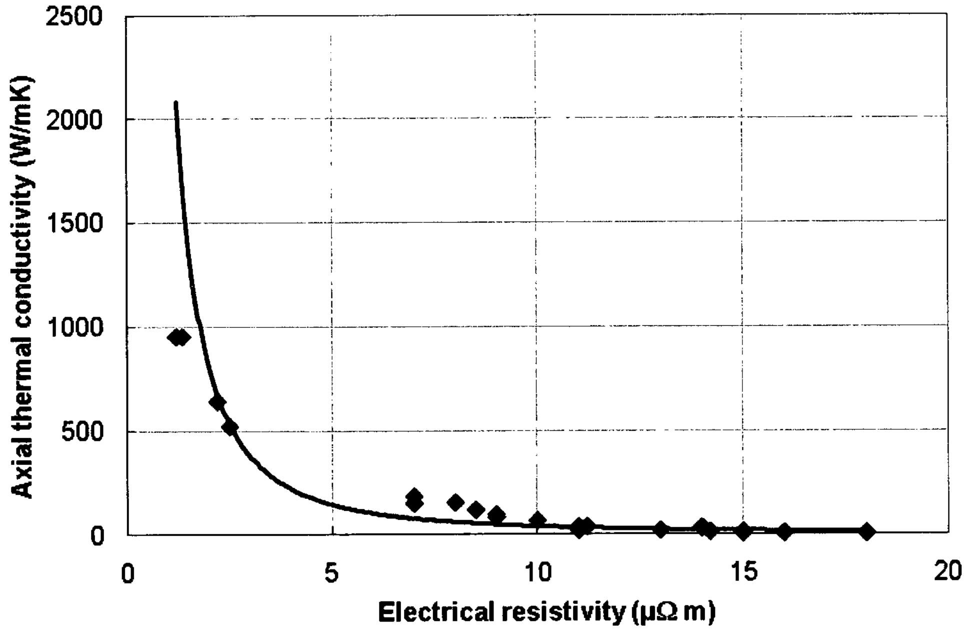

Figure 2.2: Electrical resistivity of carbon fibres as a function of their axial thermal conductivity

2.2 Analytical Models

Calculating the thermal conductivity of unidirectional composites along the fibre direction k_x from the axial thermal conductivity of the fibres k_{fa}, thermal conductivity of the resin k_m and fibre volume fraction V_f is straightforward. The rule of mixture (ROM-A) or parallel model relating the above variables, Equation (2.1), is widely acknowledged and validated. Divergence from this model is rare and can be assigned specific causes [41].

$$k_x = V_f \cdot k_{fa} + (1 - V_f)k_m \qquad (2.1)$$

The situation is more complex in the case of thermal conductivity of homogeneous unidirectional composites in the direction transverse to the fibres k_z. When transverse fibre properties are sought they are usually obtained from transverse measurements made on unidirectional composites. Different models were proposed for that purpose, and transverse thermal conductivity data for both fibres and composites depend on the model used in generating it. Although related analytical problems received attention from the late 19th century [42], models published in the context of structural continuous fibre composites are reviewed here.

In 1965 Thornburg and Pears [6] used parallel and series arrangement of the fibres and matrix in predicting PMC conductivity along and across the fibres, respectively. The former model corresponds to the ROM-A, and remains widely used as stated above. The latter model is the transverse rule of mixtures (ROM-T); it does not account for fibre shape and alignment, or for other aspects such as the presence of voids. In 1967 Springer and Tsai [43] identified the series ROM-T model as a lower bound for the transverse conductivity of unidirectional composites k_z and proposed another model where heat flows along parallel straight lines through a domain including a single fibre at its centre. This model assumes that composites are macroscopically homogeneous, fibres sections are perfectly circular, the problem can be treated as two-dimensional, thermal contact resistance between fibres and matrix is negligible and the fibres are arranged in a square array. The authors noted that alignment of fibre cross-sections in a square array better reflected experimental conductivity values than alignment in a hexagonal array, with an error of approximately 5% below $V_f = 60\%$ rising to more than 10% above $V_f = 75\%$. The authors also noted that k_z varies strongly with V_f at values relevant to yarns as found in textile reinforcements, and regarded accurate V_f values as an absolute prerequisite to the determination of k_z. Numerical methods were used in another reference [44] in demonstrating that straight heat flux lines induce an underestimation of k_z in some cases. The difference can be negligible for high V_f structural C/E PMCs, going from 7.71% at $V_f = 44.5\%$ to 0.37% at $V_f = 79\%$ for a ratio of conductivities of fibre (transverse) to matrix k_{ft} / k_m of 10. Behrens [45] developed a closed-form model of k_z for an array of cylindrical fibres in a square alignment using the method of long waves, and noted that although hexagonal alignment would be preferable in practice it makes little difference. Donea [46] obtained the same equation through other means and deemed it applicable to the cases of square and hexagonal fibre alignment. Upper and lower bound values were provided for hexagonal, square and random alignment; for a fixed V_f the random array was more conductive, followed by the square and then the hexagonal array; again differences were deemed negligible in practice. Clayton [47] proposed a semi-empirical closed-form model which was validated by Dasgupta *et al.* [8]:

$$k_z = \frac{k_m}{4}\left[\sqrt{(1-V_f)^2\left(\frac{k_{ft}}{k_m}-1\right)^2+\frac{4k_{ft}}{k_m}}-(1-V_f)\left(\frac{k_{ft}}{k_m}-1\right)\right]^2 \qquad (2.2)$$

Nielsen [48] proposed a closed-form model accounting for the aggregation of fibres into yarns:

$$k_{yt} = k_m\left[\frac{1+A\cdot B\cdot V_f}{1-B\cdot\varphi\cdot V_f}\right] \quad ; \quad B = \frac{(k_{ft}/k_m)-1}{(k_{ft}/k_m)+A} \quad ; \quad \varphi = 1+\left(\frac{1-V_f}{V_{f,\max}{}^2}\right)\cdot V_f \qquad (2.3)$$

where constant A is determined by the geometry of inclusions. Experimental data validated the model, and it was used in demonstrating that fibre aggregation into yarns must be considered if present.

In a thorough review paper from 1976, Progelhof *et al.* [49] identified Nielsen's model as the most reliable for solid-solid particle composites; however, this conclusion was reached from data relevant to particle inclusions only as insufficient data was available for highly non-spherical particles such as continuous fibres. In a recent paper Pal [50] reached the same conclusion for particles. Differences between k_z values predicted by Clayton's and Nielsen's models are small for continuous fibre composites.

Around the same time, data relevant to aerospace polymer composites began to emerge in the literature. In 1974 Knibbs and Morris [51] commented on the important effect of fibre orientation but did not provide values for k_{ft} . In 1979 Pilling *et al.* [52] conducted thorough measurements on unidirectional and [0°/90°] composites made from high modulus and high strength fibres at different V_f along, across and at 45° from the reference orientation, between 90K and 270K. All conductivity values of samples made from high modulus fibres were larger. Values for unidirectional samples measured along the fibres were larger followed by those of bidirectional samples and unidirectional samples measured across the fibres; conductivity of bidirectional samples was constant in all directions. A strong effect of T was seen along the fibres; across the fibres the effect was weaker. No sample reached maximum conductivity below 270K. Along the transverse direction, the effect of V_f varying from 45.9% to 71.9% was stronger than that of T for the range selected. Results generally agreed with those of Knibbs *et al.* [51]. It was observed that the equations of Thornburg and Pears [6], Springer and Tsai [53] and Nielsen [48] could all model the variation of k_z with V_f ; however, different values of k_{ft} were obtained from each model and for each V_f . Accuracy was estimated between ±3% and ±10%.

More work pertaining to carbon/polymer continuous fibre PMCs was reported in the 1980s. From an analytical procedure Ishikawa [34] noted that below $V_f = 60\%$ differences in k_z between square or hexagonal packing are minor for $k_{ft} / k_m < 10$, and that they are significant beyond either limit. Measurements on unidirectional composites made from fibre T300 from Toray lead to $k_{fa} = 6.3$ W/mK and $k_{ft} = 1.25$ to 1.53 W/mK. The former value compares well to that in [28], but scatter is seen on the latter, as well as on k_x and k_z.

2.3 Classical Lamination Theory

Once the thermal conductivities of homogeneous unidirectional layers of prepreg k_1 and $k_2$are obtained from the above equations, the effective in-plane thermal conductivity of laminates made of such homogeneous prepreg can be calculated along any specific direction, such as k_x for the 0° direction, from the laminate thickness $2h$, ply thickness t_i , and ply orientations θ_i , using the following equation:

$$k_x = \frac{1}{2h}\sum_{i=1}^{N}(k_1(\cos\theta_i)^2 + k_2(\sin\theta_i)^2)t_i \tag{2.4}$$

Similarly, values of the directional conductivity in unidirectional composites k_{cd} where the same material is used for all plies, can be calculated from Equation (2.5) where $\theta$is the angle between fibre and measurement directions [53]. Boundary effects in measurements where $0° < \theta < 90°$ were evaluated [34].

$$k_{cd} = k_1(\cos\theta)^2 + k_2(\sin\theta)^2 \tag{2.5}$$

The development of Equations 2.4 and 2.5 is presented in the classic textbook by Tsai and Hahn [53] and they also appears in MIL Handbook-17 [54]; it will not be repeated here. However, one important feature of the model must be highlighted in relation with the work presented in this thesis. The most common aspect of the classical lamination theory is the development of equations describing the stiffness and compliance of laminates. This starts with the superimposition of basic unidirectional expressions of Hooke's law describing the elastic constitutive behaviour along two principal and orthogonal orientations, labeled here as x and y, and expressed with stresses as the independent variable:

$$\varepsilon_x = \frac{1}{E_x}\sigma_x - \frac{\nu_y}{E_y}\sigma_y \tag{2.6}$$

$$\varepsilon_y = -\frac{\nu_x}{E_x}\sigma_x + \frac{1}{E_y}\sigma_y \tag{2.7}$$

$$\varepsilon_s = \frac{1}{E_s}\sigma_s \tag{2.8}$$

Expressed in matrix form the equations appear as stated below, where the couplings between imposed axial stresses along x and y respectively, and axial strains along y and x, respectively, are expressed clearly. Such couplings are quantified by the Poisson's ratio, and in orthotropic materials two such ratios are defined in-plane – the major Poisson's ration and the minor Poisson's ratio.

$$\begin{bmatrix} \varepsilon_x \\ \varepsilon_y \\ \varepsilon_s \end{bmatrix} = \begin{bmatrix} \frac{1}{E_x} & -\frac{\nu_y}{E_y} & 0 \\ -\frac{\nu_x}{E_x} & \frac{1}{E_y} & 0 \\ 0 & 0 & \frac{1}{E_s} \end{bmatrix} \cdot \begin{bmatrix} \sigma_x \\ \sigma_y \\ \sigma_s \end{bmatrix} \tag{2.9}$$

In reference [53] the authors demonstrate that with regards to constitutive structural behaviour, laminates featuring groups of plies containing the same number of plies laid in groups separated by angles of π/3 or less show in-plane isotropy. Practically, laminating sequences such as $[0°/60°/\text{-}60°]_s$ or $[0°/45°/\text{-}45°/90°]_s$ for example, have the same mechanical properties along all in-plane directions. On the other hand, a laminate characterised by a sequence such as $[0°/90°]_s$ will show different constitutive elastic properties along say the 0° and 45° directions.

The π/3 maximum angle separating plies in mechanically orthotropic laminates results from the *x*-*y* interaction typically quantified by the Poisson's ratio. However, an equivalent effect does not exist for thermal conductivity, where in-plane conduction through in-plane orthotropic laminates, along the two principal directions, is expressed by the following matrix which is devoid of coupling:

$$\begin{bmatrix} q_x \\ q_y \end{bmatrix} = -\begin{bmatrix} k_x & 0 \\ 0 & k_y \end{bmatrix} \cdot \begin{bmatrix} \partial T / \partial x \\ \partial T / \partial y \end{bmatrix} \tag{2.10}$$

It can demonstrated that in the case of in-plane thermal conductivity, laminates featuring groups of plies containing the same number of plies laid in groups separated by angles of π/2 or less show in-plane isotropy. Indeed, Figure 2.3 shows values of Equation 2.5 between $\theta = 0°$ and $\theta = 90°$, the same function between $\theta = 0°+90°$ and $\theta = 90°+90°$, and their sum; arbitrary values of $k_1 = 10$ W/mK and $k_2 = 1$ W/mK were used. The latter represents the values of directional conductivity of a [0°/90°]$_s$ laminate between $\theta = 0°$ and $\theta = 90°$; the graph shows that this is indeed constant.

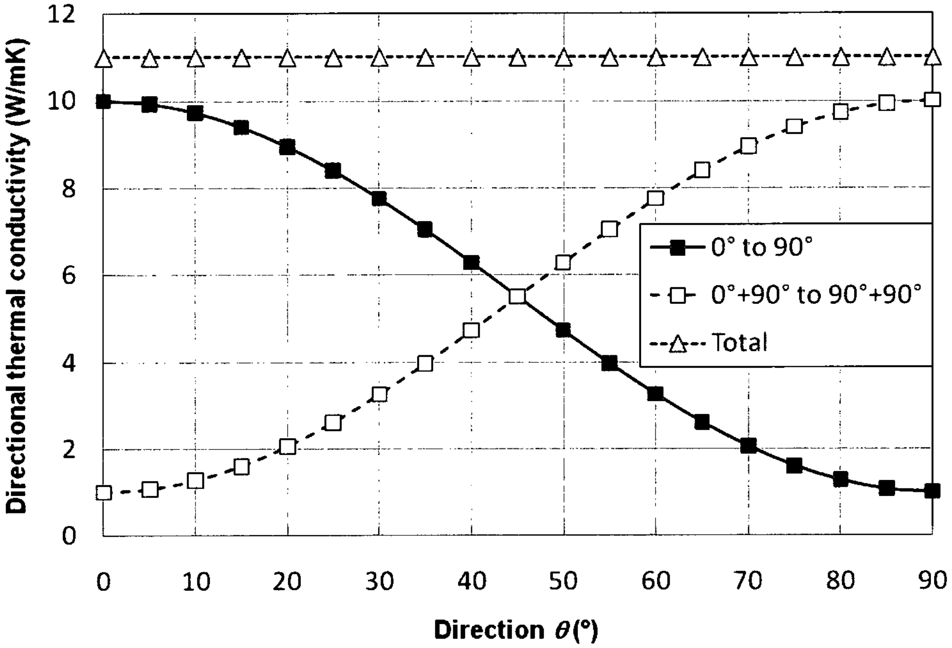

Figure 2.3: Directional in-plane thermal conductivity between $\theta = 0°$ and $\theta = 90°$ for 0° ply, 90° ply, and [0°/90°] laminate

The practical consequence is that in terms of in-plane conduction, a laminate characterised by a sequence such as [0°/90°]$_s$ will show the same conductivity along say the 0° and 45° directions. The largest angles between plies required to obtain in-plane isotropy is 60° for elastic stiffness and 90° for thermal conductivity.

Reference [53] states that it is safe to assume that the through-thickness transverse conductivity k_z of a laminate manufactured from unidirectional plies is equal to the transverse conductivity of a single ply, since the transverse conductivity for all plies is equal and independent of orientation.

2.4 Computational Models

Modelling of conduction in textile composite unit cells was reported in the literature [7-10]. Dasgupta *et al.* [7] created numerical models of single layer plain weaves with maximum V_f of 36% and yarn fibre volume fraction V_{fy} of 63%, Figure 2.4; both numbers are low when compared to those characterizing actual aerospace carbon/epoxy PMCs. The models represented PMCs used for specific purposes discussed by the authors, rather than structural composites with V_f above 55%. Large resin-rich zones were present in the models, away from the yarn crossovers. The thickness of individual textile layers was obtained by dividing laminate thickness by the number of layers, hence nesting was not modeled [8]. The presence of sizeable resin-rich zones in textile unit cells was discussed in [55]. In that work, modeling weaves as superimposed unidirectional layers gave good agreement with experimental data. Dasgupta *et al.* [8] modeled yarns of lenticular cross-sections following spline paths, Figure 2.5, whilst Ning and Chou [29] used rectangular cross section yarns and piecewise linear paths, Figure 2.6; both methods were reported to agree well with experimental data despite the major differences in geometry and geometrical modeling approximations. These results show that some aspects of reinforcement geometry must be captured when modeling the thermal conductivity of textile composites. However, accurate geometric models do not seem to be mandatory in all cases, if there is a way to adjust other material parameters to experimental data for example. Models of diverse yarns were also proposed by Bigaud *et al.* [9], Figure 2.7. These models, which are more complex, also feature relatively large resin-rich zones; they illustrate the difficulty of obtaining realistic geometries representing real woven materials using generic and therefore much simplified models.

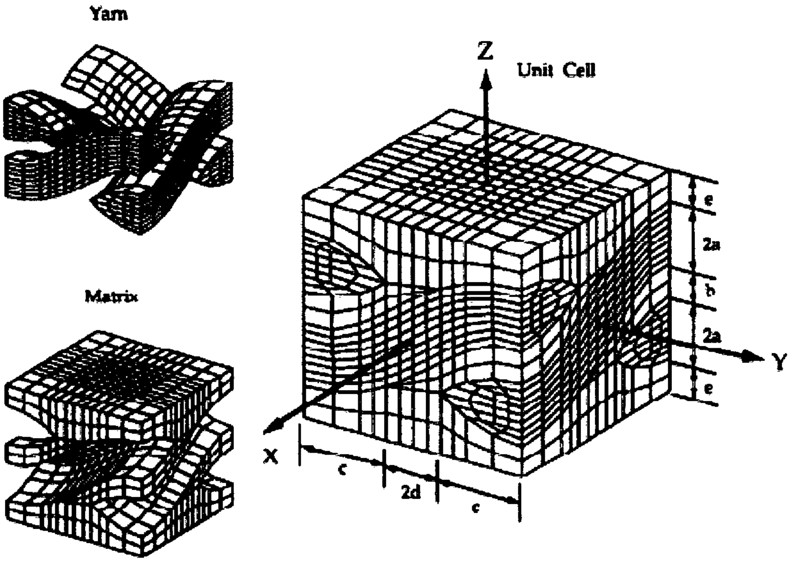

Figure 2.4: Textile unit cell models and finite element meshes, Dasgupta *et al.* 1996 [8]

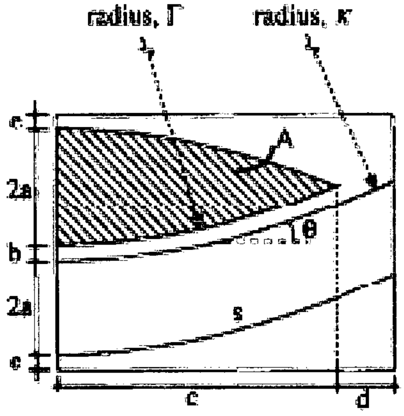

Figure 2.5: Lenticular yarn sections in models by Dasgupta *et al.* [8]

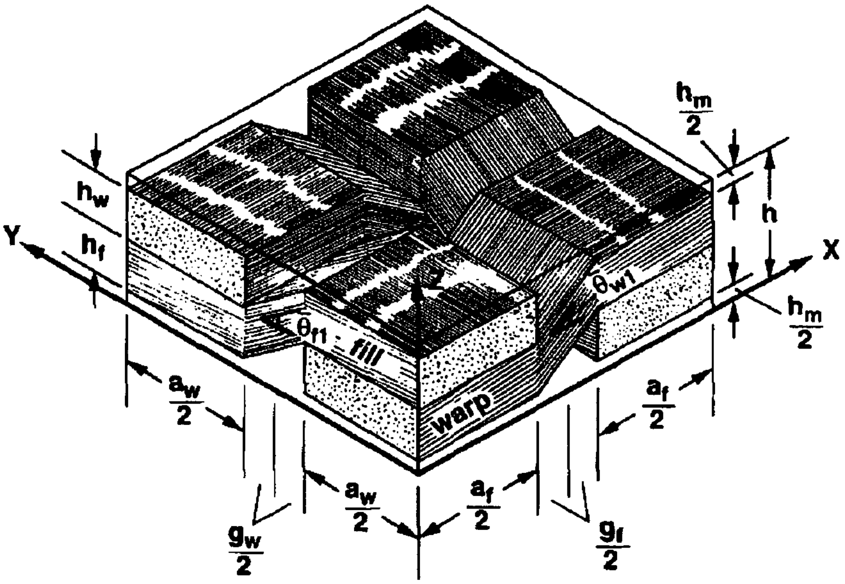

Figure 2.6: Textile unit cell models, Ning and Chou, 1995 [29]

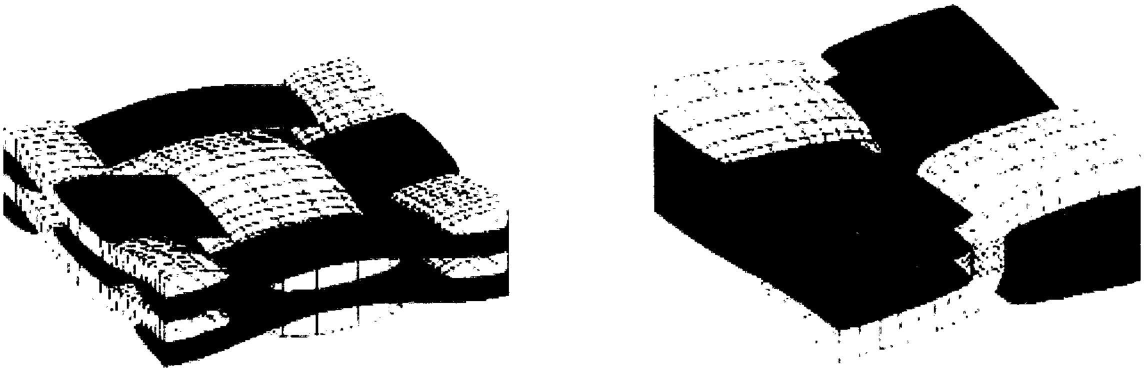

Figure 2.7: Textile unit cell models and finite element meshes, Bigaud et al, 2001 [9]

The above models were used in predicting thermal conduction, which is the transfer of heat within a material without movement of said material, resulting from an imposed temperature gradient. Fourier's Law [56] states the heat transfer rate through a material is proportional to the negative temperature gradient and the area which the heat flows through perpendicular to the gradient:

$$\bar{q} = -k\nabla T \tag{2.11}$$

where $\bar{q}$ (W/m^2) is the local heat flux, k (W/mK) is the thermal conductivity and $-\nabla T$ (K/m) is the local temperature gradient. Thermal conductivity varies as a function of the material temperature. For C/E PMCs the variation of k is limited over the temperature range of interest [5,28]. For non-isotropic materials, such as PMCs, k varies with orientation as stated above. The thermal conductivity in a particular direction can be calculated from the one-dimensional form of Fourier's Law:

$$q = -k\frac{dT}{dx} \tag{2.12}$$

where q (W/m^2) is the heat flux and dT (K) and dx (m) are the temperature difference and distance between two areas of interest.

As stated above, geometrical models of weaves have been used for predicting the conductivity of woven composites [7-10]. However, the link between accuracy in geometry and in predicted conductivity values was not assessed. More importantly, the relation between geometrical accuracy and the ensuing accuracy of predicted conductivity values was not compared to error in experimental conductivity values. This comparison is useful in assessing the relevance of techniques available for predicting the thermal conductivity of composites for different types of reinforcements. Considering the context, considerable variability on thermal conductivity was observed for PMCs, resulting from variability on fibre properties, V_f and fibre configuration. Conductivity measurement error was evaluated at 3% to 12% in [10, 23, 36]. Reference [57] quotes differences of up to 13% between predictions of k_z made using the Springer-Tsai model and numerical simulations. Discrepancies varying from 4.6% to 11.0% between predictions on textile composites and experimental results were found [9]. Larger values are reported elsewhere; a variability range of 10 to 15% is representative of reported values of thermal conductivity for fibre composites.

3 Experimental

3.1 Thermal Conductivity Measurement Devices

Experimental data were gathered using two thermal conductivity measurement devices known as THASYS and THISYS, manufactured by Hukseflux, Netherlands (Figure 3.1). THASYS is designed to measure the through-thickness transverse thermal conductivity of flat specimens while THISYS is designed to measure the in-plane thermal conductivity of flat specimens. The THASYS and THISYS devices were chosen because they enable both in-plane and through-thickness measurements from the same specimens. The following sections describe the operation of the THASYS and THISYS devices, as well as modifications made to THISYS operation that enabled the measurement of directional in-plane thermal conductivity values.

Figure 3.1: THASYS (front) and THISYS thermal conductivity measurement devices

3.1.1 THASYS Transverse Conductivity Measurement Device

The THASYS device used for measuring the through-thickness transverse thermal conductivity, is shown in Figure 3.2.

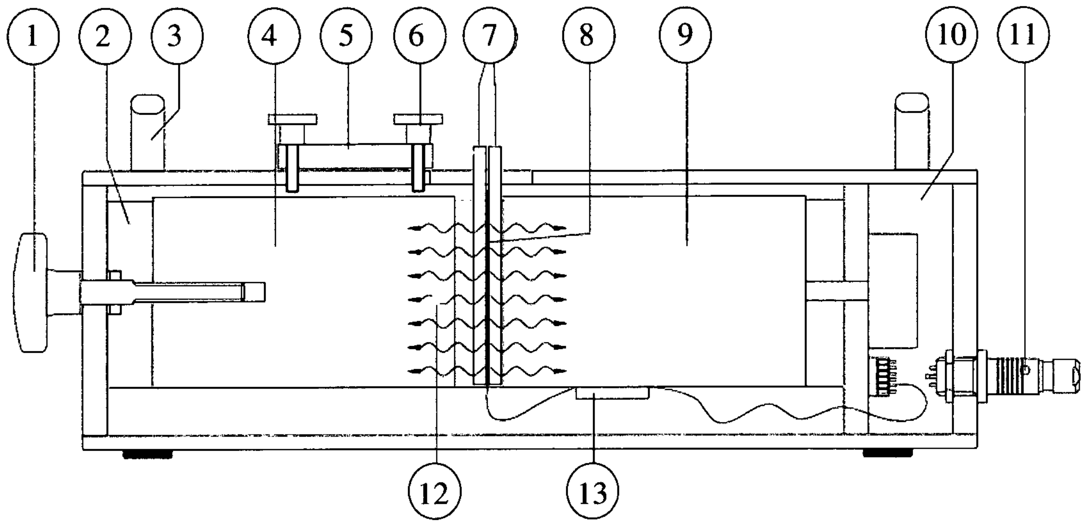

Figure 3.2: THASYS internal components [58]

1) adjustment for moving heat sink
2) glycerol bath
3) handle
4) movable heat sink
5) cover plate
6) cover plate screw
7) specimens (2)
8) heater and thermopile
9) fixed heat sink
10) empty compartment for cable connectors
11) connector for power and DAQ
12) direction of heat flux
13) thermopile connector

THASYS operation is based on principles outlined in standard test method ASTM C1114-06 (Standard Test Method for Steady-State Thermal Transmission Properties by Means of the Thin-Heaters Apparatus) [59]. In this test method a thin heater is positioned between two identical specimens and heat sinks as shown in Figure 3.2. Lateral heat flux from the thin heater is considered negligible; hence this configuration generates a homogeneous and symmetric heat flux transverse to the specimens. This heat flux and the resulting symmetric temperature field must be known to calculate the thermal conductivity of the specimens. Upon testing a heating cycle is carried out; when the device and specimens reach steady state the transverse thermal conductivity can be calculated based on the heat flux and the differential temperature across the specimens. The transverse heat flux is calculated from heater power. The differential temperature across the specimen and the specimen thickness are known, and the through-thickness transverse thermal conductivity is calculated based on Fourier's law [56], Equation (2.11). This method provides an absolute thermal conductivity since it is based on directly measured quantities. The THASYS heater contains the hot joints of the thermopile sensor, while the cold joints are located on the heat sinks Figure 3.2. A thermopile is a circuit of multiple thermocouples enabling the accurate measurement of small temperature variations as one measurement is based on the sum of voltages produced by all thermocouples. The thermopile configuration used in the THASYS device is proprietary to Hukseflux. In the THASYS device, thermal contact resistance between the specimen and device components is minimized by immersing the specimens, heater, and heat sinks in a glycerol bath. The thermal conductivity of glycerol, 0.29 W/mK [58], is one order of magnitude higher than that of air at 0.025 W/mK [58], whilst the glycerol interface contact resistance is considered negligible. Further reduction of the contact resistance is achieved by applying contact pressure to the stack of heat sinks, specimens and heater by means of a spring. Standard test method ASTM D5470-6 requires a minimum of 0.69 MPa (100 psi) of pressure between the apparatus and specimen when using a low viscosity thermal grease on specimens with low surface roughness, to as much as 3.4 MPa (500 psi) when using high viscosity thermal grease on specimens with high surface roughness.

Typical in-plane specimen dimensions are 70 mm x 110 mm with a thickness ranging from 0.1 to 6 mm. Calibration of the THASYS device is performed by measuring the conductivity of Pyrex™ 7740 material standards provided by Hukseflux and adjusting control software constants as required. The accuracy of the device depends on the thermal resistance of the specimen, which is calculated by dividing the specimen thickness by its through-thickness thermal conductivity. THASYS accuracy for the range of recommended thermal resistances to be measured is shown in Table 3.1 (all at 20°C) as reported by Hukseflux [58]. Hukseflux quote ±1% variability for conductivity measurements taken at 20°C [58].

Table 3.1: Accuracy of the THASYS device [58]

Thermal Resistance (10^{-3} m^2K/W)	Accuracy	Number of Specimens
>15	± 3%	2
>5	± 6%	2
>5	± 3%	4
>2.5	± 3%	6
>2.5	± 3%	6
>0.5	>± 14%	6

Other standard test methods such as ASTM D5470-06 (Standard Test Method for Thermal Transmission Properties of Thermally Conductive Electrical Insulation Materials [60] utilize relatively thick electrical heaters which require an additional guard heater around the specimen, to achieve homogeneous heat flux through a specimen whilst minimizing lateral heat flux. Method ASTM D5470-06 also requires the use of high quality insulation to minimize heat losses in the plane of the specimen; such losses can be relatively important with specimens of low conductivity.

3.1.2 THISYS In-Plane Conductivity Measurement Device

The THISYS device is designed for measuring the in-plane thermal conductivity of thermally isotropic specimens, or a bulk in-plane thermal conductivity for orthotropic specimens. Externally it appears similar to the THASYS device as shown in Figure 3.1, but its configuration and operation are different.

The components of THISYS are shown in Figure 3.3 and Figure 3.4. The THISYS device consists of two heat sinks, each of which featuring a cylindrical air-filled insulation cavity in the end closer to the specimen. The cavities are covered by thin heaters, which are used in THISYS for reducing lateral heat losses from the heaters to a negligible level. The housing has a slot in the top through which a single specimen is inserted between the heaters. Once installed the specimen is located between the heaters, which are adjacent to the insulation cavities and heat sinks. A heating cycle is applied where heat flows from the heaters, through the specimens along their plane, and into the heat sinks outside of the insulated cavities (label 12, Figure 3.3). Once steady state is reached an axially symmetrical temperature field develops in the specimen; in-plane gradients are present whilst temperatures are constant through the thickness. The heat flux is known from heater power. By measuring the temperature in the plane of the specimen and the specimen thickness, the thermal conductivity can be calculated. THISYS uses the Hukseflux proprietary thermopile to measure the average temperature on a line across the plane of the specimen from its center towards its edge, where the hot joints are located. The cold joints are located on one of the heat sinks. THISYS provides a measurement relative to a known standard.

Immersion of the specimen and inner components in a glycerol bath minimizes the thermal contact resistance between the specimen and the apparatus, as described in the previous section for THASYS. It should be noted that the thin heaters the insulation cavities from the glycerol. Similarly to THASYS, THISYS requires contact pressure applied on the heat sinks, heaters, and specimen via a spring.

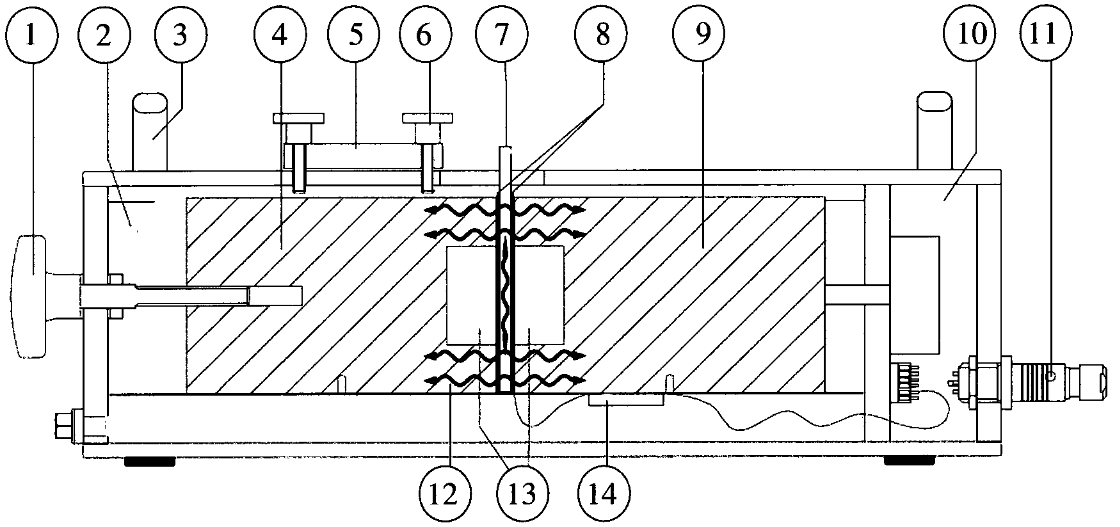
1
2
3
4
5
6
7
8
9
10
11
12
13
14

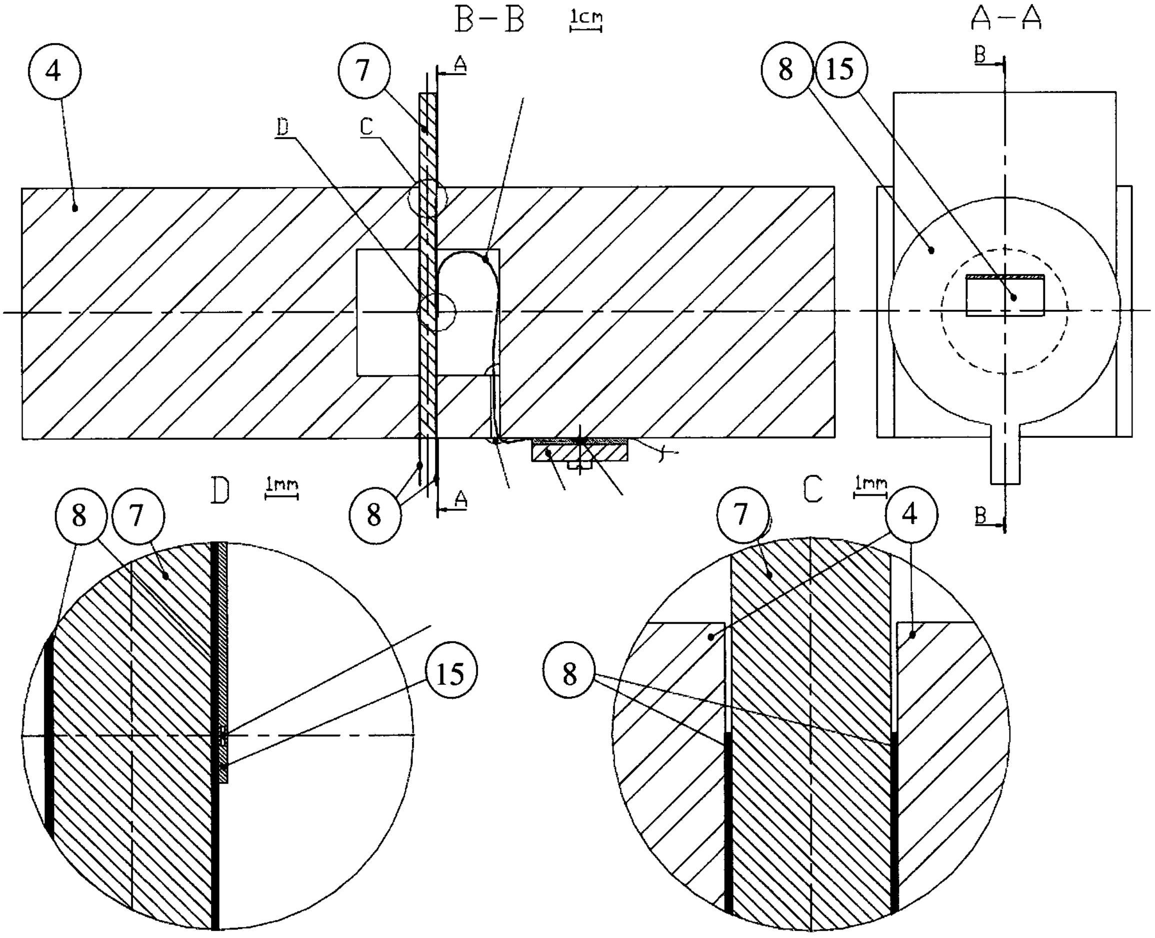
B–B
1cm
A–A
4
7
8
15
8
A
A
B
B
D
C
D
1mm
C
1mm
8
7
15
7
4
8

1) adjustment for moving heat sink
2) glycerol bath
3) handle
4) movable heat sink
5) cover plate
6) cover plate screw
7) specimen
8) heaters (2)
9) fixed heat sink
10) empty compartment for cable connectors
11) connector for power and DAQ
12) direction of heat flux
13) air filled insulation cavities
14) thermopile connector
15) thermopile

Figure 3.3: THISYS internal components [61]

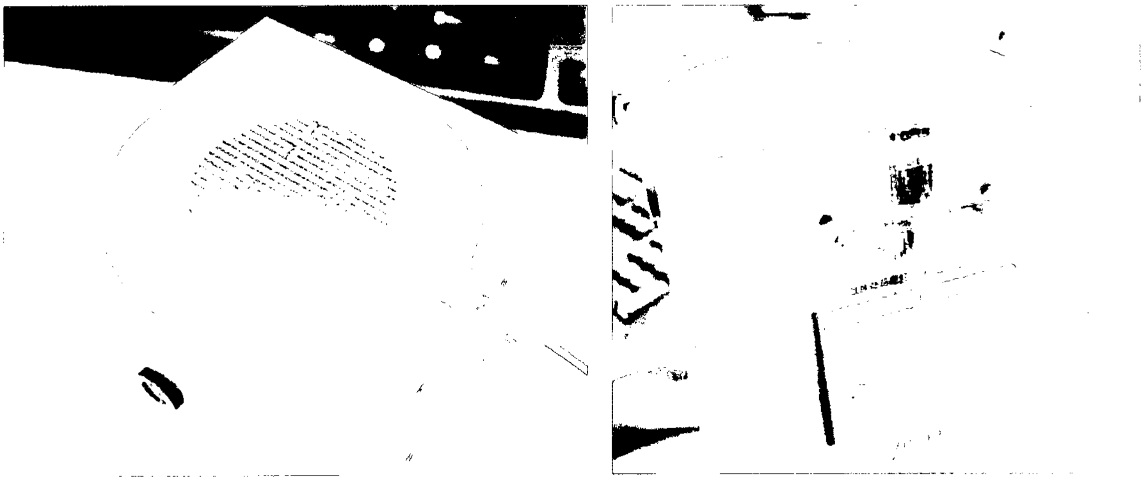

Figure 3.4: THISYS heater, heat sink and thermopile [61]

The geometry for THISYS specimens is the same as that for THASYS at 70 mm wide by 110 mm high, with thickness ranging from 0.1 to 6 mm. Calibration of the system is performed by measuring Pyrex™ 7740 material standards provided by Hukseflux and adjusting control software constants as required. THISYS can measure thermal conductivities ranging from 0.1

W/mK up to 200 W/mK [61]. The product of specimen thermal conductivity and thickness should be between 1 x 10^{-3} W/K and 5 x 10^{-3} W/K [61]. Experimental data obtained by Hukseflux with the THISYS device are provided for accuracy demonstration, Figure 3.5. The measurements were taken with Pyrex 7740™ specimens with thicknesses ranging from 2 mm to 7 mm, a Perspex reference standard with a thickness of 5.62 mm, and stainless steel 304L specimens with thicknesses ranging from 0.1 mm to 0.7 mm. All measurements were taken at 20°C. Figure 3.5 demonstrates an overall in-plane thermal conductivity measurement accuracy of ±6% compared to values available in the literature. Hukseflux quote ±2% variability for measurements taken at 20°C [61].

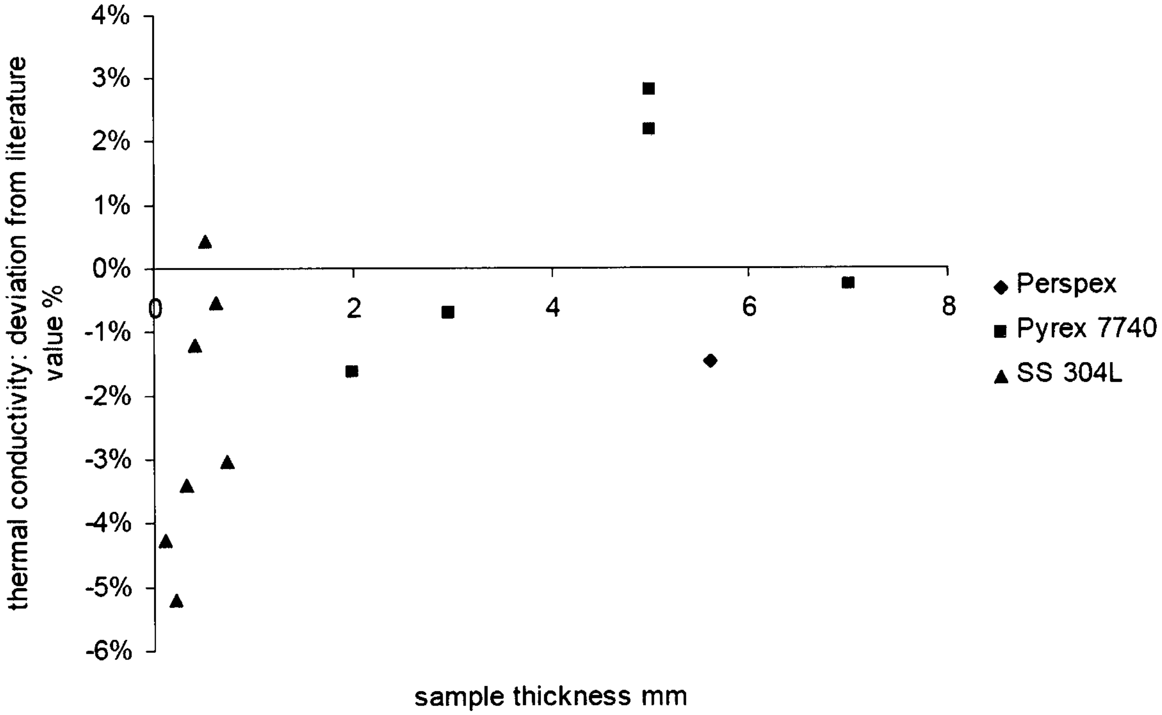

Figure 3.5: THISYS measurement accuracy – deviation from literature values [61]

3.1.3 Directional Conductivity Measurement Using THISYS

As described in section 3.1.2 the THISYS device is designed to measure the in-plane thermal conductivity of thermally isotropic specimens, or a bulk in-plane thermal conductivity for orthotropic specimens. For complete experimental validation of the model predictions presented in this thesis, and for work with polymer composites in general, directional in-plane measurements of orthotropic specimens are required. After extensive discussions and review of the THISYS device operation with Hukseflux staff a modification to the specimen geometry was proposed by the author, which would enable the measurement of thermal conductivity along a specific in-plane direction. This section and subsections describe precisely how THISYS operates in its standard and directional configurations.

3.1.3.1 Standard Configuration

In the standard THISYS configuration, Figure 3.6, heat generated in the portion of the heaters that covers the insulation cavity flows through the specimen along its plane, from the center of the specimen towards its edge at the heat sink. It is important to note that in Figure 3.6 the second heat sink is not shown for simplicity only; the THISYS device is symmetrical along its main axis with respect to the specimen mid-plane, except for the thermal sensor located in one heater only. Power is supplied to both heater elements; heat flows from both elements, into the specimen, and into the heat sinks. Heat that is generated by the portion of the heaters that is sandwiched between the specimen and the insulation cavities is primarily directed into the specimen. Heat that is generated by the portion of the heaters that is sandwiched between the specimen and heat sinks goes partly in the specimen and partly in the heat sinks. A temperature field, theoretically with axial symmetry, is generated in the specimen. Once the system reaches steady state, in-plane temperature gradients remain but specimen temperature variations through the thickness become negligible. A temperature difference is measured between the average recorded by the thermopile and the heat sink. Specimens of higher thermal conductivity generate less in-plane thermal resistance and a smaller temperature difference. Accounting for thickness, the thermal conductivity of the specimen can be calculated from the measured heat flux which is related to heater power, and the temperature difference.

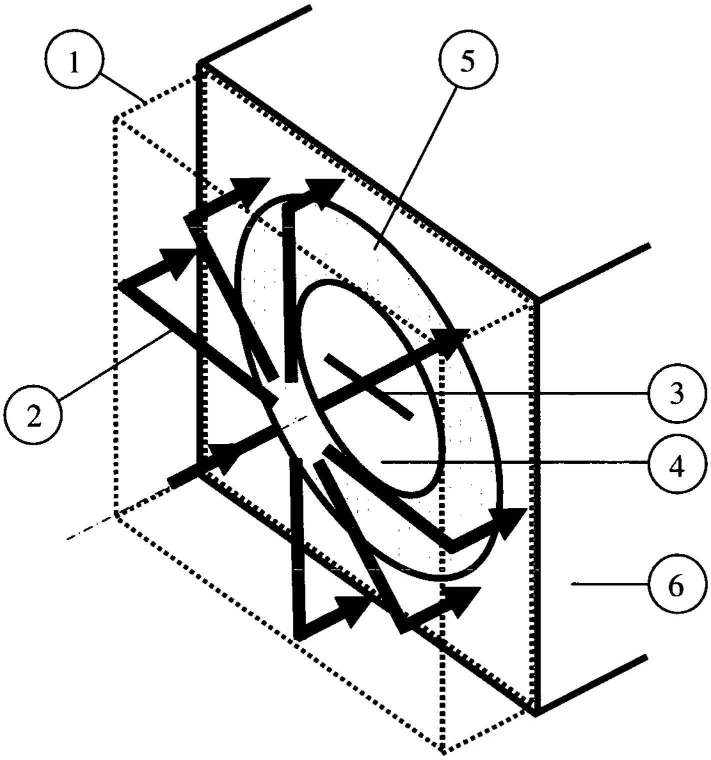

Figure 3.6: THISYS – Heat flux in standard operation

1) specimen	2) heat flux
3) thermopile	4) insulation cavity
5) circular heater (covers cavity)	6) heat sink

3.1.3.2 Directional Configuration

The principle and operation of THYSIS in the directional configuration are similar to the above, with changes in specimen geometry and installation procedure only. The objective behind the introduction of the directional configuration was to generate a heat flux along a specific in-plane direction, enabling measurement of the in-plane thermal conductivity in that direction. Apart from the specimen and its installation the directional THISYS operating procedure is unchanged from that seen in the standard configuration.

The directional THISYS configuration is shown in Figure 3.7. A specimen measuring 22 mm in width and 110 mm in length is aligned vertically and centered over the thermopile. The 22 mm width was chosen to ensure coverage of the entire thermopile which is 20 mm wide. Device operation is unchanged, but the heat flux generated in the specimen is predominantly oriented along its length before it reaches the heat sink.

As the thinner directional specimen does not cover the entire heater width, closed-cell foam was used to displace the glycerol away from the portion of the heaters not in contact with the specimen. This also minimized convective heat losses through the edges of the specimen. Pieces of Starfoam PAF1254 rolled material measuring 110 mm by 22 mm by 3.2 mm were stacked until their total thickness exceeded the specimen thickness, and taped to either edge of the specimen. The thermal conductivity of the closed-cell foam is close to that of air at 0.025 W/mK, negligible compared to that of glycerol at 0.29 W/mK. Many trials were conducted in order to establish this configuration.

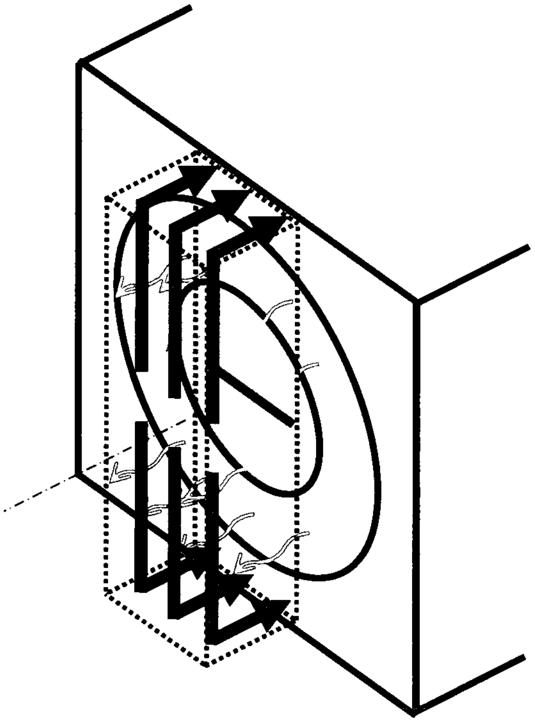

Figure 3.7: THISYS – Directional orientation

As the thinner directional specimen does not cover the entire heater width, some of the heat generated by the element during testing will flow elsewhere. Heat may also be lost to the glycerol film present on the side edges of the specimen. As the objective is to direct heat along the length of the specimen, the directional geometry will be generally more accurate for measuring along directions of high conductivity where the in-plane transverse direction has a much lower thermal conductivity, say along the carbon fibres in a unidirectional laminate. Conversely, the directional configuration will be potentially less accurate in directions of low conductivity if the in-plane transverse direction has a much higher thermal conductivity, say across the carbon fibres in a unidirectional laminate. In the latter case the heat will be drawn to the side edges of the specimen where losses to the glycerol will occur.

For any given material including thermally isotropic materials, the directional specimen design described above produces measured value that differ from those obtained by using the standard configuration. Directional THISYS measurements of isotropic materials were plotted against THASYS measurements of the same materials in order to generate a calibration curve, which can be used to convert directional THISYS measurements of non-isotropic materials to directional in-plane thermal conductivity. Directional THISYS configuration specimens cut from a variety of isotropic materials were tested and their conductivity as provided by the THISYS software was plotted against standard specimens of the same materials measured in THASYS. THASYS was chosen for its superior accuracy. The resulting calibration curve, Figure 3.8, was used to determine the thermal conductivity of non-isotropic specimens measured with THISYS in the directional configuration. Measurements were performed for eight materials including Teflon™, two unidentified polymers, silicone, HDPE, glass, stainless steel and a composite of copper spheres suspended in epoxy. Measurement records are available in Appendix A. The equation of the linear calibration curve appearing in Figure 3.8 is $y = 0.28282x + 0.0602$ with an R^2 value of 0.998.

To minimize directional THISYS measurement error the insulation foam must be replaced each time a new specimen is installed. This prevents any potential saturation of the foam with glycerol. Directional THISYS measurement errors are associated with the following causes: 1) non-directionality of heat flux due to the width of the specimen (22 mm) which cannot be further reduced since it must cover the entire thermopile, 2) thermal losses due to the foam,

3) thermal losses due to small volumes of glycerol which are not displaced by the foam, and 4) improper specimen location with respect to the thermal sensor.

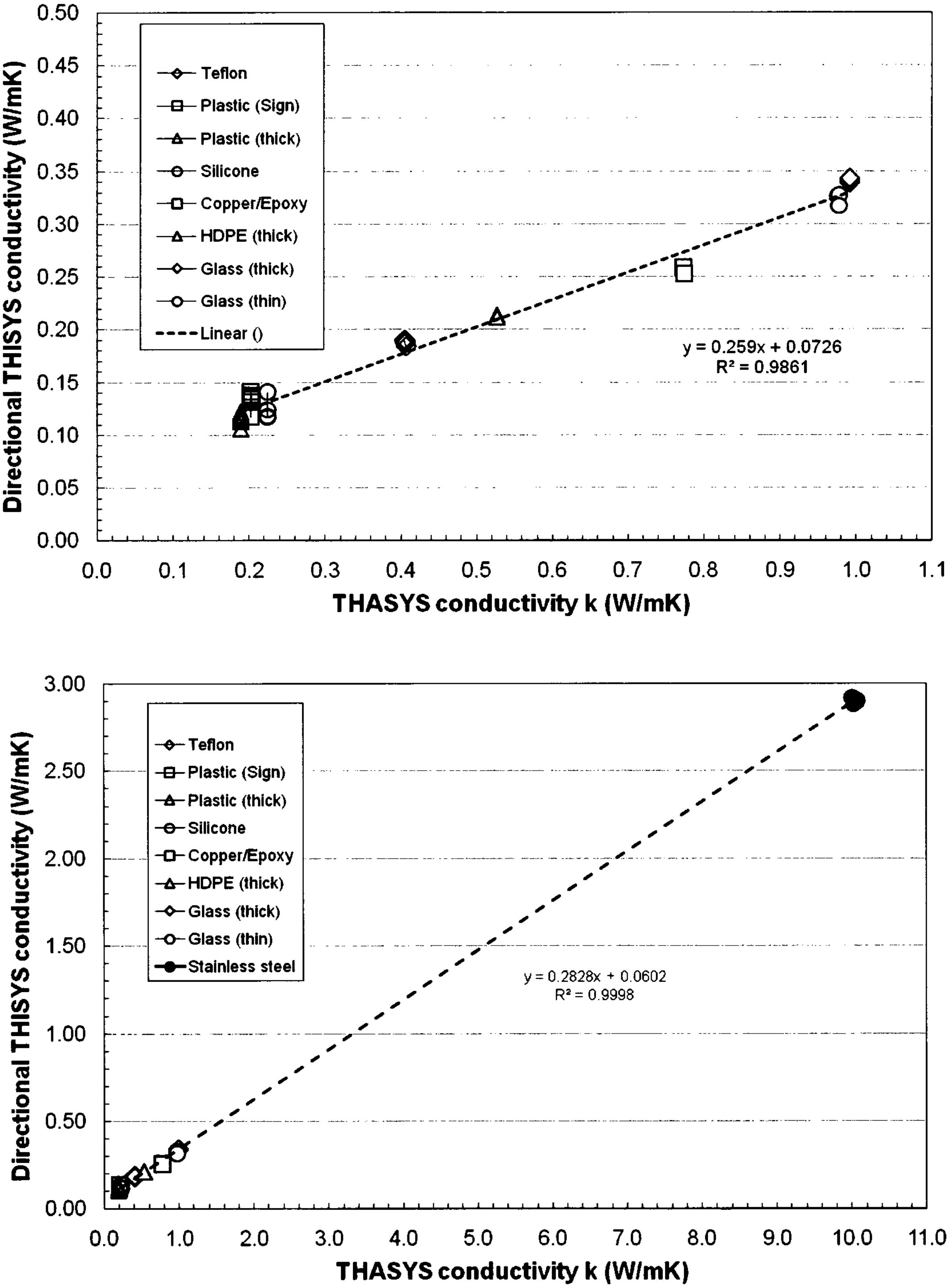

Figure 3.8: Directional THISYS calibration curve

3.1.3.3 Confirmation

Measurements performed during the course of the experimental work confirmed the validity of the directional THISYS measurement configuration.

In-plane transverse directional THISYS measurements taken across the fibre direction of unidirectional laminates manufactured from unidirectional prepreg were compared with through-thickness transverse measurements taken on the same laminates using THASYS. Panel 1 described below is a unidirectional laminate $[0]_6$ manufactured from unidirectional carbon/epoxy prepreg. In-plane transverse conductivity values measured using the directional THISYS configuration averaged at 0.700 W/mK. The through-thickness transverse thermal conductivity measured using THASYS averaged at 0.730 W/mK. Whilst not necessarily equal these two averages should be close. In this case the difference is 4.1% of the latter value.

Also, theoretical predictions made for laminates manufactured from unidirectional prepreg were confirmed as outlined in section 4.1 and Table 4.1. The predictions correlated well and were within the limits of variability described in chapter 2.

Finally, the high level of linearity shown by the calibration curve in the above section provided clear indication of consistency in the effect of the configuration.

3.2 Composite Panel Manufacturing

Fourteen carbon/epoxy panels were manufactured from three polymer composite material systems, with the aim of measuring directional thermal conductivity. The following sections describe the material systems, processing methods, lamination sequences and non-destructive inspection technique used for the panels.

3.2.1 Material Systems

Three different carbon/epoxy composite systems were used in manufacturing panels: material 1) unidirectional prepreg tape AS4/3501-6 from Hexcel [Appendix B], material 2) plain weave prepreg HexPly F263 from Hexcel [Appendix B], and material 3) unidirectional woven fabric style 1152 from Fabric Development impregnated with Mia-epoxy 100 resin and hardener 95 [Appendix B]. The material system specifications are detailed in Table 3.2. Panels manufactured from prepreg materials 1 or 2 typically measured 30 cm by 30 cm whilst panels manufactured from unidirectional fabric material 3 measured 15 cm x 30 cm.

Table 3.2: Carbon/epoxy material systems

Material	**1**	**2**	**3**
Designation	AS4/3501-6	HexPly F263 W3T282-42"-F263	Tape weave Fabric style 1152
Manufacturer	Hexcel	Hexcel	Fabric Development
Form	UD prepreg	Woven prepreg	UD dry fibre
Weave style	N/A	Plain weave	UD weave
Fibre	AS4	T300	T300
Surface density (g/m^2)	150	194	366.7
Roll width (cm)	107	107	7.5
Cured ply thickness (mm)	0.25	0.18	0.37
Fibre volume fraction	0.62	0.61	0.55

3.2.2 Processing

Panels made from materials 1 and 2 were manufactured in an autoclave, whilst panels made from material 3 were made using hybrid hand-layup. Panel information appears in Table 3.3. It is important to note that in the case of material 2, each lamina or ply of woven prepreg is effectively a layer with the same amount of fibres in both orientations hence described as [0/90]. As seen in Table 3.3 the first two panels manufactured for each material type - panels 1 and 2, 7 and 8, and 10 and 11 - were duplicated to ensure manufacturing and measurement consistency.

Table 3.3: Laminate summary

Panel	**Material**	**Form**	**Layup**	**Processing**	**C-Scan**
1	1	UD Prepreg	$[0]_6$	Autoclave	Acceptable
2	1	UD Prepreg	$[0]_6$	Autoclave	Acceptable
3	1	UD Prepreg	$[0/90/0/90]_s$	Autoclave	n/a
4	1	UD Prepreg	$[0/90/0]_s$	Autoclave	Acceptable
5	1	UD Prepreg	$[0/45/-45/90]_s$	Autoclave	Acceptable
6	1	UD Prepreg	$[0/30/-30]_s$	Autoclave	Acceptable
7	2	Woven Prepreg	$[(0/90)]_8$	Autoclave	Acceptable
8	2	Woven Prepreg	$[(0/90)]_8$	Autoclave	Acceptable
9	2	Woven Prepreg	$[(0/90)/(45/-45)/(45/-45)/(0/90)]_s$	Autoclave	Acceptable
10	3	UD Woven	$[0]_6$	Hand-Layup	n/a
11	3	UD Woven	$[0]_6$	Hand-Layup	n/a
12	3	UD Woven	$[0/90]_s$	Hand-Layup	n/a
13	3	UD Woven	$[0/90/0]_s$	Hand-Layup	n/a
14	3	UD Woven	$[0/60/-60]_s$	Hand-Layup	n/a

The Baron – Blakeslee autoclave model BAC-46, serial A38801 used for manufacturing panels from materials 1 and 2 is shown in Figure 3.9. Panels manufactured in the autoclave from these materials were cured according to Hexcel's data sheet [Appendix B]. All panels cured in the autoclave were vacuum-bagged as detailed in Figure 3.10. The autoclave cure cycles for materials 1 and 2 are shown Figure 3.11 and Figure 3.12 respectively.

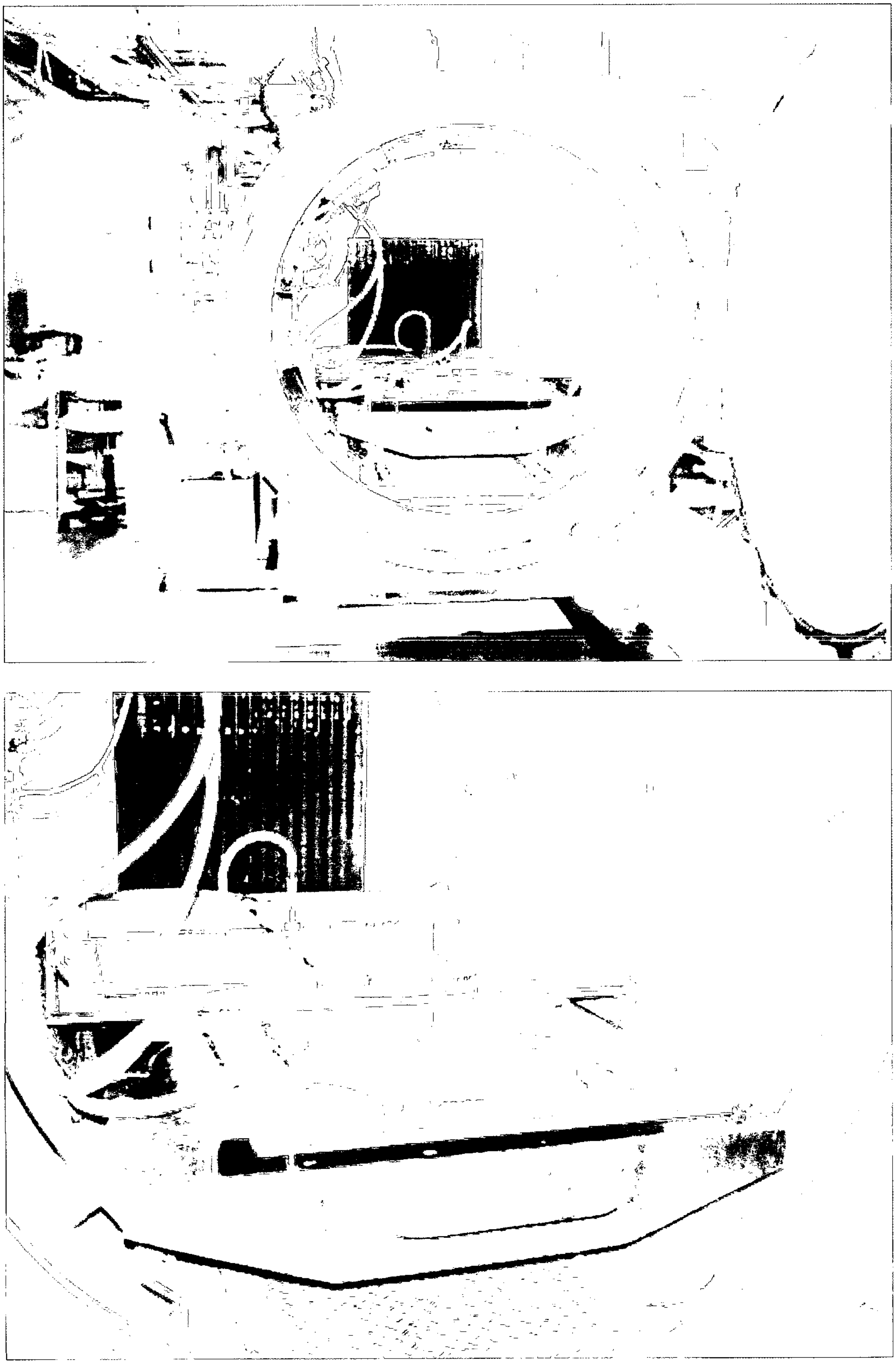

Figure 3.9: Baron – Blakeslee autoclave with vacuum bagged panels

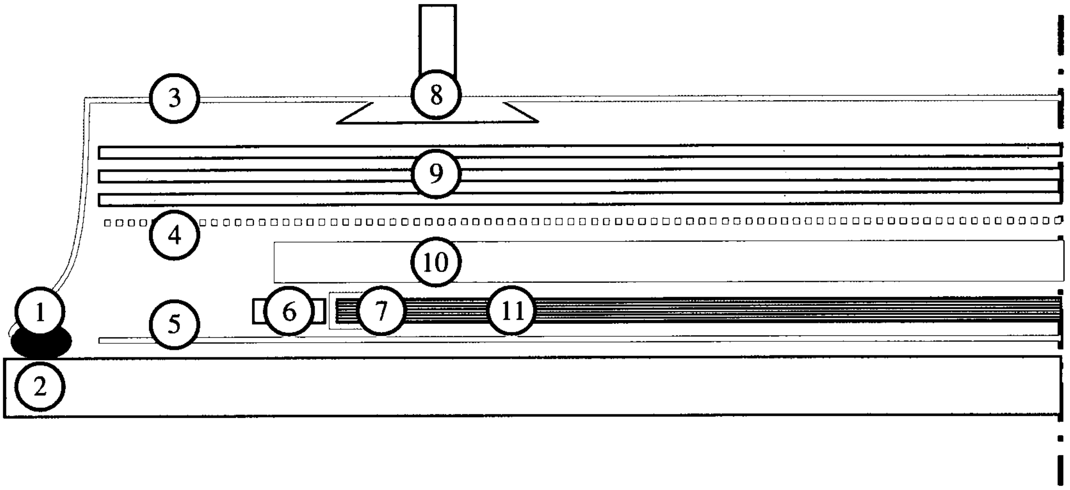

1) bag seal
2) tool plate
3) vacuum bag
4) perforated release film
5) non-perforated release film
6) thickness dam
7) polyimide tape edge seal
8) vacuum port
9) breather material
10) caul plate wrapped in release film
11) composite panel

Figure 3.10: Vacuum bagging configuration for autoclave cured composite panels

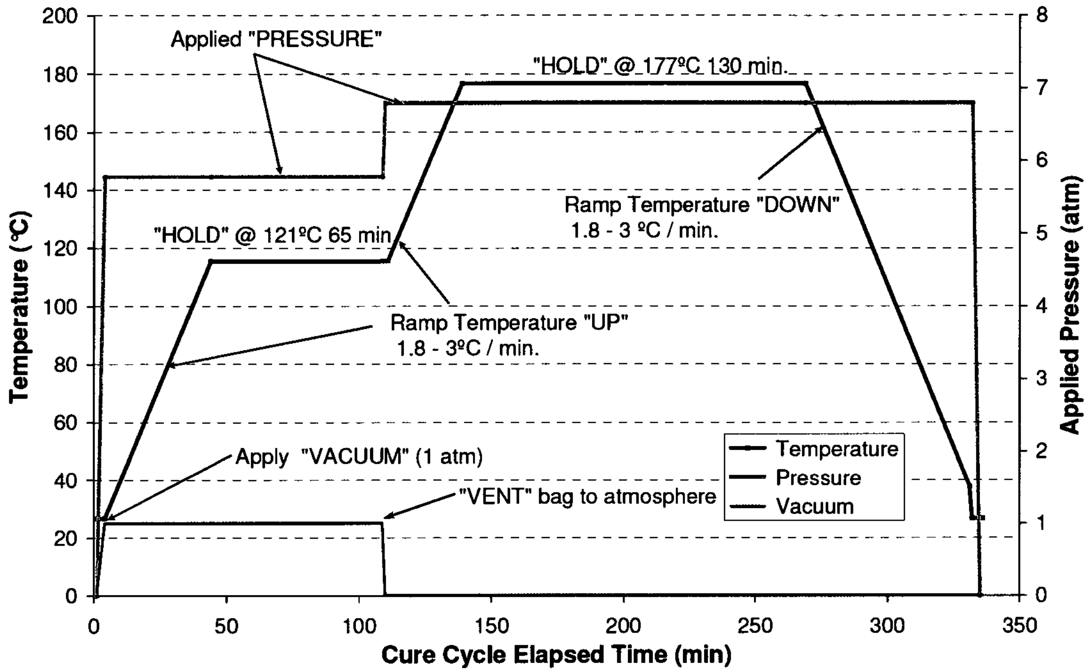

Step	Step Time	Temp.	Pressure	Next	Applied	Check	Step Description	Cycle Time	
#	(min.)	(°C)	(atm)	Step	Vac. / Vent		(action type)	(min.)	(hrs.)
0	1	27	0	1	Full Vac.		Re-set Setpoints to "Base"	Start	Start
1	3	27	6	2	Full Vac.		Ramp Press. "Up"	1	0.0
2	40	116	6	3	Full Vac.		Ramp Temp. "Up" (+2.2°C/min)	4	0.1
3	65	116	6	4	Full Vac.		Dwell (cure)	44	0.7
4	1	116	7	5	Full Vac.		Ramp Press. "Up"	109	1.8
5	1	116	7	6	Vac. To Vent		"VENT" Bag - Vac. Pump "Off"	110	1.8
6	28	177	7	7	Vent		Ramp Temp. "Up" (+2.2°C/min)	111	1.9
7	130	177	7	8	Vent		Dwell (final cure)	139	2.3
8	62	38	7	9	Vent		Ramp Temp. "Down" (-2.2°C/min)	269	4.5
9	1	27	7	10	Vent		Ramp Temp. "Down" (fast)	331	5.5
10	3	27	0	11	Vent		Ramp Press. "Down"	332	5.5
11	1	27	0	11	Vent		Hold - Complete	335	5.6
HOLD							"Base" Setpoints	336	5.6
					CURE CYCLE COMPLETE				

Figure 3.11: Autoclave cure cycle, material 1 – Hexcel AS4/3501-6

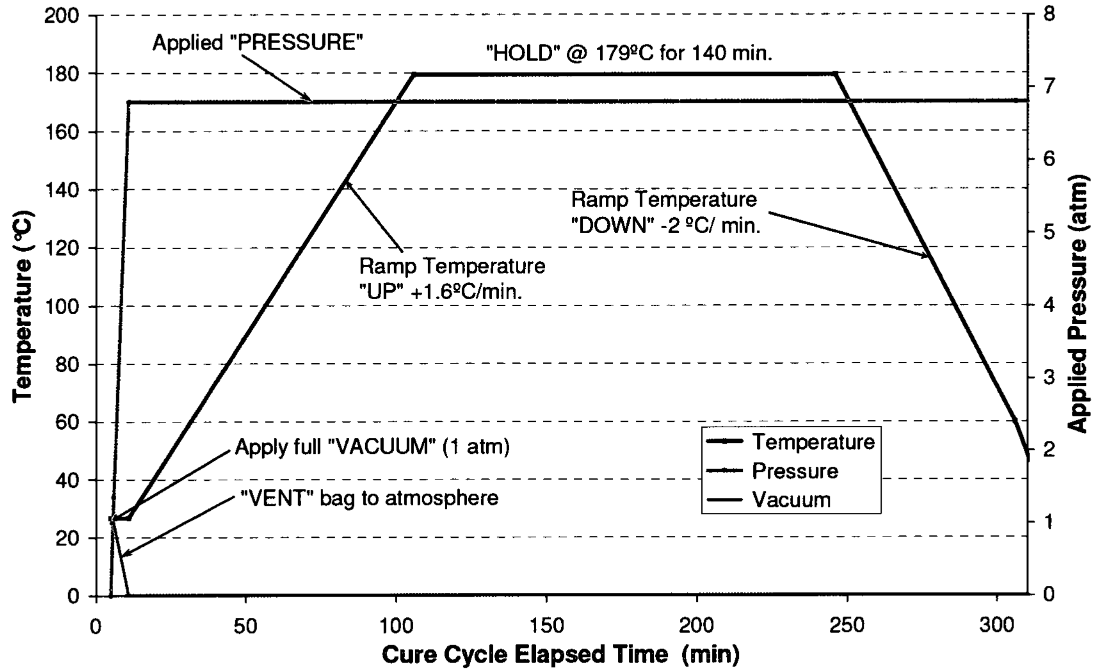

Step #	Step Time (min.)	Temp. (°C)	Pressure (atm)	Next Step	Applied Vac. / Vent	Check	Step Description (action type)	Cycle Time (min.)	(hrs.)
0	5	27	0	1	Full Vac.		Re-set Setpoints to "Base"	Start	Start
1	1	27	1	2	Full Vac.		Ramp Press. "Up"	5	0.1
2	5	27	7	3	Vent		"VENT" @20 psi. - Vac. Pump "Off"	6	0.1
3	95	179	7	4	Vent		Ramp Temp. "Up" (+1.6ºC/min)	11	0.2
4	140	179	7	5	Vent		Dwell 355ºF (±10ºF) min 120min.	106	1.8
5	60	60	7	6	Vent		Ramp Temp. "Down" (-2.0ºC/min)	246	4.1
6	12	27	7	7	Vent		Ramp Temp."Down" fast (-2.8ºF/min)	306	5.1
7	2	27	0	8	Vent		Ramp Press. "Down"	318	5.3
8	1	27	0	8	Vent		Hold - Complete	320	5.3
HOLD							"Base" Setpoints	321	5.4
					CURE CYCLE COMPLETE				

Figure 3.12: Autoclave cure cycle, material 2 – Hexcel HexPly F263

For hybrid hand-layup of panels made of material 3 the dry fibre bed was impregnated with Mia-epoxy 100 resin and hardener 95 mixed at 100:24 mass ratio, and then cured and post-cured at 43°C for 60 minutes as recommended by the resin supplier. The panels were produced in a Carver press at controlled thickness, Figure 3.13.

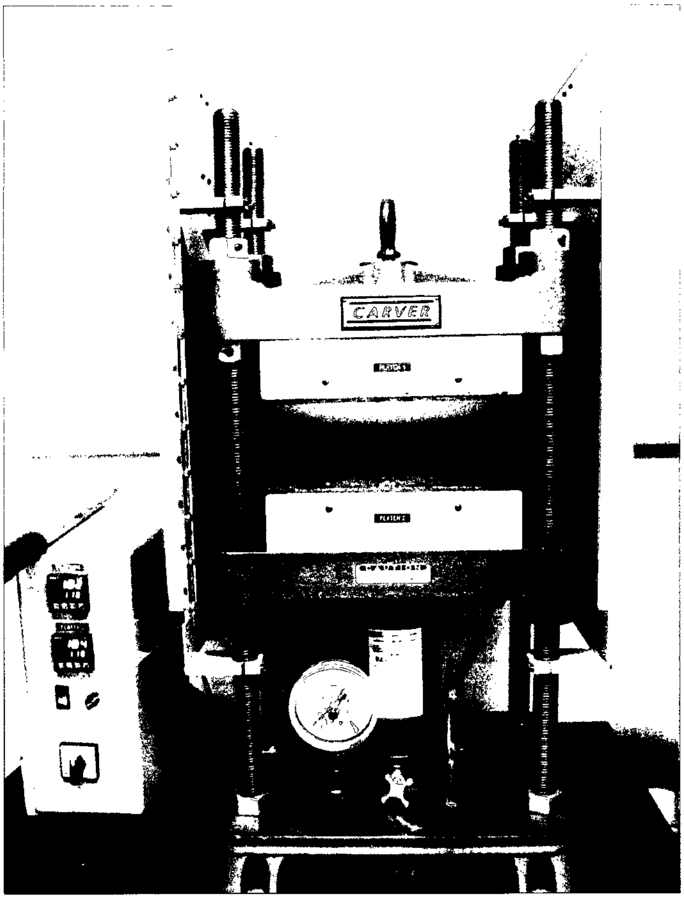

Figure 3.13: Carver heated press

3.2.3 Non-Destructive Inspection

Through-thickness transmission ultrasonic c-scans of panels 1, 2 and 4 through 9 were conducted to ensure consolidation quality. The scans appear in Figure 3.14. The panels were immersed in water and a reflector bar was located behind them as usual practice. Qualitative assessment of the C-scan images indicates suitable levels of quality for all panels, with no discontinuities. Variations in colour seen in the images result from minor changes in laminate thickness. C-scans were not conducted on panel 3 due to c-scan availability or on panels 10 to14 due to reinforcement heterogeneity.

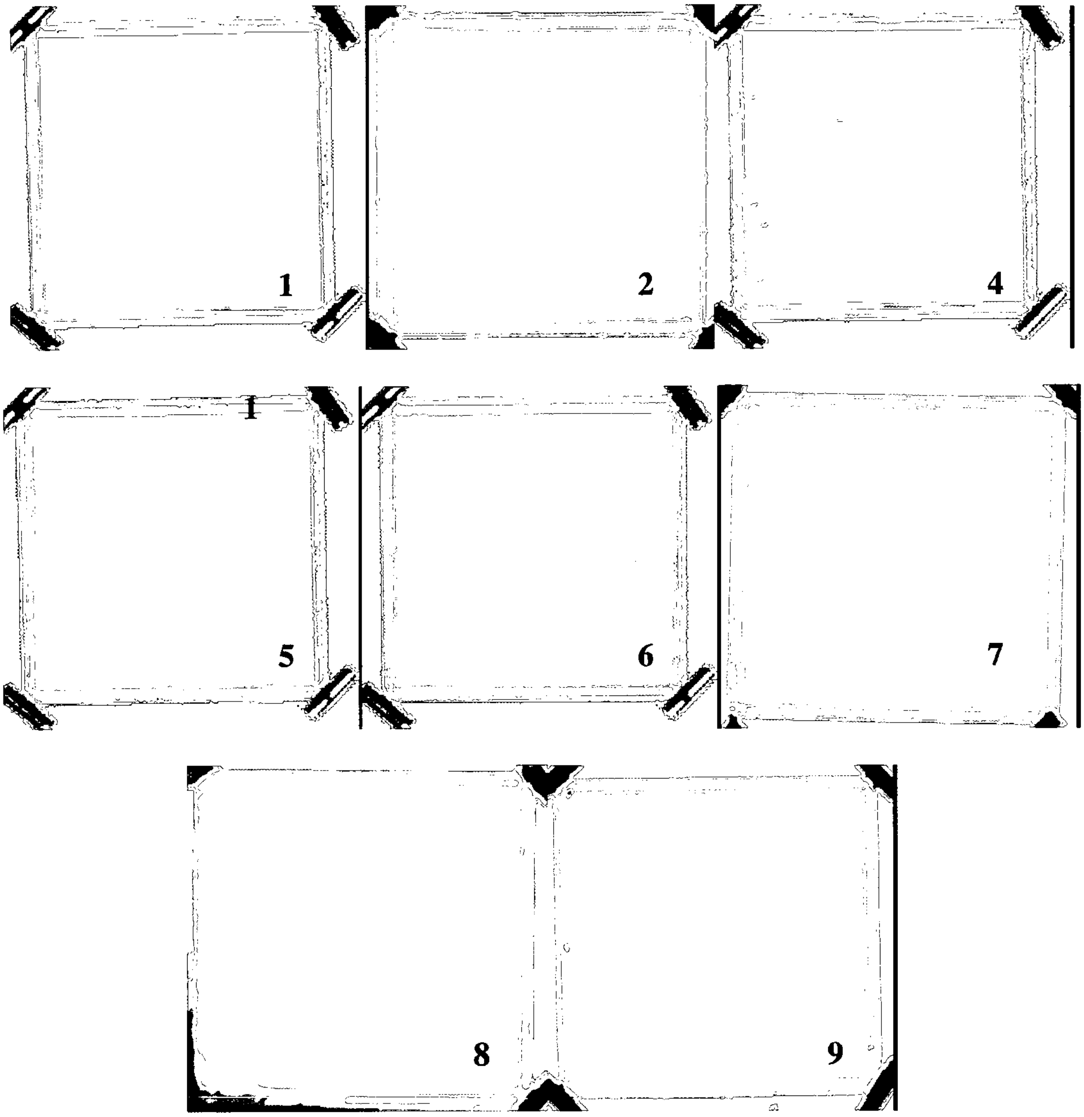

Figure 3.14: Ultrasonic c-scan images of panels 1, 2 and 4 through 9

3.2.4 Micrographs of Panels

This section describes selected cross-section micrographs of panels made from materials 1, 2 and 3. Differences in reinforcement architecture and variation within material structures are highlighted. A section of panel 5 made of UD prepreg material 1 with laminating sequence [0/45/-45/90]s is shown in Figure 3.15. The eight separate plies are clearly visible and one is measured as 0.269 mm thick compared to the manufacturer's cured ply thickness of 0.250 mm (Table 3.2). The overall laminate thickness is 2.022 mm compared to the manufacturer's 2.000 mm estimate.

Figure 3.15: Cross section of panel 5 made of UD prepreg material 1 with laminating sequence $[0/45/-45/90]_s$

A section of panel 7 made of woven prepreg material 2 with laminating sequence [(0/90)]8 is shown in Figure 3.16. The bi-directional reinforcement structure of each ply is visible. Irregular interaction of the eight plies complicates identification of individual plies. The micrographs shows areas of full yarn nesting as well as areas with no nesting. Some vertical yarn gaps appear constant while others are variable. The micrograph features areas of yarn contact and interference. Resin rich zones are also clearly visible. Yarn cross-section height and laminate thickness and inter-yarn distance of 0.136 ± 0.003 mm, 1.493 ± 0.042 mm, and 2.260 ± 0.175 mm were, respectively, determined from Figure 3.16. On the basis of measured yarn thickness, a laminate made of eight superimposed layers of plain weave prepreg with no nesting should have a thickness of 2.176 mm. Alternatively, a laminate made of eight staggered prepreg layers featuring full nesting should have a thickness of at least 1.632 mm. Both predicted thicknesses are larger than the actual laminate thickness, highlighting the prevalence of nesting.

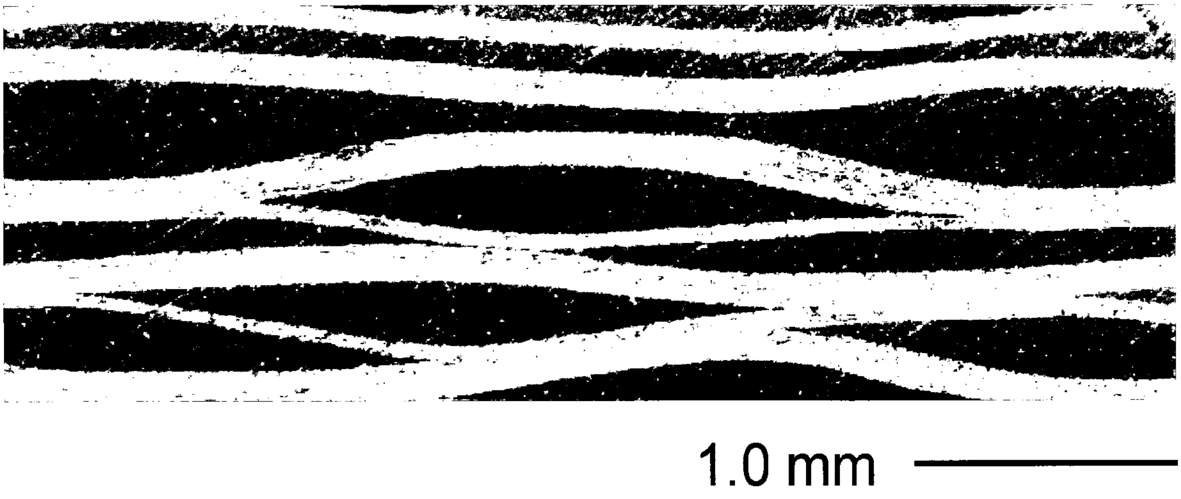

Figure 3.16: Cross section of panel 7 made of woven prepreg material 2 with laminating sequence $[(0/90)]_8$

Sections of panel 13 made of UD woven fabric material 3 with laminating sequence [0/90/0]s are shown in Figure 3.17. The textile reinforcement is made from distinct yarns separated by inter-yarn gaps; yarns and gaps segregated by manual analysis appear in the lower part of the figure. In-plane inter-yarn gaps are larger than through-thickness ones, and as a result k_z is larger than k_y for unidirectional panel 11 (Section 3.3 Table 3.4). The micrographs feature a high degree of nesting between the two central plies with significant yarn section deformation compared to the outer plies. Variable inter-yarn gaps are observed along with resin rich zones.

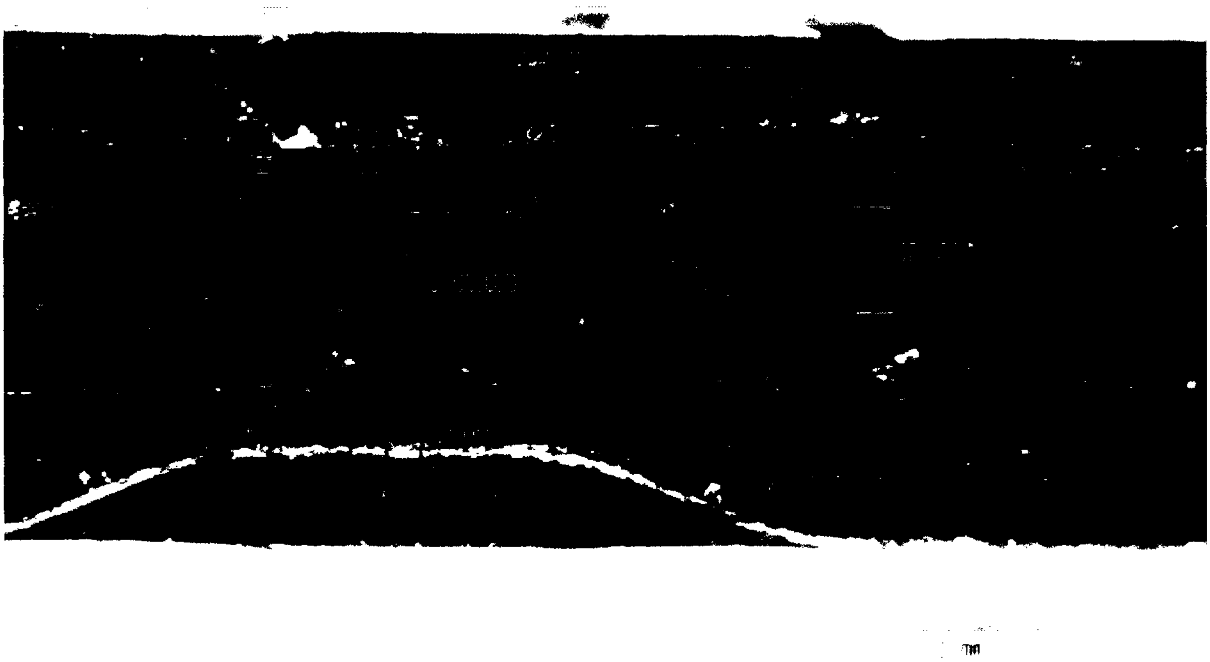

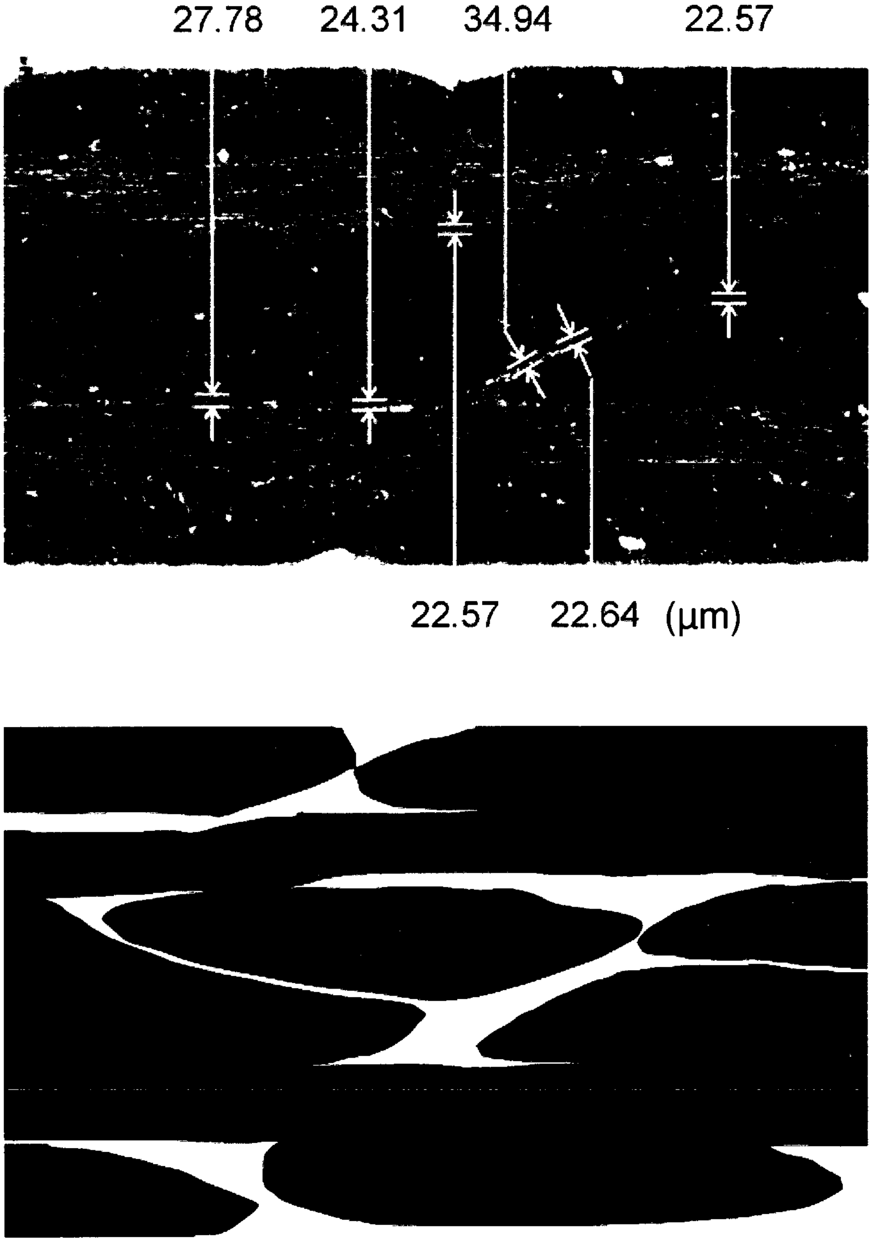

Figure 3.17: Cross sections of panel 13 made of UD woven fabric material 3 with laminating sequence $[0/90/0]_s$

3.3 Directional Thermal Conductivity Measurements

The following experimental results are presented in Table 3.4 for panels 1 to 14: the bulk in-plane thermal conductivity measured using the THISYS device in its original configuration, referred to as bulk THISYS; the through-thickness transverse thermal conductivity measured using the THASYS device, referred to as THASYS; and values of the directional in-plane thermal conductivity measured using the THISYS in its directional configuration, referred to as directional THISYS. It is important to note that measurements taken with THISYS in its original configuration correspond to a bulk in-plane thermal conductivity as described in section 3.1.2, and do not have a directional character. THISYS measurements taken in the directional configuration are directionally dependent.

Measurement direction is identified by the angle along which each specimen was cut from the panel. Specimens for measurements made with bulk THISYS, THASYS and directional THISYS were oriented in the 0°, 45° and 90° as shown in Figure 3.19. Bulk THISYS and THASYS in-plane specimen dimensions measure 70 by 110 mm while directional THISYS specimens measure 22 by 110 mm. Eighteen specimens were cut with a diamond saw from panels 1 through 9 including three bulk THISYS/THASYS specimens for each of the three directions – the same specimens were used for both measurements – and three directional THISYS specimens for each of the three directions. Directional THISYS specimens were cut out of bulk THISYS/THASYS specimens after measurement. A minimum of three measurements were taken for each specimen, for a typical total of 54 measurements for each of these panels. Nine specimens were typically cut from panels 10 through 14 including two bulk THISYS/THASYS specimens and six directional THISYS specimens, two for each direction. Each entry in Table 3.4 is an average of at least three measurements, and as many as twelve measurements depending on the number of specimens used. A typical specimen cut plan is shown in Figure 3.19. Raw experimental data is available in Appendix C.

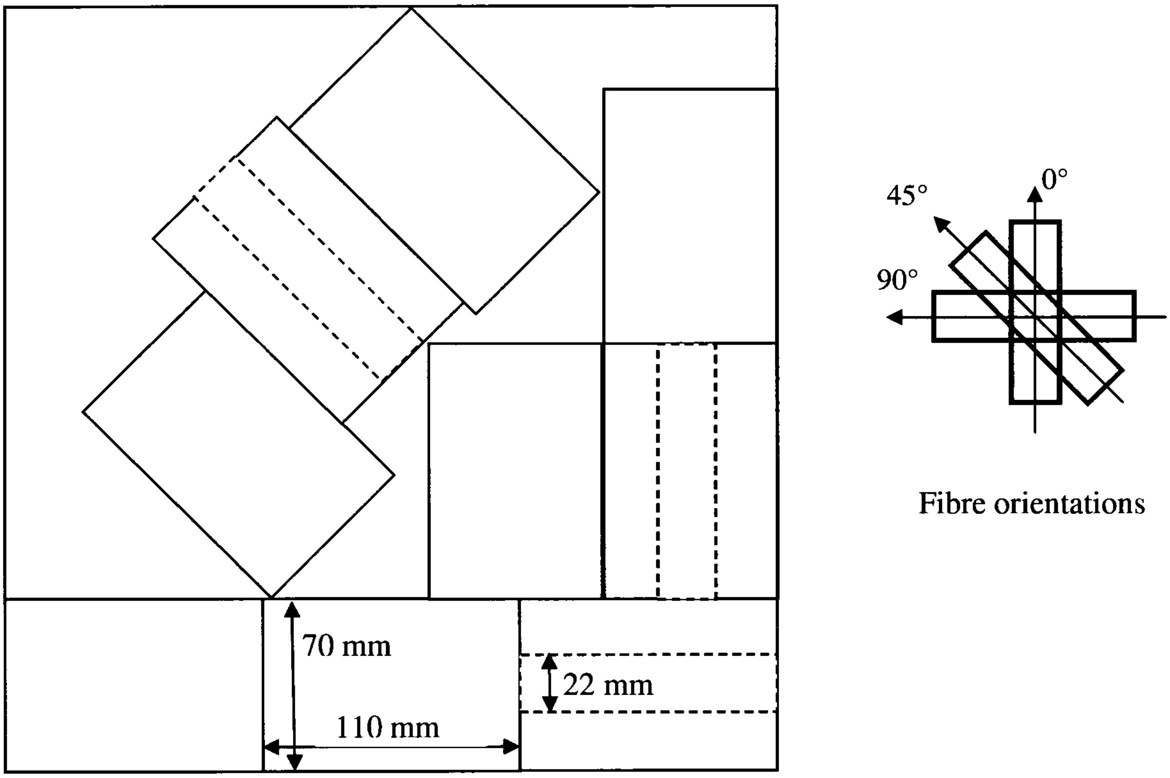

Fibre orientations

Figure 3.19: Typical thermal conductivity specimen cut plan with orientations

Table 3.4: Experimental thermal conductivity results

Panel	Material	Layup Sequence	Thermal Conductivity (W/mK)						
			Standard THISYS			THASYS	Directional THISYS		
			k_x 0°	k_y 90°	k_{45} 45°	k_z	k_x 0°	k_y 90°	k_{45} 45°
1	1	$[0]_6$	3.16 ±0.03	3.10 ±0.15	2.94 ±0.05	0.73 ±0.06	6.40 ±0.30	0.70 ±0.08	2.74 ±0.03
2	1	$[0]_6$	3.15 ±0.07	3.37 ±0.01	3.33 ±0.02	0.81 ±0.04	7.33 ±0.35	0.85 ±0.11	3.25 ±0.12
3	1	$[0/90/0/90]_s$	2.90 ±0.01	3.06 ±0.03	3.00 ±0.10	0.74 ±0.02	3.87 ±0.02	3.73 ±0.06	3.89 ±0.02
4	1	$[0/90/0]_s$	3.18 ±0.03	3.22 ±0.01	3.13 ±0.01	0.74 ±0.01	4.72 ±0.09	2.79 ±0.09	3.52 ±0.06
5	1	$[0/45/-45/90]_s$	3.16 ±0.03	3.12 ±0.03	3.03 ±0.05	0.74 ±0.02	3.50 ±0.12	3.57 ±0.05	3.59 ±0.06
6	1	$[0/30/-30]_s$	3.03 ±0.02	3.05 ±0.01	3.09 ±0.08	0.71 ±0.01	5.43 ±0.02	1.70 ±0.14	3.51 ±0.01
7	2	$[(0/90)]_8$	2.60 ±0.07	2.57 ±0.03	2.51 ±0.04	0.62 ±0.01	2.97 ±0.04	2.97 ±0.04	2.96 ±0.06
8	2	$[(0/90)]_8$	2.56 ±0.04	2.55 ±0.02	2.58 ±0.02	0.60 <0.01	3.04 ±0.02	2.90 ±0.05	2.90 ±0.19
9	2	$[(0/90)/(45/-45)/$ $(45/-45)/(0/90)]_s$	2.42 ±0.03	2.42 ±0.04	2.37 ±0.03	0.58 ±0.01	2.81 ±0.08	2.79 ±0.02	2.74 ±0.04
10	3	$[0]_6$	2.04 <0.01	▨	▨	0.45 <0.01	4.77 ±0.13	▨	▨
11	3	$[0]_6$	2.05 ±0.02	▨	▨	0.46 <0.01	4.95 ±0.07	0.36 <0.01	1.68 <0.01
12	3	$[0/90]_s$	2.27 ±0.01	▨	▨	0.45 <0.01	2.62 ±0.02	2.72 ±0.21	3.04 ±0.14
13	3	$[0/90/0]_s$	2.43 <0.01	▨	▨	0.52 <0.01	3.53 ±0.01	2.03 ±0.03	2.77 ±0.02
14	3	$[0/60/-60]_s$	2.42 ±0.01	▨	▨	0.51 <0.01	2.59 ±0.13	2.81 ±0.03	2.78 ±0.01

For panel 1, made of UD prepreg material 1 laid up as $[0]_6$, through-thickness transverse THASYS measurements of the thermal conductivity average at 0.73 W/mK with a standard deviation of ±0.06 W/mK (±5%). The manufacturer of the device, Hukseflux, suggests that THASYS has an accuracy of ±3%. Bulk in-plane THISYS measurements for panel 1 range from 2.94 W/mK to 3.16 W/mK (7% variation) along 0°, 90°, and 45°directions with a maximum standard deviation of ±0.15 W/mK (±5%). Hukseflux suggests that in its original configuration the THISYS device has an accuracy of ±6%. It should be noted that the bulk THISYS measurements are expected to be equal along all in-plane directions for any given lamination sequence. Directional THISYS in-plane thermal conductivities were measured at 6.40 W/mK, 2.74 W/mK and 0.70 W/mK for the 0°, 45°, and 90° directions respectively. The high degree of dependence on direction is expected for the unidirectional laminate in panel 1. It should be noted that the in-plane transverse directional thermal conductivity across the fibres in the 90° direction at 0.70 W/mK compares well to the through-thickness transverse conductivity at 0.73 W/mK, for a difference of 4%. The in-plane orthotropy ratio k_x / k_y is 9.14for panel 1.

Panel 2, made of UD prepreg material 1 laid-up as $[0]_6$, was manufactured from the same material and has the same lamination sequence as panel 1; both panels are nominally identical. Through-thickness transverse THASYS measurements average at 0.81 W/mK with a standard deviation of ±0.04 W/mK (±5%). This generally compares to the panel 1 average value of 0.73 W/mK for a 10% difference, which can be generally accounted for by standard deviation on both values. Bulk in-plane THISYS measurements for panel 2 range from 3.15 W/mK to 3.37 W/mK (7% variation) with a maximum standard deviation of ±0.07 W/mK

(±2%). The range of all bulk THISYS measured values obtained on unidirectional panels manufactured from UD prepreg material 1 (panels 1 and 2) extends from 2.94 W/mK to 3.37 W/mK (13% variation). For panel 2, directional THISYS in-plane thermal conductivities were measured at 7.33 W/mK, 3.25 W/mK and 0.85 W/mK for the 0°, 45° and 90° directions respectively. Comparing these values with the directional in-plane THISYS thermal conductivity values obtained for panel, 1 the difference between measurements for the 0°, 45°, and 90° directions are 13%, 16% and 18% respectively. Note that for panel 2 the transverse in-plane thermal conductivity across the fibres in the 90° direction at 0.85 W/mK, compares well to the through-thickness transverse conductivity at 0.81 W/mK for a difference of 5%. The in-plane orthotropy ratio k_x / k_y is 8.62 for panel 2 compared to 9.14 for panel 1.

For panel 3 made of UD prepreg material 1 laid-up as $[0/90/0/90]_s$, through-thickness transverse THASYS measurements of the thermal conductivity average at 0.74 W/mK with a standard deviation of ±0.02 W/mK (±3%). This falls within the range of THASYS measurements for panels 1 to 6 manufactured from UD prepreg material 1, which extends from 0.73 W/mK to 0.81 W/mK (10% variation). Bulk in-plane THISYS measurements for panel 3 range from 2.90 W/mK to 3.06 W/mK (5% variation) with a maximum standard deviation of ±0.03 W/mK (±1%). The range of all bulk THISYS measurements obtained for panels 1 to 6 manufactured from UD prepreg material 1 extends from 2.90 W/mK to 3.37 W/mK (14% variation). For panel 3, directional THISYS in-plane thermal conductivities ranged from 3.73W/mK to 3.89 W/mK (4% variation) with a maximum standard deviation of ±0.06 W/mK (±2%). The small in-plane conductivity difference observed for panel 3 was expected due to the panel being thermally quasi-isotropic. A skew in data is seen when comparing in-plane conductivity values obtained from THYSIS in its original and directional configurations; this skew should not be present in theory. A similar skew was observed for panels 5, 7, 8 and 9. No firm explanation was developed for this. In developing the calibration method for the directional measurements based on isotropic materials it was decided to use the THASYS data as reference as this technique is deemed more precise by Hukseflux. The difference observed above may be caused by inequalities in THASYS and THISYS data for the isotropic reference materials, or by a difference in the temperature fields generated in composite samples that are thermally isotropic in their plane only. Extensive results where THASYS and THISYS data are systematically compared for the same isotropic samples were not available from Hukseflux. This aspect of the method and results will require further investigation.

For panel 4 made of UD prepreg material 1 laid-up as $[0/90/0]_s$, through-thickness transverse THASYS measurements of the thermal conductivity average at 0.74 W/mK with a standard deviation of ±0.01 W/mK (±1%). This value falls within the overall range of THASYS measurements for panels manufactured from UD prepreg material 1 (0.73 W/mK to 0.81 W/mK, 10% variation). Bulk in-plane THISYS measurements for panel 4 range from 3.13 W/mK to 3.22 W/mK (3% variation) with a maximum standard deviation of ±0.03 W/mK (±1%). Directional THISYS in-plane thermal conductivities were 4.72 W/mK, 3.44 W/mK and 2.79 W/mK for the 0°, 45° and 90° directions respectively. The difference observed between these in-plane directional measurements was expected since there are twice as many fibres aligned in the 0° direction as there are in the 90 °direction. The in-plane orthotropy ratio k_x / k_y is 1.69 for panel 4, compared to 9.14 and 8.62 for panels 1 and 2 respectively.

For panel 5 made of UD prepreg material 1 laid-up as $[0/45/-45/90]_s$, through-thickness transverse THASYS measurements of the thermal conductivity average at 0.74 W/mK with a standard deviation of ±0.02 W/mK (±3%). This value falls within the range of all THASYS values measured for panels manufactured from UD prepreg material 1, which extends from 0.73 W/mK to 0.81 W/mK. Bulk in-plane THISYS measurements for panel 5 range from 3.03 W/mK to 3.16 W/mK (4% variation) with a maximum standard deviation of ±0.05 W/mK (±2%). These values fall within the overall range of all bulk in-plane THISYS measurements for panels manufactured from UD prepreg material 1, which extends from 2.90 W/mK to 3.37 W/mK. Directional in-plane thermal conductivities measured with THISYS in the directional configuration on panel 5 range from 3.50 W/mK to 3.59 W/mK (3% variation) with a maximum standard deviation of ±0.12 W/mK (±3%). The range of directional THISYS measurements for quasi-isotropic panels 3 and 5 manufactured from UD prepreg material 1 extends from 3.50 W/mK to 3.89 W/mK (10% variation); whilst values generated with the THISYS device are generally consistent for a given measurement technique, the aforementioned skew remains.

For panel 6 made of UD prepreg material 1 laid-up as $[0/30/-30]_s$, through-thickness transverse THASYS measurements of the thermal conductivity average at 0.71 W/mK with a standard deviation of ±0.01 W/mK (±1%). This extends the range of all THASYS values measured for panels 1 to 5 manufactured from UD prepreg material 1, to 0.71 W/mK to 0.81

W/mK (12% variation). Bulk in-plane THISYS measurements for panel 6 range from 3.03 W/mK to 3.09 W/mK (2% variation) with a maximum standard deviation of ±0.08 W/mK (±3%). These values fall within the range of all THISYS measurements for panels manufactured from UD prepreg material 1, which extends from 2.90 W/mK to 3.37 W/mK. Directional in-plane thermal conductivities measured with THISYS on panel 6 were 5.43 W/mK, 3.51 W/mK and 1.70 W/mK for the 0°, 45° and 90° directions respectively. The large degree of dependence of directional thermal conductivity on direction was expected for the laminate. The in-plane orthotropy k_x / k_y ratio is 3.19 for panel 6, compared with 9.14, 8.62 and 1.69 for panels 1, 2 and 4 respectively.

For panel 7 made of plain weave prepreg material 2 laid-up as $[(0/90)]_8$, through-thickness transverse THASYS measurements of the thermal conductivity average 0.62 W/mK with a standard deviation of ±0.01 W/mK (±2%). The average through-thickness transverse thermal conductivity for panel 7 is lower than those of panels 1 through 6 manufactured from UD prepreg tape material 1, even with a difference in V_f of only 0.01. This is believed to originate from a lower transverse thermal conductivity of the T300 fibre used in the reinforcement, with values available in the literature grouped around 0.84 W/mK compared with 2.1 W/mK for the AS4 fibre used in material 1. Whilst crimp in present in the reinforcement of material 2 its influence on through-thickness thermal conductivity is believed to be minor. Bulk in-plane THISYS measurements for panel 7 range from 2.51 W/mK to 2.60 W/mK (3% variation) with a maximum standard deviation of ±0.07 W/mK (±3%). Directional in-plane thermal conductivities measured with THISYS on panel 7 range from 2.96 W/mK to 2.97 W/mK with a maximum standard deviation of ±0.06 W/mK (±2%).

The limited variation in in-plane conductivity is a direct consequence of in-plane quasi-isotropy in the laminate construction. The skew between bulk and directional in-plane measurements can be seen again with this panel.

Panel 8 made of plain weave prepreg material 2 laid-up as $[(0/90)]_8$ is nominally identical to panel 7. Through-thickness transverse THASYS measurements average at 0.60 W/mK with a standard deviation of <±0.01 W/mK. This compares to the average value obtained with panel 7, 0.62 W/mK, for a 3% variation. Bulk in-plane THISYS measurements for panel 8 range from 2.55 W/mK to 2.58 W/mK (1% variation) with a maximum standard deviation of ±0.04 W/mK (±2%); this is within the range of comparable values obtained for panel 7. Directional in-plane thermal conductivities measured with THISYS range from 2.90 W/mK to 3.04 W/mK (5% variation) with a maximum standard deviation of ±0.19 W/mK (±7%). This overlaps comparable values obtained for panel 7, with a wider variation, extending the range of directional THISYS measurements for quasi-isotropic panels manufactured from plain weave prepreg material 2.

For panel 9 made of plain weave prepreg material 2 laid-up as $[(0/90)/(45/-45)/(45/-45)/(0/90)]_s$, through-thickness transverse THASYS measurements of the thermal conductivity average at 0.58 W/mK with a standard deviation of ±0.01 W/mK (±2%), extending the range of these values measured for panels manufactured from material 2 to 0.58 W/mK to 0.62 W/mK for a 6% variation. Bulk in-plane THISYS measurements for panel 9 range from 2.37 W/mK to 2.42 W/mK (2% variation) with a maximum standard deviation of ±0.04 W/mK (±2%). When considering all bulk-in plane THISYS values measured for panels manufactured from plain weave prepreg material 2, this data extends the range to 2.37 W/mK to 2.60 W/mK for a 9% variation. Directional in-plane thermal conductivities measured with THISYS range from 2.74 W/mK to 2.81 W/mK (2% variation) with a maximum standard deviation of ±0.08 W/mK (±3%). When considering all directional in-plane THISYS measurements for panels manufactured from plain weave prepreg material 2, this data extends the range to 2.74 W/mK to 3.04 W/mK for a 10% variation.

For panel 10 made of impregnated UD woven fabric material 3 laid-up as $[0]_6$, through-thickness transverse THASYS measurements of the thermal conductivity average at 0.45 W/mK with a standard deviation of <±0.01 W/mK. The lower through-thickness transverse conductivity compared with that of panels manufactured from materials 1 or 2 is believed to result from the lower V_f of 0.55 for composites made from material 3. Bulk in-plane THISYS measurements for panel 10 in the 0° direction average at 2.04 W/mK with a standard deviation of <±0.01 W/mK. Directional in-plane thermal conductivities measured with THISYS in the 0° direction average at 4.77 W/mK with a standard deviation of ±0.13 W/mK (±3%). Measurements for other directions are not available since the panel size would only allow the preparation of a limited number of specimens.

Panel 11 made of impregnated UD woven fabric material 3 laid-up as $[0]_6$, is nominally identical to panel 10. Through-thickness transverse THASYS measurements of the thermal conductivity average at 0.46 W/mK with a standard deviation of <±0.01 W/mK, extending the range of such values obtained for panels made of UD woven fabric material 3 to 0.45 W/mK to 0.46 W/mK for a 2% difference. Bulk in-plane THISYS measurements for panel 11 in the 0° direction average at 2.05 W/mK with a standard deviation of ±0.02 W/mK (±1%); again the value is very similar to that obtained for panel 10, with a difference of <1%. Directional in-plane thermal conductivities measured with THISYS were 4.95 W/mK, 1.68 W/mK and 0.36 W/mK for the 0°, 45° and 90° directions respectively. The high degree of dependence on direction was expected for the unidirectional laminate. Panel 11 orthotropy ratio k_x / k_y was 13.75, larger than similar ratios recorded with any other panel investigated in this work. It should be noted that the in-plane thermal conductivity across the fibres in the 90° direction, at 0.36 W/mK, is significantly lower than the through-thickness transverse thermal conductivity at 0.46 W/mK (22% variation). This difference is thought to result from the presence of in-plane inter-yarn gaps that are larger than the through-thickness ones as confirmed by microscopy. The 0° in-plane measurement of 4.95 W/mK for panel 11 can be compared to the similar measurement made on panel 10, at 4.77 W/mK (4% variation).

For panel 12 made of impregnated UD woven fabric material 3 laid-up as $[0/90]_s$, through-thickness transverse THASYS measurements average at 0.45 W/mK with a standard deviation of <±0.01 W/mK. The value is very close to those recorded for panels 10 and 11. Bulk in-plane THISYS measurements for panel 12 along the 0° direction average at 2.27 W/mK with a standard deviation of ±0.02 W/mK (±1%), extending the range of similar values for panels made of UD woven fabric material 3 to 2.04 W/mK to 2.27 W/mK (10% variation). Directional in-plane thermal conductivities measured with THISYS measurements for thermally quasi-isotropic panel 12 range from 2.62 to 3.04 W/mK (14% variation) with a maximum standard deviation of ±0.07 W/mK (±1%).

For panel 13 made of impregnated UD woven fabric material 3 laid-up as $[0/90/0]_S$, through-thickness transverse THASYS measurements average at 0.52 W/mK with a standard deviation of <±0.01 W/mK. Considering the above THASYS measurements reported for panels made of UD woven fabric material 3, this extends the range 0.45 W/mK to 0.52 W/mK for a 13% variation. Bulk in-plane THISYS measurements made along the 0° direction average at 2.43 W/mK with a standard deviation of <0.01 W/mK. Directional in-plane thermal conductivity THISYS measurements were 3.53 W/mK, 2.77 W/mK and 2.03 W/mK along the 0°, 45° and 90° directions respectively. The dependence of these values on direction was expected for the non-quasi isotropic laminate. The orthotropy ratio k_x / k_y was 1.74 for panel 13.

For panel 14 made of impregnated UD woven fabric material 3 laid-up as $[0/60/-60]_S$, T through-thickness transverse THASYS measurements average at 0.51 W/mK with a standard deviation of <±0.01 W/mK. When considering all THASYS measurements conducted on panels made of UD woven fabric material 3, the range extends from 0.45 W/mK to 0.52 W/mK (13% variation). Bulk in-plane THISYS measurements along the 0° direction average at 2.42 W/mK with a standard deviation of ±0.01 W/mK (<1%). Directional in-plane THISYS measurements for quasi-isotropic panel 14 range from 2.59 W/mK to 2.81 W/mK (8% variation) with a maximum standard deviation of ±0.13 W/mK (±5%). When considering all directional THISYS measurements of quasi-isotropic panels manufactured from UD woven fabric material 3, the range of in-plane directional thermal conductivity values goes from 2.59 W/mK to 3.04 W/mK (15% variation).

Conductivity values presented in Table 3.4 are generally close to those of polymers when compared with the conductivity of materials such as copper at 415 W/mK [56] and CVD carbon fibres at 1100 W/mK along the axial direction [2, 4]. Values measured along the fibres in unidirectional laminates are also relatively low as carbon fibres AS4 and T300 are aimed at structural applications rather than heat transfer management.

In-plane thermal conductivity data for panels 1 and 2 show that directional THYSIS measurements clearly captured the thermal orthotropy of the laminates. Orthotropy ratios of approximately 9 are generally in line with those reported for fibres similar to those used. The variability of in-plane thermal conductivity values recorded for individual panels is largest for k_y at 11% and 13%; this is in line with published values from chapter 2. Other values of the variability obtained in this work range from 1.0% to 4.7%, indicating very good data reproducibility. Overlap of in-plane transverse and through-thickness transverse conductivities k_y and k_z is excellent for both panels 1 and 2 as expected of tape prepreg material 1; variability is larger in data obtained from THISYS, and more so for the directional configuration. Directional values of k_x and k_{45} recorded for panels 1 and 2 do not overlap. Similarly, the in-plane data measured with THYSIS in its original configuration tends not to overlap for the two panels. Differences in in-plane thermal conductivity results for these laminates result from the panels rather than from THYSIS, as explained by the average thicknesses measured for panels 1 and 2 at 1.501 mm and 1.439 mm respectively: the differences between the experimental values obtained for both panels result from variations in V_f between the panels.

Panels 3 and 5 are thermally isotropic in their plane as shown by the in-plane directional thermal conductivity values; this was expected from the laminating sequence. Low variability is seen both in-plane and through the thickness at less than 3.5%. In-plane directional conductivity values are consistently larger for panel 3 with no overlap of directional in-plane conductivity ranges between both panels. This result, also seen with panels 1 and 2, is surprising for this material and manufacturing route; better reproducibility was expected from panel to panel. Panel 4 shows a higher thermal conductivity along the 0° direction as expected from its laminating sequence; k_x measured for panel 4 is larger than the directional conductivity of panels 3 and 5, while k_y is smaller. Variability remains low with panel 4. Panel 6 also shows higher conductivity along the 0° direction as expected; k_x measured on panel 6 is larger than that of panel 4 while k_{45} is in line with the in-plane conductivity values measured on the panels that are thermally quasi-isotropic. As expected from the laminating sequences, panel 6 shows the lowest in-plane thermal conductivity along k_y compared to all other in-plane values apart from the in-plane directional value of k_y for the unidirectional panels 1 and 2. All trends predicted for panels made of tape prepreg material 1 were confirmed by the experimental data; differences observed between panels 1 and 2, and between 3 and 5, were unexpected. Also, the skew in data between the bulk in-plane and directional in-plane data for panels that are thermally quasi-isotropic in their plane was unexpected.

Directional in-plane conductivity data for panels 7 to 9 indicate isotropy. The variability of these in-plane results is largest at 7% and lower than 2% in most cases. However, differences between the lower and higher average values for the different laminates are close to 10%. All values measured using THISYS in its original configuration are lower than directional values as mentioned previously. Thermal conductivity values for in-plane thermally isotropic panels 7 to 9 are only marginally larger than those recorded for panels 12 and 14 made of the same fibres, despite their larger V_f. This unexpected finding may result from fibre waviness in material 2; differences in the thermal conductivity of resins, which strongly affects the result, may also constitute an explanation. Other than the aforementioned skew in in-plane data all results obtained with panels made of material 2 confirm the trends predictable from analysis.

Directional in-plane thermal conductivity values recorded for panel 11 show in-plane orthotropy as expected. The in-plane longitudinal to in-plane transverse orthotropy ratio is larger than the in-plane longitudinal to through-thickness transverse orthotropy ratio as a result of horizontal inter-yarn gaps being larger than vertical inter-yarn gaps, Figure 3.18. This is reflected by larger values of the through-thickness transverse conductivity k_z compared with the in-plane transverse values k_y. Directional in-plane thermal conductivity values obtained from THISYS for panels 12 and 14 do not reflect perfect thermal isotropy; this may be a consequence of the less reproducible materials and manufacturing route used for producing panels made of material 3. Panel 14 is essentially isotropic in the plane as expected. Variability is limited, ranging from less than 0.1% to 8%. All conductivity values are lower than those measured for material 1 as expected from the lower V_f. The orthotropy ratios of panel 13 and panel 4 are almost equal, and both panels have the same laminating sequence.

Through-thickness transverse thermal conductivity data measured using THASYS shows low variability. For each material, most variability ranges overlap though differences are observed in cases such as panel 2 as a result of thickness fluctuations. Transverse conductivity values were largest for material 1, followed by material 2 and material 3 in a trend similar to decreasing V_f values.

Experimental data show that variability in thermal conductivity for composites can range from less than 1% to more than 10%. In-plane and through-thickness transverse conductivity values can differ significantly depending on reinforcement type. The results also show that THISYS allows quantification of the directional conductivity.

4 Modelling

The general goal of the modelling work undertaken in this thesis was to explore and develop a capability for predicting values of the directional in-plane and through-thickness transverse thermal conductivity k_{ci} and k_z of composite materials. In the wider context where one needs thermal conductivity data say for the design of a mould, such predictions may be used on their own or as complement to a limited array of experimental values. Beyond predicted values, the work reported here also aimed at documenting the process, effort and level of information needed as well as the variability of predicted values, in order to gauge the practical applicability of the capability. Different methods were evaluated towards these aims. A number of closed form models exist for predicting thermal conductivity values of homogeneous unidirectional composites [23, 62]. Analytical methods applicable to textile-reinforced composites are also reported in the open literature but these were not subjected to extensive analysis or applied to practical design cases.

This chapter features prediction methods applied to domains representative of the materials discussed in chapter 3. In contrast to material 1, one major feature of materials 2 and 3 is the presence of a reinforcement architecture resulting from the weaving of distinct yarns. Material 1 can be regarded as homogeneous with a fibre volume fraction V_f that is generally constant over representative volumes with characteristic dimensions equal to a few fibre diameters. The same can be said of the individual yarns woven into reinforcements for materials 2 and 3. On the other hand materials 2 and 3 are heterogeneous with marked fluctuations in V_f in the resin-rich zones – or inter-yarn gaps – extending between the yarns. In this work the classical lamination theory (CLT) and models of the thermal conductivity applicable to homogeneous composites were used in determining the thermal conductivity of tape prepreg laminates and impregnated textile yarns. Unit-cell simulations of heat transfer in textile-based composites were developed to quantify the effect of changes in reinforcement architecture – or geometry – on thermal conductivity. Steady-state finite element simulations were conducted for non-crimped and crimped woven textile reinforced composites as described below. Comparisons are made with the results of experimental measurements presented in chapter 3. This chapter concludes with a discussion of the applicability of different modelling methods for predicting the thermal conductivity of composite materials.

4.1 Modelling Tape Prepreg Using the Classical Lamination Theory

The CLT was used for modelling the thermal conductivity of panels 1 to 6 manufactured with homogeneous tape prepreg material 1, Table 3.3. The conductivity along any specific direction, such as k_x for the 0° direction, can be calculated from the laminate thickness $2h$, ply thickness t_i , ply conductivity along and across the fibres k_{fa} and k_{ft}, and ply orientations θ_i in the lamination sequence using eqn 2.4 [53].

Because of poor consistency in published axial thermal conductivity data and general lack of radial thermal conductivity data for AS4 fibres produced by Hexcel, properties for the fibres were calculated from experimental data measured on panel 1 $[0]_6$ using the rule of mixtures by volume (ROMv), eqn 2.1 [53] and Clayton's model for aligned fibres, eqn 2.2 [47]. The fibre volume fraction V_f for panels made from tape prepreg material 1 was 0.62 and k_m was set at 0.2 W/mK. From these calculations the axial and radial conductivity values k_{fa} and k_{ft} of AS4 fibre were determined as10.2 W/mK and 2.1 W/mK respectively.

Measurements made on panel 2 $[0]_6$ are directly comparable to those made on panel 1. Values of in-plane thermal conductivities k_x, k_y, and k_{45} for panel 2 are 7.33 W/mK, 0.85 W/mK and 3.25 W/mK respectively compared to 6.40 W/mK, 0.70 W/mK and 2.74 W/mK for panel 1 – differences of 13%, 18% and 16%. Causes for these differences, seen with highly reproducible material and manufacturing methods, were discussed in chapter 3; they represent the largest variability observed with thermal conductivity measurements. Prediction of k_{cd} was performed for other tape prepreg lamination sequences. The CLT predicts a quasi-isotropic k_{cd} value of 3.56 W/mK that can be compared with experimental measurements made on panels 3 and 5. Panel 3 with lamination sequence $[0/90/0/90]_s$ returned experimental values of 3.87 ± 0.02 W/mK, 3.73 ± 0.06 W/mK and 3.89 ± 0.02 W/mK along the 0°, 90° and 45° directions respectively, for a largest difference of 8% compared to the CLT. Panel 5 with lamination sequence $[0/45/-45/90]_s$ returned experimental values of 3.5 ± 0.12 W/mK, 3.57 ± 0.05 W/mK and 3.59 ± 0.06 W/mK along the 0°, 90° and 45° directions respectively for a largest difference of 2% compared to the CLT. The calculated thermal conductivity values k_x, k_y, and k_{45} for panel 4 with lamination sequence $[0/90/0]_s$ were 4.51 W/mK, 2.62 W/mK and 3.56 W/mK respectively. These CLT predictions can be compared with experimental measurements of 4.72 ± 0.09 W/mK, 2.75 ± 0.09 W/mK and 3.52 ± 0.06 W/mK along the 0°, 90°, and 45° directions respectively for a largest difference of 6%. For panel 6 with lamination sequence $[0/30/-30]_s$ the CLT predicts values of 5.45 W/mK, 1.67 W/mK and 3.56 W/mK for k_x, k_y, and k_{45} compared to measured values of 5.43 ± 0.02 W/mK, 1.70 ± 0.14 W/mK and 3.51 ± 0.01 W/mK along the 0°, 90°, and 45° directions respectively, for a largest difference of 2%.

The above CLT modelling data for AS4/3501-6 tape prepreg material 1 is summarised in Table 4.1 where the reference values used for calculating the fibre conductivities are bracketed. A 23% difference was observed between the predicted and measured values of k_{45} for panel 1. For panel 2 the same difference was only 9%, again highlighting differences between nominally similar laminates. With the exception of the k_{45} value for panel 1 the maximum difference between experimental measurements and CLT predictions is 16%, which is of the same order of magnitude as the experimental variability on conductivity seen for the same panels. Possible sources of error include minute deviations from directions stated in the laminating sequence and specimen cutting orientations, as well as similar deviations arising upon the installation of specimens into the THISYS device.

Table 4.1: CLT modelling summary for AS4/3501-6 tape prepreg material 1

		Thermal conductivity (W/mK)					
		Directional THISYS			Classical lamination theory		
Panel	Layup	k_x 0° st. dev.	k_y 90° st. dev.	k_{45} 45° st. dev.	k_x 0° % diff.	k_y 90° % diff.	k_{45} 45° % diff.
1	$[0]_6$	(6.40)	(0.70)	2.74	-	-	3.56
		±0.30	±0.08	±0.03			-23%
2	$[0]_6$	7.33	0.85	3.25	6.40	0.73	3.56
		±0.35	±0.11	±0.12	15%	16%	-9%
3	$[0/90/90/0]_S$	3.87	3.73	3.89	3.56	3.56	3.56
		±0.02	±0.06	±0.02	9%	5%	9%
4	$[0/90/0]_S$	4.72	2.79	3.52	4.51	2.62	3.56
		±0.09	±0.09	±0.12	5%	6%	-1%
5	$[0/45/-45/90]_S$	3.50	3.57	3.59	3.56	3.56	3.56
		±0.12	±0.05	±0.06	-2%	<1%	1%
6	$[0/30/-30]_S$	5.43	1.70	3.51	5.45	1.67	3.56
		±0.02	±0.14	±0.01	<1%	2%	-1%

With the exception of k_{45} for Panel 1, agreement between CLT predictions and experimental data is within expected limits for material 1. Differences between corresponding predicted and measured values are comparable to the variability of experimental results, and with variability levels reported in the literature for thermal conductivity data measured on polymer composites. The use of CLT is appropriate in the case of tape prepreg material 1, which is homogeneous. Heterogeneity issues such as yarn crimp, the nesting of neighbouring textile layers or the presence of lateral and through-thickness inter-yarn gaps preclude the use of reverse calculation, the ROMv and of the CLT for materials 2 and 3. The modelling of these materials is reported in the following sections.

4.2 Finite Element Modelling of Textile Composites: Overview

Finite element models of generic textile composite unit cells were developed as a predictive tool for the assessment of directional thermal conductivity as a function of reinforcement geometry and constituent properties. The following is an overview of the model development plan for this thesis.

Unidirectional textile modelling was performed in three separate stages. In stage 1 initial unidirectional modelling efforts focused on the development of a generic three-dimensional meso-scale composite unit cell model consisting of two layers of parallel non-crimp yarns in an epoxy matrix. In iteration 1 a total of nine full yarn crossovers were modelled. The objective was to develop a geometric modelling approach as well as to assess boundary conditions. The model featured unrealistically large inter-yarn gaps to simplify meshing. The mesh density was constant throughout the domain of each model. A convergence study determined appropriate element size for the meso-scale thermal analysis.

For iteration 2 the unidirectional textile model was refined with realistic reinforcement geometry parameters based on values from literature. Variable mesh densities were introduced where larger elements were located in the center of the yarn section and became progressively smaller towards the edge where the smallest elements were located in the inter-yarn gaps. The variable mesh density successfully reduced the number of elements required. A convergence study was performed to assess discretization error associated with the new mesh and geometry. The refined geometry with smaller inter-yarn gaps resulted in an expected increase of k_z compared to the initial unidirectional model. Time and processing resources to run the simulations were deemed unacceptably high.

In iteration 3 further unidirectional textile model refinement consisted of modeling ¼ of a yarn crossover rather than nine complete crossovers previously modelled. A convergence study was performed with multiple meshes which revealed the same k_z results compared to the nine crossover model while simulation solving time was reduced from hours to minutes.

Stage 2 of the unidirectional textile modelling consisted of a parametric study varying V_f. Varying reinforcement geometry was shown to have a clear effect on k_z values. Models and results were presented at the Sixth Joint Canada-Japan Workshop on Composites, August 2006 [63].

Stage 3 consisted of a parametric study with constant V_f. The objective was to investigate the variability in k_z as well as k_{ci} caused by subtle changes in reinforcement geometry while maintaining a constant V_f. Reinforcement geometry and material properties were based on measured values. Results were compared to experimental data where variability was consistent with expectations based on literature. Models and results were presented at the 9th International Conference on Textile Composites, October 2008 [64].

Woven textile modelling was performed in two separate stages. In stage 1 initial woven modelling efforts focused on the development of geometric models of plain weaves that were as similar as possible to the unidirectional modelling work so that the effect of weaving could be clearly distinguished. Models containing four quarters of crossovers were created. The objective of iteration 1 was to demonstrate the capability of assigning local orientation to yarn elements which was required to model the orthotropic material.

Iteration 2 sought to model more realistic geometry. A study was performed to analyze the effect of section change due to crimp. Yarns were assigned three different cross sections which became progressively thinner towards the area of maximum crimp. The results demonstrate a clear effect of crimp on k_z.

In iteration 3 a parametric study included the same parameters as those examined during the unidirectional model development stage 2. The models successfully demonstrated the geometric modeling approach for woven textile reinforcements and again highlighted that reinforcement geometry has an effect on k_z in addition to constituent material properties and

V_f. Results were presented at the 8th International Conference on Textile Composites, October 2006 [65].

Stage 3 of the woven model development sought to generate more realistic reinforcement geometry based on measured values from experimental materials. Models featured plain weave textiles at $[0°/90°]_n$ and [0°/+45°/-45°/90°]. Values for k_{ci} as well as k_z were predicted. Modelling constant vertical inter-yarn gaps at all crossover points maximized nominal unit cell fibre volume fraction. The method resulted in resin rich zones which were addressed by creating models where single layers of reinforcements were cut through their horizontal mid-plane to increase the overall V_f of the unit cell. The results demonstrated expected trends and were compared to experimental data. Models and results were presented at the 9th International Conference on Textile Composites, October 2008 [64].

4.3 Non-Interlaced Reinforcements Stage 1: Convergence Studies

The first stage of work on modelling non-interlaced reinforcements consisted in convergence studies performed in a cycle of three iterations.

4.3.1 Non-Interlaced, Stage 1, Iteration 1

In iteration 1, 4 models featuring 6 identical resin-saturated straight yarns with constant cross-sections were laid in 2 layers of 3 parallel yarns oriented at 0° and 90°, Figure 4.1. The yarns were separated by void-free resin-rich zones in the horizontal and vertical directions;

no attempt at modelling contact and nesting was made. Each model featured 9 yarn resin-rich crossovers. The geometry detailed below did not change from model to model; it features unrealistically large inter-yarn gaps to ease the initial attempts at meshing these zones undertaken in iteration 1. Mesh density was uniform in each model but varied between models with the aim of assessing numerical convergence on through-thickness transverse thermal conductivity for this first case.

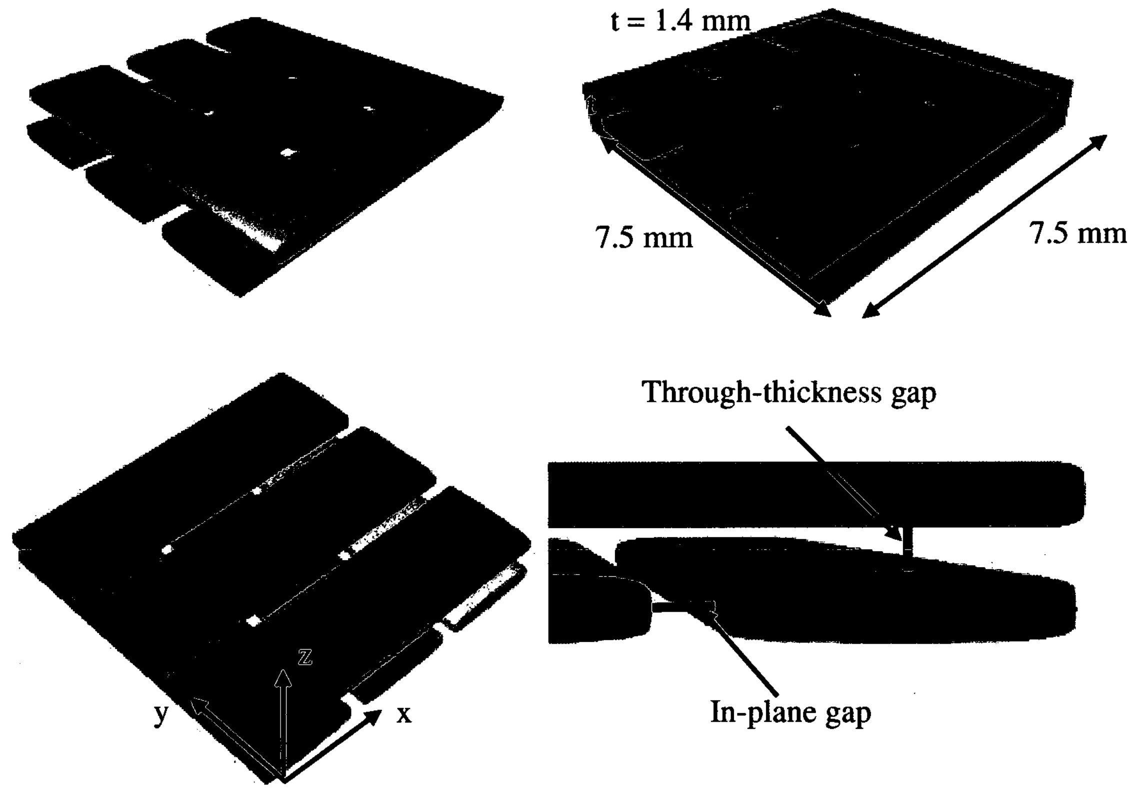

Figure 4.1: Non-interlaced reinforcements, stage 1, iteration 1

Yarn cross-sections were modelled as hyperellipses in the local x-y section plane, where y is perpendicular to the plane of the fabric:

$$y = \pm\left(1 - \frac{x^2}{a^2}\right)^n \qquad (4.1)$$

where a and n are constants. Values of power n lower than 0.5 indicate a fuller section closer to a square; a is the aspect ratio of yarn width to height. Yarns had a major radius of 1 mm and a minor radius of 0.2 mm, corresponding to yarn dimensions of material 3. Power n was set at 0.3. The minimum heights of in-plane and through-thickness inter-yarns gaps were 0.5 mm and 0.2 mm respectively. The domain measured 7.5 mm by 7.5 mm by 1.4 mm with yarns positioned symmetrically in the unit-cell. TexGen 2 was used for creating the geometric unit-cell models [66] and Gambit™ 2.2.30, the pre-processor to the computational fluid dynamics (CFD) code Fluent™ 6.2.16 [67], was used for meshing. All meshes featured 4-noded linear tetrahedral elements.

Boundary conditions replicating experimental THASYS through-thickness measurements were defined. Uniform temperatures were imposed on the upper and lower boundaries of the unit-cell models whilst heat flow through the lateral faces was set to zero. Temperatures were specified at all nodes located on the upper and lower boundaries. Side walls were forced adiabatic. An average through-thickness heat flux was determined through simulation and used in calculating k_z based on Fourier's law, eqn. 2.12. Contact resistance between fibres and resin was not modelled as justified from section 2.2 of this thesis.

Carbon/epoxy yarns were modelled as isotropic materials in this first iteration, using the transverse properties of yarns of AS4 fibres as provided by Hexcel. The fibre and resin thermal conductivities k_{ft} and k_m were set at 1.19 W/mK and 0.25 W/mK respectively. Yarn conductivity k_{yt} was calculated using the parallel rule of mixtures by volume (pROMv) with a typical yarn fibre volume fraction V_{fy} assumed at 0.75. The relation between the yarn fibre volume fraction V_{fy}, unit cell fibre volume fraction V_f and actual fibre volume fraction in material 3 was not queried in iteration 1 as the inter-yarn gaps were kept intentionally large to ease meshing.

Meshes were converted to MSC Patran™ [68] neutral files using code written by the author for this project. Material properties and boundary conditions were defined in MSC Patran™ and simulations were performed in MSC Nastran™ [69]. The effect of temperature on thermal conductivity was neglected in the steady-state simulations. Results of a convergence studies on through-thickness transverse thermal conductivity k_z for unit-cells featuring large inter-yarn gaps appear in Table 4.2. The typical element side length is based on the smallest elements that are located in the through thickness yarn gaps. A large difference between the transverse conductivity of the yarns k_{yt} and the through-thickness transverse conductivity of the composite k_z was observed, indicating the need for meso-scale modelling.

Table 4.2: Convergence study results for non-interlaced reinforcements, stage 1, iteration 1.

Mesh	Number of elements (thousands)	Through-thickness transverse thermal conductivity (W/mK)
NI S1 I1-1	426	0.4133
NI S1 I1-2	608	0.4138
NI S1 I1-3	715	0.4139
NI S1 I1-4	1 221	0.4139

4.3.2 Non-Interlaced, Stage 1, Iteration 2

A second modelling iteration was conducted where the unit-cell geometry was made more faithful to the actual reinforcement by reducing the in-plane and through-thickness inter-yarn gaps to typical dimensions. A single geometry was produced for reasons stated below. The geometry featured 6 straight yarns laid in two superimposed layers oriented at 0° and 90° as seen in iteration 1. Material properties, boundary conditions and the constant yarn cross-section were unchanged. In-plane inter-yarn gaps were set as a ratio of yarn width to inter-yarn gap of 15:1 and through-thickness transverse inter-yarn gaps were set as a ratio of yarn thickness to inter-yarn gap of 20:1. These ratios lead to in-plane and through-thickness transverse inter-yarn gaps of 0.133 mm and 0.020 mm respectively, the latter being equivalent to 3 typical carbon fibre diameters. Mesh density was constant throughout the model. The mesh appears in Figure 4.2; a temperature plot and a heat flux magnitude plot are presented in Figures 4.3 and 4.4. It can be observed that the distribution of heat flux magnitude at each crossover takes an elongated pattern along the direction of the yarns, despite the fact that these are modelled as isotropic with an underestimated axial conductivity. This results from the yarn cross-section shape and associated increasing thickness of the transverse through-thickness resin gaps when measured from the yarn centreline and towards its edges.

A convergence study was performed on 6 meshes labelled NI S1 I2-1 to NI S1 I2-6, Table 4.3. Meshes NI S1 I2-1 to NI S1 I2-3 had uniform mesh density throughout the domain while meshes NI S1 I2-4 to NI S1 I2-6 featured larger elements inside the yarns; the largest element density and smallest elements were located in zones of greatest temperature gradient, namely the inter-yarn resin gaps. Lower temperature gradients were found in the yarn interiors.

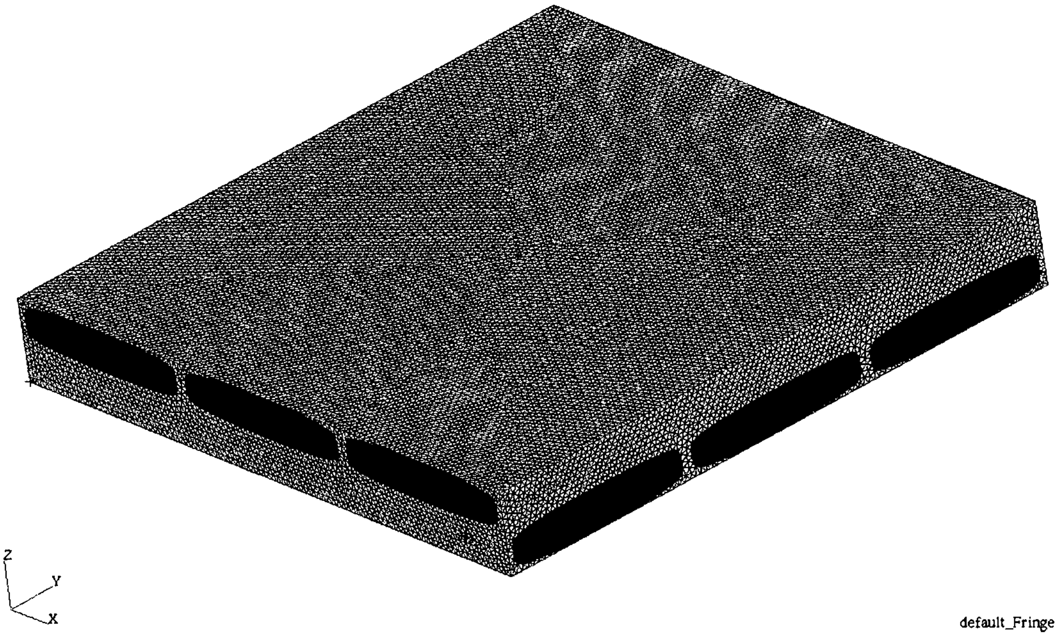

Figure 4.2: Non-interlaced reinforcements, stage 1, iteration 2: mesh

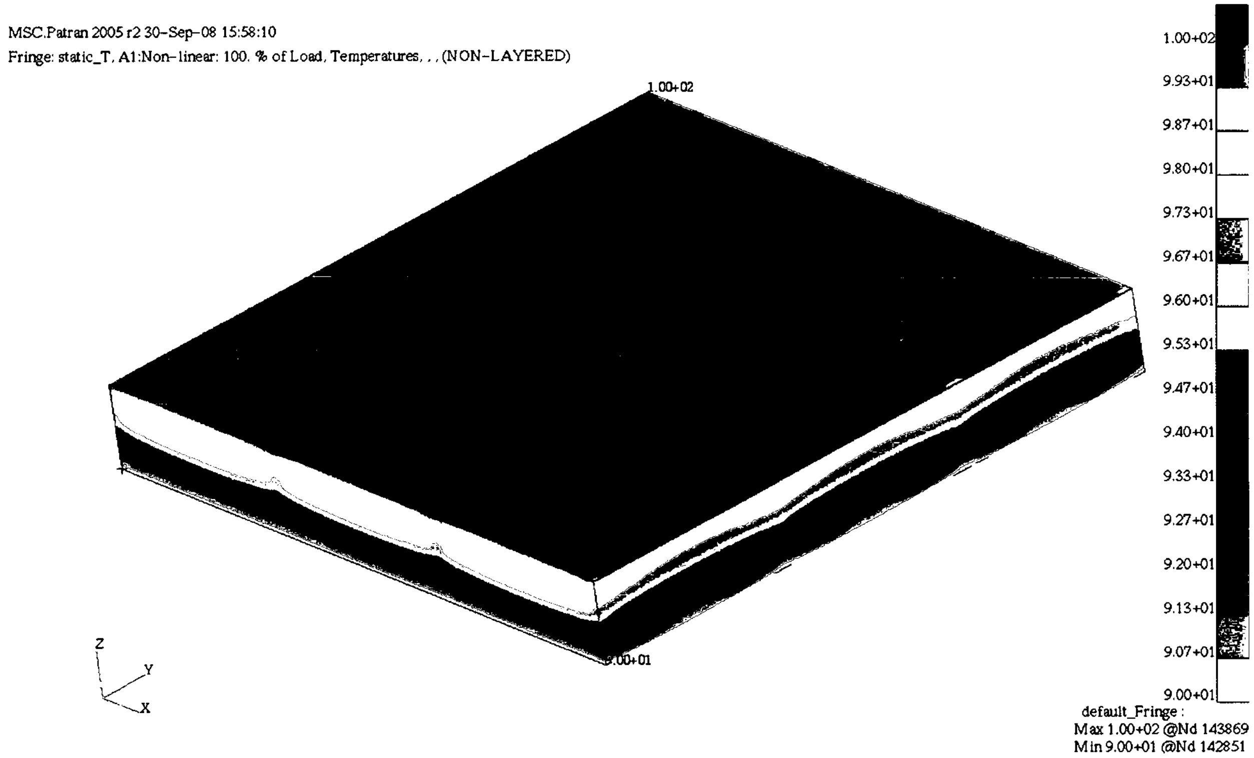

Figure 4.3: Non-interlaced reinforcements, stage 1, iteration 2: temperature distribution (°C)

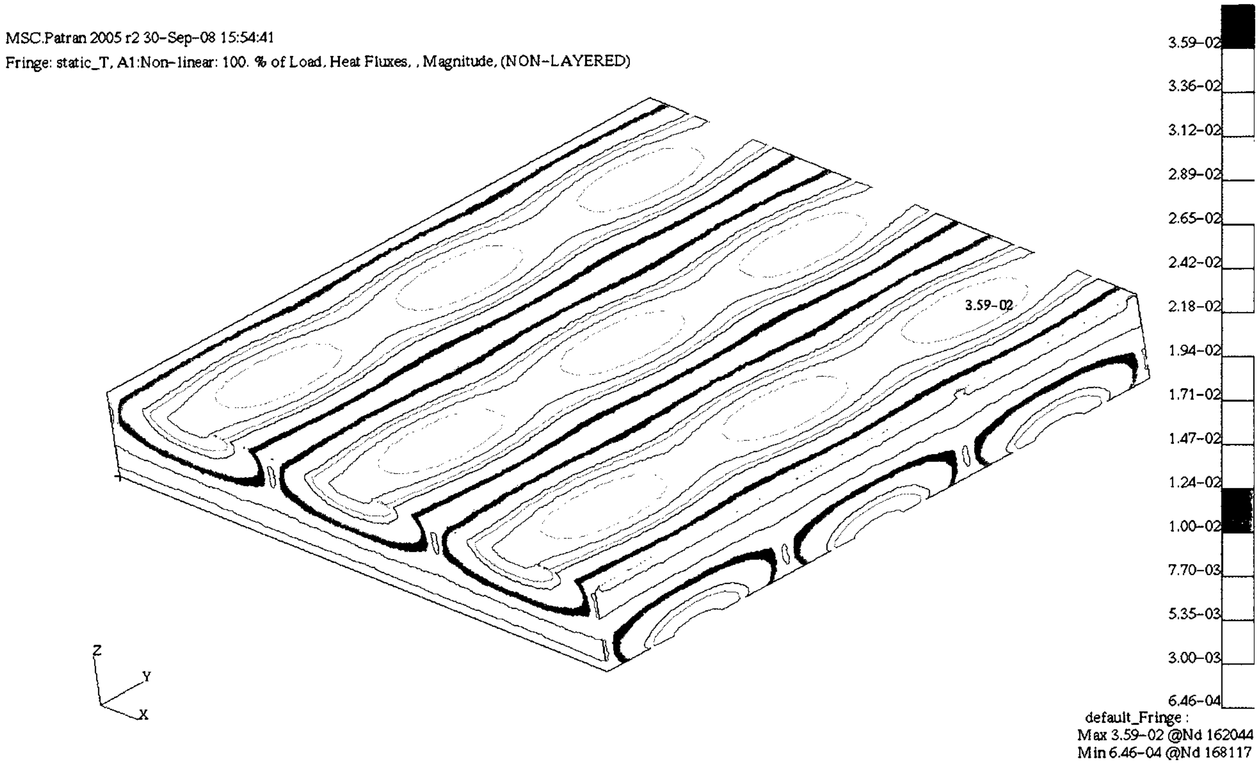

Figure 4.4: Non-interlaced reinforcements, stage 1, iteration 2: heat flux (W/mm^2)

Table 4.3: Convergence study results for non-interlaced reinforcements, stage 1, iteration 2

Mesh	Typical element side length (mm)	Number of elements (thousands)	Through-thickness transverse thermal conductivity (W/mK)
NI S1 I2-1	0.070	843	0.504
NI S1 I2-2	0.060	838	0.542
NI S1 I2-3	0.050	1840	0.506
NI S1 I2-4	0.045	1313	0.505
NI S1 I2-5	0.040	1696	0.506
NI S1 I2-6	0.035	2233	0.506

Based on the values of k_z shown in Table 4.3 the element size used in mesh NI S1 I2-3 was deemed appropriate. Meshes NI S1 I2-1 and NI S1 I2-2 were considered inadmissible as they featured a large number of skewed elements in the through-thickness yarn gaps. Coarser meshes would not be viable for the same reason. Meshes NI S1 I2-4 to NI S1 I2-6 demonstrated the possibility of using fewer elements by reducing the mesh density in zones of small gradients. When compared with iteration 1, the results of iteration 2 indicate that the models are capable of detecting changes in reinforcement geometry as they predicted the increase in k_z expected of a decrease in through-thickness transverse inter-yarn gaps.

At this stage of model development the general correspondence of simulated and measured values was probed for the first time for through-thickness conductivity; this was not attempted with iteration 1 as inter-yarn gaps were unrealistically large in that case. Samples as described in chapter 3 were cut from a CFRP plate laminated from Hexcel's Hexply 6376 unidirectional prepreg tape (Appendix B) laid as $[0/90]_{22}$. The laminate was cured in an autoclave at 177°C and 689 kPa for 130 minutes as recommended by Hexcel. Two samples were sent to Hukseflux, supplier of the thermal conductivity measurement devices described in chapter 3, for evaluation of this equipment. The values of k_z measured by Hukseflux were 0.56 and 0.60 W/mK at 20°C. The 7% difference between these measurements was within the expected variability limits discussed in chapter 3. These results are not directly comparable to those of simulations performed in iteration 2 as the materials differed. However, the lower simulated value of 0.506 W/mK was deemed encouraging in view of the resin-rich zones present the simulated materials. The simulated results were also compared to previous data generated at NRC-IAR in the context of Duval's thesis [70] on modelling heat transfer through composite tooling. The experimentally measured through-thickness thermal conductivity of CFRPs made of 2/2 twill carbon fabric prepreg LT 33 CFO 700T manufactured by ACG (Advanced Composites Group) was reported at 0.57 W/mK. Nature of constituent materials withstanding, a value higher than that obtained for the unidirectional composite is explained by the interlacing of yarns in the reinforcement. Finally, the early simulation value of 0.506 W/mK obtained in iteration 2 can be compared in retrospect to the experimental data presented in chapter 3. Panels 10 through 14, made from a non-interlaced reinforcement, returned measured values of k_z ranging from 0.45 to 0.52 W/mK.

Iteration 2 returned promising values of the through-transverse conductivity. However, resources and CPU time required to run the simulation were deemed unacceptable. A third modelling iteration was conducted, aiming at reducing requirements for processing resources.

4.3.3 Non-Interlaced, Stage 1, Iteration 3

The third iteration took advantage of symmetry. Model extents were reduced from covering nine full yarn crossovers to one quarter of a single crossover as illustrated in Figure 4.5 where resin elements appear in red and yarn elements in white. Only half of each yarn cross-section was modelled; the geometry was otherwise unchanged from that used in iteration 2. The single geometry produced for iteration 3 was meshed with seven densities as listed in Table 4.4. The variable mesh density introduced in iteration 2 was featured in all meshes created for iteration 3, as shown in Figure 4.5. Based on the results shown in Table 4.4, the element size associated with mesh NI S1 I3-4 leading to a value of the through-thickness transverse conductivity of 0.505 W/mK was selected. Good agreement with solutions obtained in nine-crossover iteration 2 was observed. The reduced domain cut computing time from hours to minutes for the mesh selected.

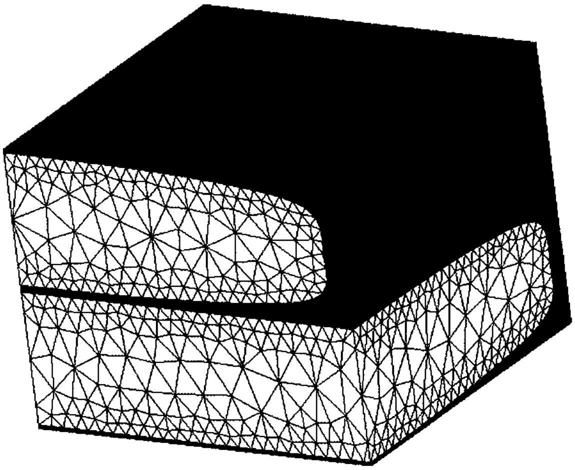

Figure 4.5: Non-interlaced reinforcements, stage 1, iteration 3: mesh

Table 4.4: Convergence study results for non-interlaced reinforcement, stage 1, iteration 3

Mesh	Typical element side length (mm)	Number of elements (thousands)	Through-thickness transverse thermal conductivity (W/mK)
NI S1 I3-1	0.050	32	0.502
NI S1 I3-2	0.045	40	0.505
NI S1 I3-3	0.040	54	0.503
NI S1 I3-4	0.035	69	0.505
NI S1 I3-5	0.030	93	0.505
NI S1 I3-6	0.025	141	0.506
NI S1 I3-7	0.020	251	0.505

Heat flux magnitude in the iteration model 3, mesh NI S1 I3-4 is shown in Figure 4.6. Temperature gradients in the same model, shown in Figure 4.7, further demonstrate the rationale for meshing the inter-yarn gaps with maximum element density while decreasing the mesh density inside the yarns, where these gradients are smallest.

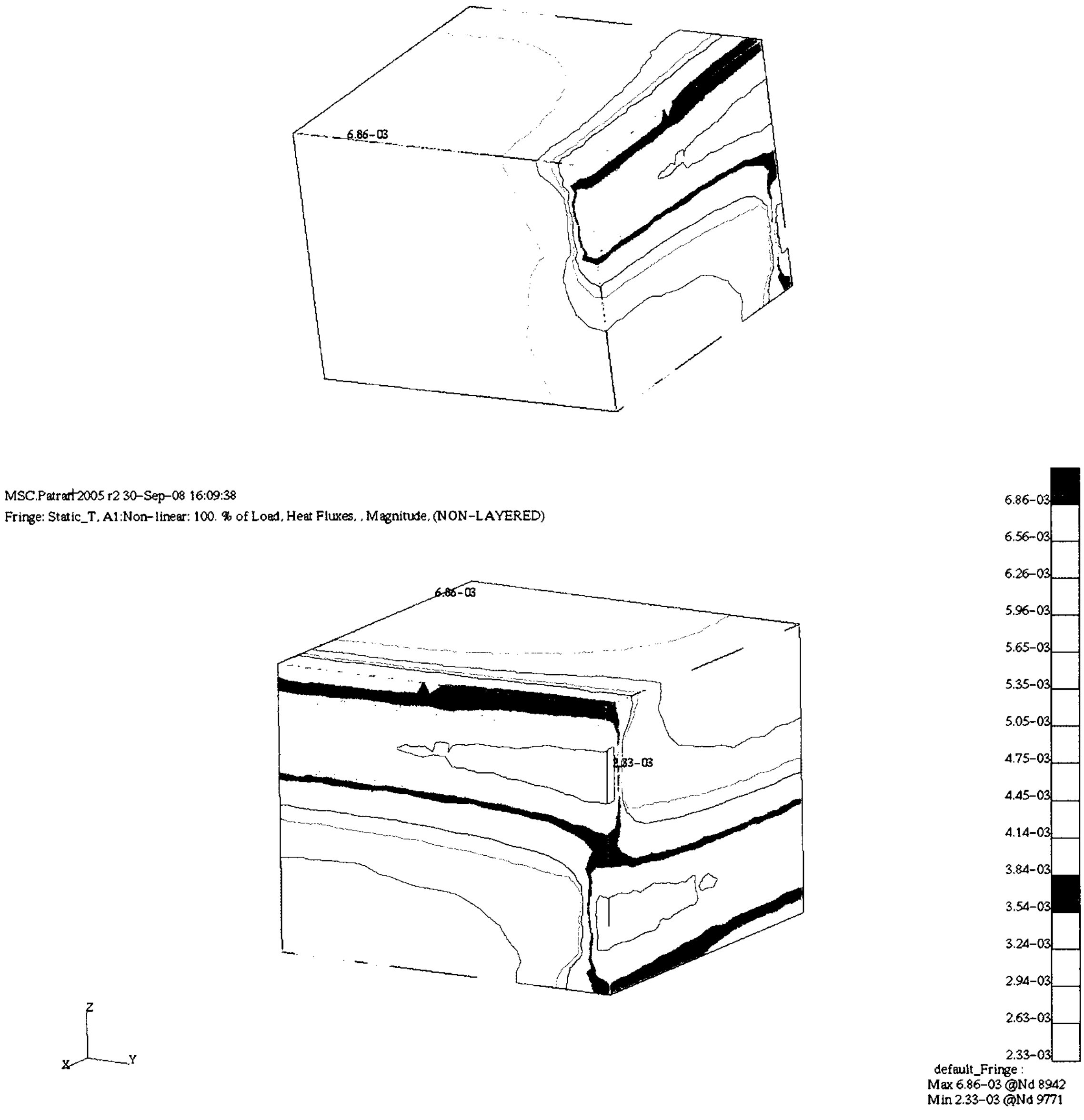

Figure 4.6: Non-interlaced reinforcements, stage 1, iteration 3: heat flux (W/mm^2)

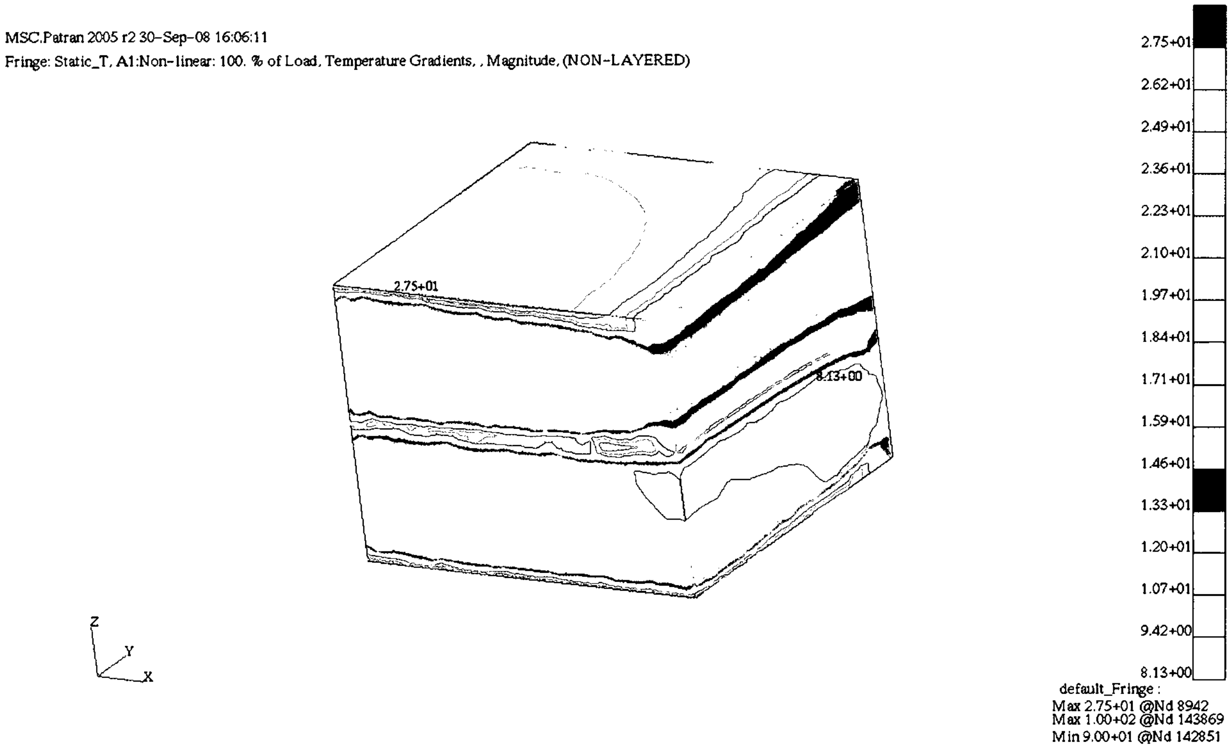

Figure 4.7: Non-interlaced reinforcements, stage 1, iteration 3: temperature gradients (°C/mm)

4.4 Non-Interlaced Reinforcement Stage 2: Parametric Study, Varying V_f

Once satisfactory models and meshes were obtained a parametric study was performed where eight geometric and material parameters were varied as listed in Table 4.5. The objective was to quantify and compare the effects of these parameters on the through-thickness thermal conductivity. Parameter P1, the yarn aspect ratio, was expressed as a width-to-height ratio of the yarn cross-section with baseline value of 5:1. Parameter P2 was the hyperellipse yarn section shape power *n* with baseline value of 0.3. Parameters P3 and P4 quantified the in-plane and through-thickness transverse inter-yarn gaps using ratios of the yarn width and height respectively; baseline values were 15:1 and 20:1. As P3 and P4 ratios increased the gaps between the yarns decreased and the overall V_f increased. It should be noted that the unit cell height and width as well as the fibre volume fraction differed in each trial. Parameters P5, P6, P7 and P8 were the yarn transverse thermal conductivity, yarn specific heat, resin thermal conductivity and resin specific heat respectively. A total of 33 models and associated parametric trails were conducted. Table 4.5 lists 25 of them only as changes in specific heat did not alter the steady-state conductivity, as expected.

The effects of parameters P1 to P5 and P7 on the through-thickness thermal conductivity k_z are illustrated in Figure 4.8. It is seen that:

- Parameter P1: k_z decreases slightly as the yarn aspect ratio (width-to-height) increases;
- Parameter P2: k_z increases as the yarn section shape power n decreases; smaller power values correspond to a more rectangular yarn section and to an increased V_f.
- Parameters P3 and P4: k_z increases as the ratio of yarn width to inter-yarn gap increases for both the in-plane and through-thickness transverse directions. As the ratios increase the gaps become smaller and V_f increases.
- Parameters P5 and P7: k_z increases as the yarn and/or resin conductivity increase. For the chosen parameter values an increase in yarn conductivity has a greater effect than a similar increase in resin conductivity.

Table 4.5: Parametric study results for non-interlaced reinforcements, stage 2

Simulation	**Parameters**						
	P1 Yarn aspect ratio	**P2** Yarn section shape power	**P3** Yarn spacing - ratio of width	**P4** Yarn spacing - ratio of thickness	**P5** Yarn transverse conductivty [W/mK]	**P7** Resin conductivity [W/mK]	Effective composite through-thickness transverse conductivity [W/mK]
NI S2 1	**5:1**	**0.3**	**15:1**	**20:1**	**0.613**	**0.25**	**0.505**
NI S2 2	**6:1**	0.3	15:1	20:1	0.613	0.25	0.504
NI S2 3	**7:1**	0.3	15:1	20:1	0.613	0.25	0.502
NI S2 4	**8:1**	0.3	15:1	20:1	0.613	0.25	0.501
NI S2 5	**9:1**	0.3	15:1	20:1	0.613	0.25	0.500
NI S2 6	5:1	**0.1**	15:1	20:1	0.613	0.25	0.535
NI S2 7	5:1	**0.2**	15:1	20:1	0.613	0.25	0.519
NI S2 8	5:1	**0.4**	15:1	20:1	0.613	0.25	0.494
NI S2 9	5:1	**0.5**	15:1	20:1	0.613	0.25	0.484
NI S2 10	5:1	0.3	**5:1**	20:1	0.613	0.25	0.472
NI S2 11	5:1	0.3	**10:1**	20:1	0.613	0.25	0.495
NI S2 12	5:1	0.3	**20:1**	20:1	0.613	0.25	0.513
NI S2 13	5:1	0.3	**25:1**	20:1	0.613	0.25	0.515
NI S2 14	5:1	0.3	15:1	**10:1**	0.613	0.25	0.482
NI S2 15	5:1	0.3	15:1	**15:1**	0.613	0.25	0.496
NI S2 16	5:1	0.3	15:1	**25:1**	0.613	0.25	0.510
NI S2 17	5:1	0.3	15:1	**30:1**	0.613	0.25	0.514
NI S2 18	5:1	0.3	15:1	20:1	**0.5**	0.25	0.433
NI S2 19	5:1	0.3	15:1	20:1	**0.7**	0.25	0.556
NI S2 20	5:1	0.3	15:1	20:1	**0.8**	0.25	0.612
NI S2 21	5:1	0.3	15:1	20:1	**0.9**	0.25	0.664
NI S2 26	5:1	0.3	15:1	20:1	0.613	**0.15**	0.434
NI S2 27	5:1	0.3	15:1	20:1	0.613	**0.20**	0.475
NI S2 28	5:1	0.3	15:1	20:1	0.613	**0.30**	0.529
NI S2 29	5:1	0.3	15:1	20:1	0.613	**0.35**	0.548

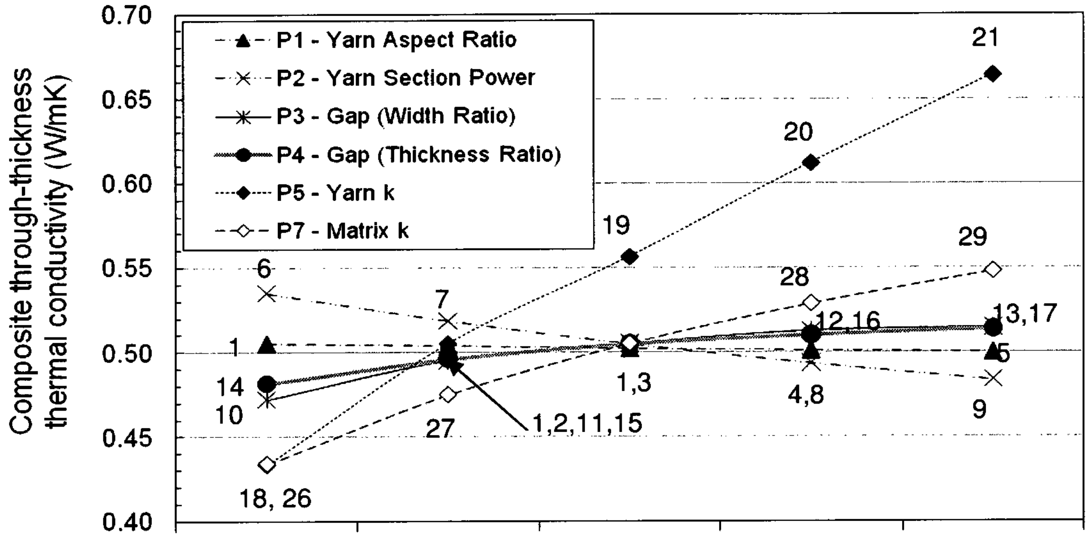

P1	5:1	6:1	7:1	8:1	9:1
P2	0.1	0.2	0.3	0.4	0.5
P3	5:1	10:1	15:1	20:1	25:1
P4	10:1	15:1	20:1	25:1	30:1
P5	0.5	0.613	0.7	0.8	0.9
P7	0.15	0.20	0.25	0.30	0.35

Figure 4.8: Non-interlaced reinforcements, stage 2, effect of parameters P1 to P5 and P7; point labels are model numbers (NI S2 X) with horizontal axis values to be read on line corresponding to relevant variable parameter

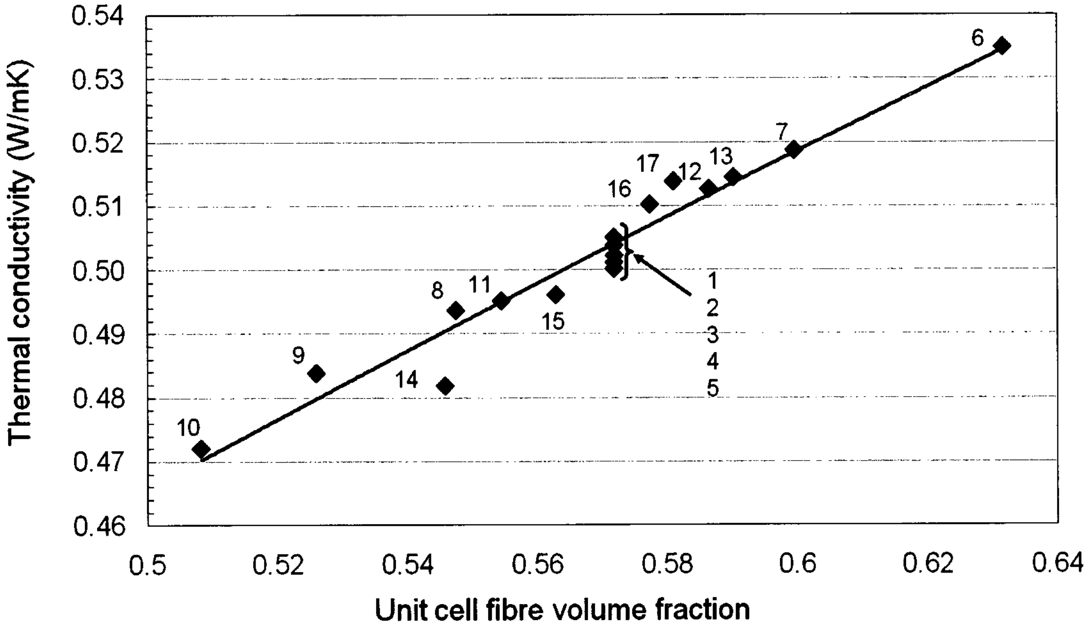

Figure 4.9: Non-interlaced reinforcements, stage 2, effect of fibre volume fraction

Figure 4.9 shows the relation between the through-thickness thermal conductivity k_z and the overall fibre volume fraction V_f for constant material properties – simulations beyond NI S2 17, which show the effect of different conductivities in constituent materials, were omitted from this figure. Whilst the general trend is clear the figure also shows the effect of small variations in the geometry as induced by parameters P1 to P4. The reinforcement geometry has a visible effect on k_z that is distinct from that of overall V_f, highlighting a very probable source of variability in experimental data and suggesting that there may be potential to tailor textile reinforcement geometries for different heat transfer responses. Although the range of predicted k_z values resulting from changes in reinforcement geometry is limited to 0.472 W/mK to 0.535 W/mK, differences could be more significant in the case of composites manufactured from pitch-based carbon fibres where the thermal conductivity is up to three orders of magnitude higher than those typical of PAN-based fibres which are the focus of this thesis.

For the ranges of parameter values selected in stage 2 of the work on composites made of non-interlaced reinforcements, the transverse thermal conductivities of the yarn and resin had the stronger effects on the through-thickness transverse thermal conductivity of the composites. This was expected as all models of the thermal conductivity of non-homogeneous materials feature the constituent's conductivities as their main parameters. Beyond this, an effect of reinforcement geometry was observed clearly. In stage 2 this takes the form of an essentially linear relationship between the through-thickness thermal conductivity and fibre volume fraction. Amongst the geometric parameters chosen the yarn cross-section power (parameter P2) had the strongest effect, followed by the in-plane and through-thickness transverse inter-yarn gap widths (parameters P3 and P4). The width-to-height ratio of the yarns, parameter P1, had relatively little effect. The results also showed a variation superimposed on the linear trend. This is well illustrated by simulations 1 to 5: whilst the effect of parameter P1 was weak, the fact that V_f was constant in these simulations clearly shows an effect of the geometry beyond that associated with changes in the fibre volume fraction, even for the relatively mild geometric variations featured in stage 2. In practice this can be ascribed to experimental variability, which was discussed in chapter 3.

4.5 Non-Interlaced Reinforcement Stage 3: Parametric Study, Constant V_f

A last round of simulations of composites made of non-interlaced reinforcements was conducted. Definitions of the geometry and material properties were further refined; values of the thermal conductivity in-plane and through-thickness were obtained. All unit cells modelled in stage 3 are characterized by a constant V_f value of 55% corresponding to panels 10 to 12 made of material 2; the aim of the simulations was to better probe the variability in conductivity induced by subtle changes in reinforcement geometry in isolation of changes in V_f.

The relation between geometry and resulting in-plane and through-thickness conductivities was quantified through 8 simulations run using unidirectional and bi-directional balanced unit-cell models NI S3 1 to NI S3 8. The main geometric characteristics of the models, which were used as simulation parameters, appear in Table 4.6; examples are shown in Figure 4.10 for a unidirectional and a bidirectional material. The hyperellipse was retained to represent the section of the straight yarns; in stage 3 the yarn width, yarn height and power n were kept constant at 2.0 mm, 0.5 mm and 0.5 in all cases. Ranges for in-plane yarn gaps *gh* and through-thickness yarn gaps *gv* were set at 0.2 mm to 0.4 mm and 0.02 mm to 0.04 mm respectively. Models with [0°] and [0°/90°] laminating sequences were created, Straight yarns occupy a large fraction of unit cells hence nesting was not modeled specifically.

Table 4.6: Parameters for non-interlaced reinforcements, stage 3

Simulation	Transverse gaps gv (mm)	In-plane gaps gh (mm)	Laminating sequence (-)	Yarn fibre volume fraction (-)
NI S3 1	0.02	0.2	[0°]	0.800
NI S3 2	0.04	0.2	[0°]	0.831
NI S3 3	0.02	0.4	[0°]	0.872
NI S3 4	0.04	0.4	[0°]	0.906
NI S3 5	0.02	0.2	[0°/90°]	0.800
NI S3 6	0.04	0.2	[0°/90°]	0.831
NI S3 7	0.02	0.4	[0°/90°]	0.872
NI S3 8	0.04	0.4	[0°/90°]	0.906

The composite V_f was held constant at 55% in all models. The proportion of unit cell volume occupied by yarns, termed nominal fibre volume fraction, varied as a function of the geometric parameters. Consequently, the yarn fibre volume fraction V_{fy} also varied. Published axial and transverse conductivities for T300 fibres k_{fa} = 8.4 W/mK and k_{ft} = 0.84 W/mK were used with resin conductivity k_m = 0.2 W/mK [10]. Yarn axial and transverse thermal conductivities k_{ya} and k_{yt} were calculated for each model using the ROM [53] and Nielsen's model [48] with A = 0.5 and $V_{f,max}$ = 0.906. Meshes featuring 100 000 to 500 000

4-noded tetrahedral elements were created in Gambit™ 2.2.30 [67]; Steady-state simulations were conducted in Fluent™ 6.2.16. Constant temperatures were imposed on the boundary faces normal to the heat flux; other boundaries were adiabatic. Fourier's law [56] was used in calculating the conductivity of the composite from the imposed temperature gradient and area-weighted surface heat flux q". A typical temperature distribution appears in Figure 4.11.

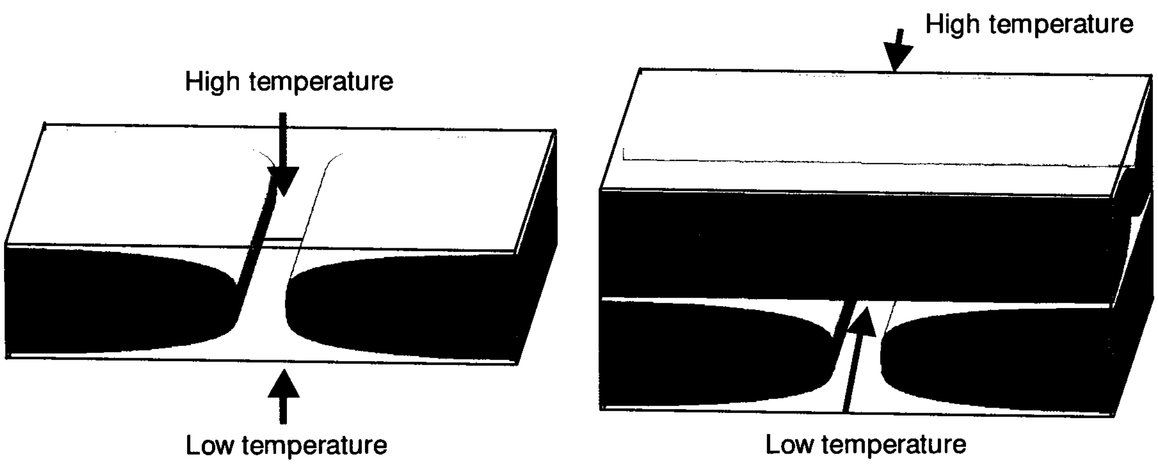

Figure 4.10: Non-interlaced reinforcements, stage 3: examples of geometry representative of models NI S3 1 to NI S3 4 (left) and NI S3 5 to NI S3 8 (right)

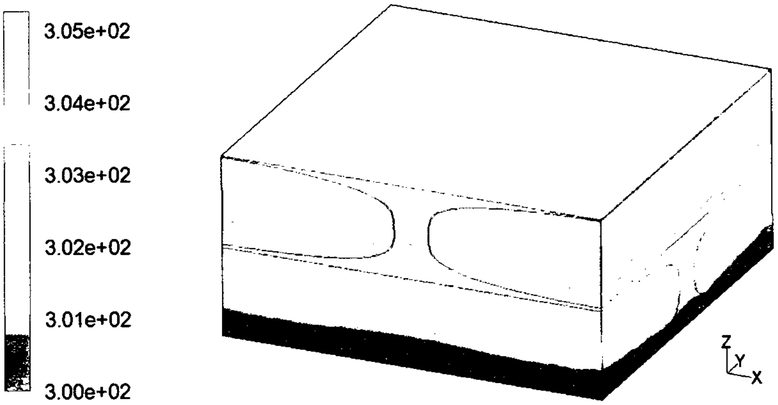

Figure 4.11: Non-interlaced reinforcements, stage 3: examples of temperature distribution, through-thickness simulation (K)

Simulation results appear in Table 4.7. Regarding through-thickness transverse composite conductivities, realistic parameter values lead to predictions that are between 1.0% and 11.0% above k_z values measured on panels 11 and 12. Modeling the composite as a homogeneous material with $V_f = 55\%$ without accounting for the yarn structure leads to a k_z value of 0.394 W/mK, 14% lower than the measured value.

Table 4.7: Parametric study results for non-interlaced reinforcements, stage 3

Simulation	Axial yarn conductivity	Transverse yarn conductivity	Transverse composite conductivity	Δ THASYS – prediction through-thickness	In-plane composite conductivity along yarns	Δ Directional THISYS – prediction along yarns	In-plane composite conductivity across yarns	Δ Directional THISYS – prediction across yarns
	k_{ya} (W/mK)	k_{yt} (W/mK)	k_T (W/mK)	- -	$k_{IP\ along}$ (W/mK)	- -	$k_{IP\ across}$ (W/mK)	- -
NI S3 1	6.76	0.626	0.484	-5.1%	5.37	-7.8%	0.494	-27.2%
NI S3 2	7.01	0.673	0.464	-1.0%	5.38	-8.0%	0.501	-28.2%
NI S3 3	7.35	0.747	0.516	-11.0%	5.37	-7.8%	0.486	-26.0%
NI S3 4	7.63	0.818	0.491	-6.3%	5.25	-5.7%	0.495	-27.3%
NI S3 5	6.76	0.626	0.481	-6.4%	N/A	N/A	N/A	N/A
NI S3 6	7.01	0.673	0.466	-3.4%	3.10	-10.0%	N/A	N/A
NI S3 7	7.35	0.747	0.503	-10.5%	N/A	N/A	N/A	N/A
NI S3 8	7.63	0.818	0.485	-7.2%	3.39	-17.6%	N/A	N/A

The variability on simulated k_z values resulting from geometry changes is limited: the largest difference between values for models NI S3 2 and NI S3 3 is 10.0%. Through-thickness transverse conductivity values for [0°] and [0°/90°] models are generally close, hence modeling a single layer of material is appropriate. Regarding in-plane conductivity, predicted values of k_{ci} along and across the yarns were between 5.7% and 27.2% above values measured on panel 11. The variability on predicted k_{ci} values resulting from changes in geometry was especially limited in the unidirectional case. For the bidirectional case models NI S3 5 and NI S3 7 did not converge for the k_{ci} simulation, whilst models NI S3 6 and NI S3 8 did converge with k_{ci} values 10.0% and 17.6% above the average conductivity measured from panel 12. All expected trends were detected. Variability at constant V_f was observed. Better results obtained with simulations of heat transfer along the yarns in unidirectional materials are consistent with higher confidence levels towards the parallel models used for homogeneous yarns, when compared with the series models used in the homogeneous transverse case. Generally, the variability levels obtained in stage 3 are comparable to those expected of measured values, as reflected in the literature.

4.6 Woven Reinforcements Stage 1: Introduction of Interlacing

The first stage of work on woven reinforcements aimed at creating geometric models of plain weaves that were as similar as possible to the non-interlaced reinforcements described in section 4.3, and at conducting a comparable parametric study of the effect of selected geometric parameters on thermal conductivity. The rationale was to highlight the effect of interlacing on thermal conductivity through comparison of the simulation data generated in both parametric studies. However, it must be noted that creating models of a woven fabric that feature yarn sections similar to those described in section 4.3 and credible yarn curvatures in unit cells of similar V_f is not possible. Therefore, comparisons made in stage 1 are to be viewed in the light of the effects of interlacing and lower V_f. Stage 1 was completed in two iterations. Iteration 1 consisted of geometry development work in the crimped section of the yarns, whilst a parametric study was conducted in iteration 2.

4.6.1 Woven, Stage 1, Iteration 1

Iteration 1 started with the creation of generic models and meshes representative of a plain woven reinforcement. This first stage was aimed at establishing a modeling functionality and not at accurate geometrical modeling. As with other cases the geometry was created in TexGen and exported in Gambit™ where it was meshed; the mesh was then converted for import in Patran™ using dedicated software written by the author. Figures 4.12 and 4.13 show one such generic mesh imported in Patran™ and a typical temperature distribution. Variable mesh density featured from the start in models of woven reinforcement. The latter figure clearly shows a distortion induced by yarn crimp. The main purpose of these models was to demonstrate the capability of assigning local orientation axes to each element representing a yarn. This capability is required for modeling orthotropic yarns. Figure 4.14 shows vectors illustrating the main orientation for each element as visible in TexGen; the determination of actual orientations is discussed below. The lower density of vectors in the centre of the yarns, which is associated with a lower mesh density in these zones, is visible in the figure. Physical dimensions and other properties are not discussed for these early models as interest to further model development is limited.

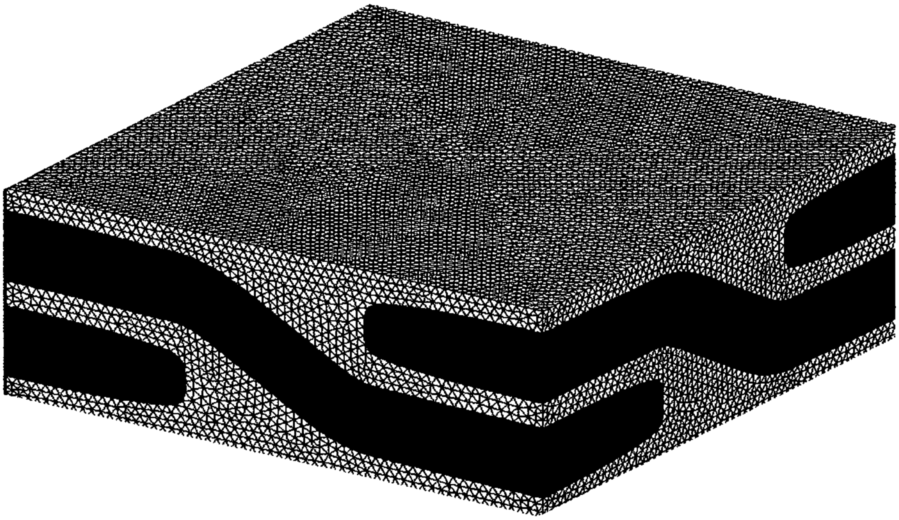

Figure 4.12: Woven reinforcement, stage 1, iteration 1

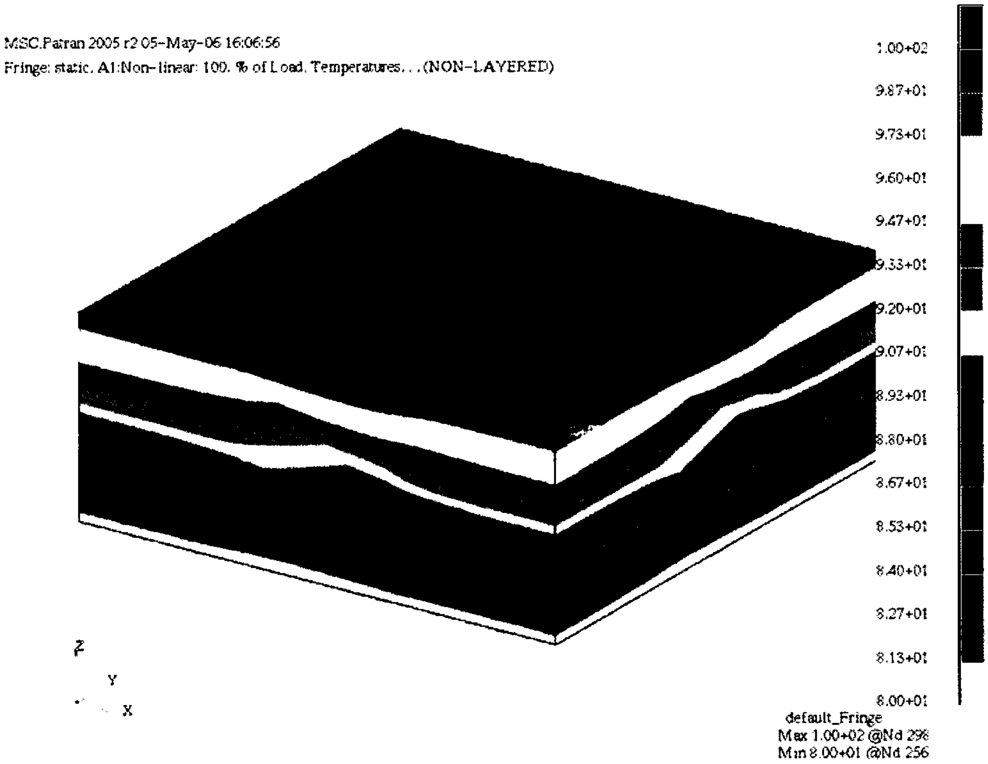

Figure 4.13: Woven reinforcement, stage 1, iteration 1: temperature distribution (°C)

Figure 4.14: Woven reinforcement, stage 1, iteration 1: fibre orientations

4.6.2 Woven, Stage 1, Iteration 2

In iteration 2 a significant effort was devoted to refining the geometry of models from those presented in the above section, with the aims of: 1) increasing the overall V_f of the modeled unit cells to values as close as possible to those of actual materials, whilst maintaining the yarn fibre volume fraction V_{fy} to realistic levels, and 2) besides interlacing, keeping the geometric models as close as possible to those used for non-interlaced materials so that the effect of interlacing on thermal conductivity may be quantified. The creation of appropriate geometric models using TexGen v2 is discussed in this section as iteration 2 to highlight practical issues and place the significance of thermal conductivity results in this context. A parametric study based on the models developed in iteration 2 was conducted as iteration 3 and is presented in the following section.

A geometric model and its associated finite element mesh are created in TexGen v2 and Gambit™ respectively, as follows. Each yarn in the unit cell is built from a set of initial points defined beforehand by the user. For each yarn a continuous line corresponding to the central path of the yarn is created as a Bezier curve that goes though all initial points. Segments of the Bezier curve extending between the initial points are separated by a number of curve points; the number of curve points per segment is set by the user. Curve points are used for positioning yarn sections along the length of the yarn. The user can create any number of yarn cross-sections by specifying section points in a flat plane, and assign any cross-section to any curve point. The plane of a cross-section assigned to a curve point is normal to the Bezier curve at that curve point. Once sections are assigned, TexGen v2 creates yarn envelopes - continuous surfaces made of flat triangles defined from the section points making up neighboring cross-sections along a given yarn. The creation of the geometric model is completed by specifying the dimensions of the unit cell; the volume inside the unit cell but outside of the yarn envelopes corresponds to inter-yarn gaps filled with resin in the composite.

Once a geometric model is created TexGen v2 generates a Gambit™ command text file, or journal file, for export to that software. The purpose of this is to use the powerful functionalities of the Gambit™ mesh generator for creating finite element meshes. When loaded into Gambit™ the journal file instructs the software to create points, line, surfaces and volumes, to perform Boolean operations on them as required, and to create meshes for each yarn in the unit cell and for the inter-yarn volume defined between the yarns. This task is not trivial as the inter-yarn volume can be very intricate and feature very thin sections with high aspect ratios. Gambit™ journal files are text based and it is often necessary to remove the command lines associated with meshing, so that this may be performed in smaller steps to ensure correct progress. Contrary to TexGen v2, which essentially creates surfaces defined in a 3D space, Fluent™ is a proper solid modeler based on the ACIS™ 3D modeling kernel. As such the geometrical tools used in creating the different geometrical entities differ. Therefore the different volumes corresponding to yarns and inter-yarn gaps in the unit cell will not be rigorously similar in TexGen v2 and Gambit™; differences will be small if sufficient numbers of curve points and section points are used when creating the TexGen v2 model. Then again, as 4-noded linear tetrahedral elements are used in the finite element meshes the outer surface of the meshed volumes in Gambit™ will not be rigorously similar to those of the geometric volumes from which they are defined.

Gambit™ features excellent tools enabling the evaluation of the finite element meshes that it generates. Once a suitable mesh has been generated it is exported back into TexGen v2 as a neutral text file. The mesh is superimposed to the geometric model, so that an orientation can be assigned to each element in the mesh; this operation is required for specifying the longitudinal and transverse thermal conductivities of the yarns in the correct orientations. The orientation vector assigned to any given element located inside a yarn envelope is parallel to the Bezier curve defining the yarn path, at the point of the curve corresponding to the centerline of a yarn cross-section going through the centre of that element. TexGen v2 also features an export function to the finite element software ABAQUS™. This function was used for importing the meshes featuring orthotropic elements into PATRAN™ using a converter written by the author.

TexGen v2 –generated ABAQUS™ files do not list a specific orientation for each element; this would make ABAQUS™ input files far too large given the way orientations are specified. Instead, the elements contained in a given yarn are separated into a user-specified number of groups that share a common orientation; this is also the case for PATRAN™ files. Similarly, values of yarn V_{fy} are assigned to groups of elements.

The work conducted in iteration 2 consisted of identifying combinations of initial points and section dimensions that would produce good quality meshes out of geometric models with satisfactory V_f, whilst remaining generally comparable to corresponding non-interlaced models. There was also a need for latitude in altering the models around the above points and dimensions, so that the effect of unit cell geometry on thermal conductivity could be assessed in iteration 3. Models covering four quarters of crossovers were built. Vertical unit-cell boundaries cutting yarn mid-lines enabled the use of adiabatic boundary conditions on those walls. Numerous attempts were made in creating yarns with smooth envelopes in the Gambit™ models; Figure 4.15 shows typical geometrical issues characterizing early attempts. Figures 4.16 to 4.24 show different aspects of a satisfactory geometric model and corresponding finite element mesh.

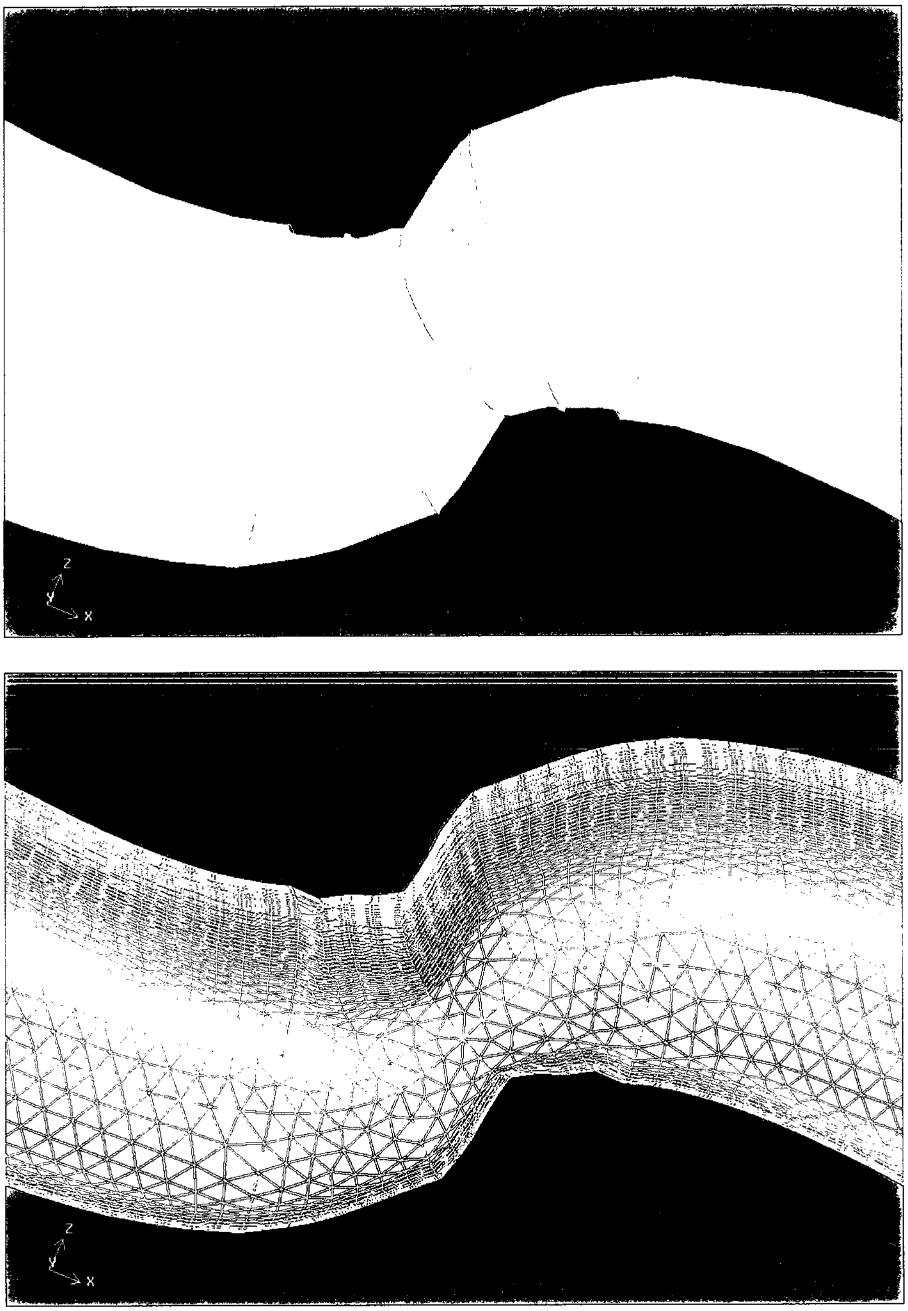

Figure 4.15: Woven reinforcement, stage 1, iteration 2: early models, geometrical issues

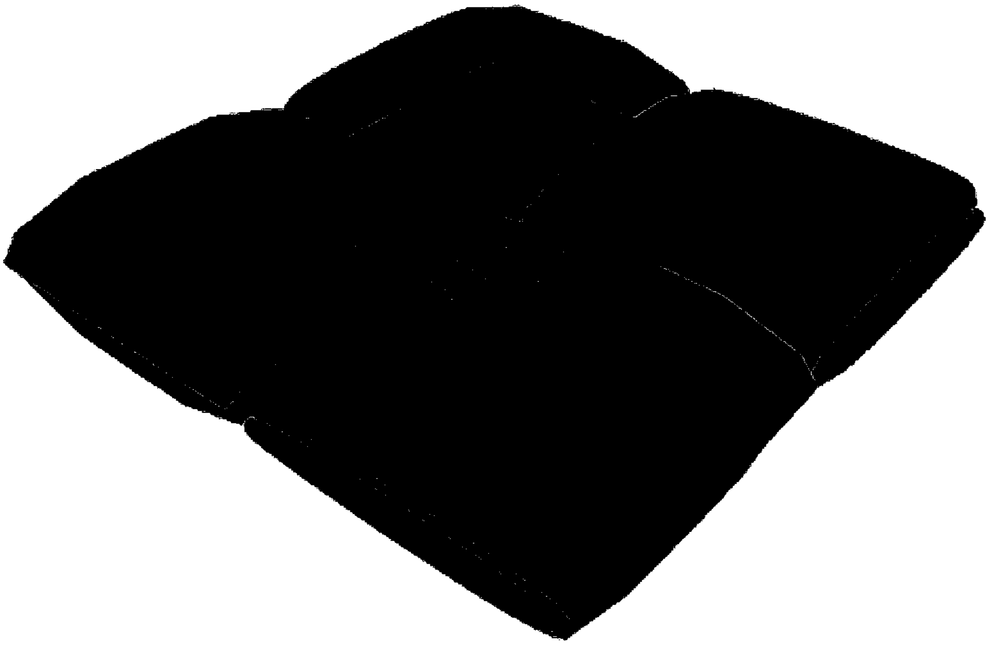

Figure 4.16: Woven reinforcement, stage 1, iteration 2: geometric model WR S1 I2-2 featuring 4 interlaced yarns, with computational domain highlighted in grey

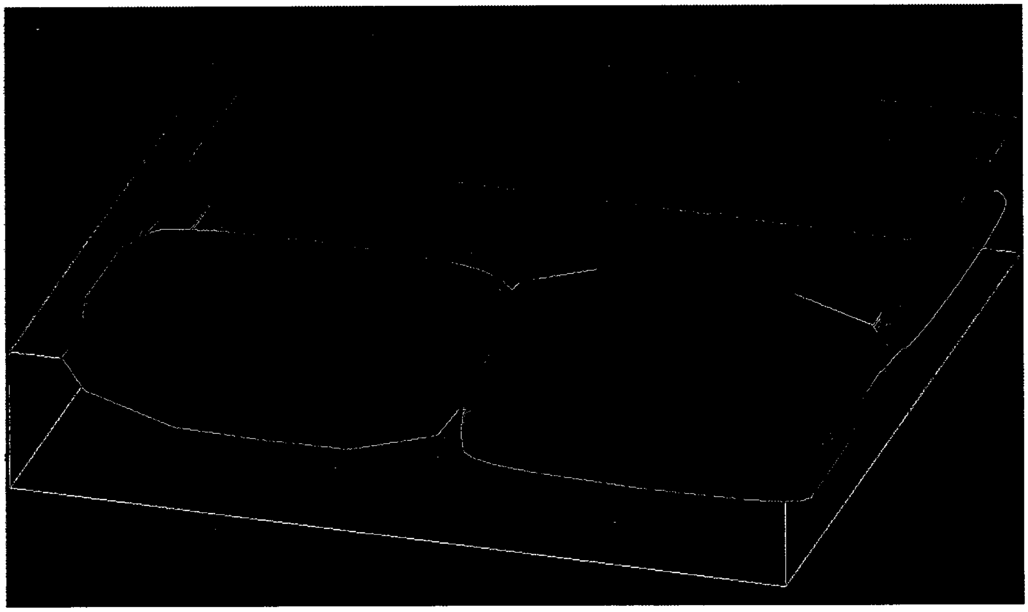

Figure 4.17: Woven reinforcement, stage 1, iteration 2: geometric model WR S1 I2-2; cross-section showing vertical inter-yarn gaps and intricacy of inter-yarn volume

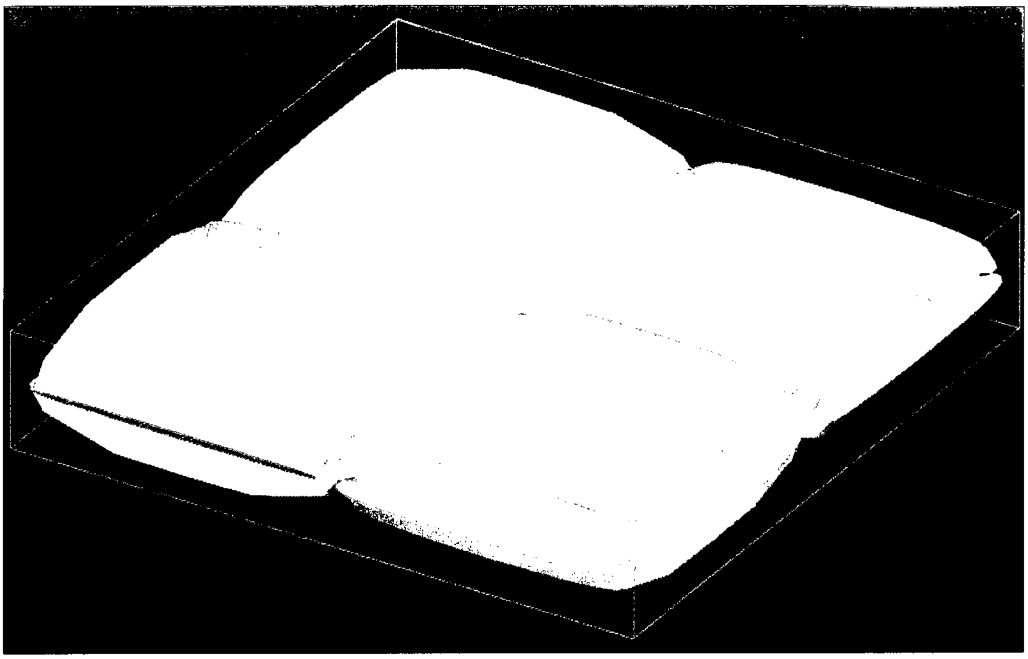

Figure 4.18: Woven reinforcement, stage 1, iteration 2: geometric model WR S1 I2-2; alternative cross-section

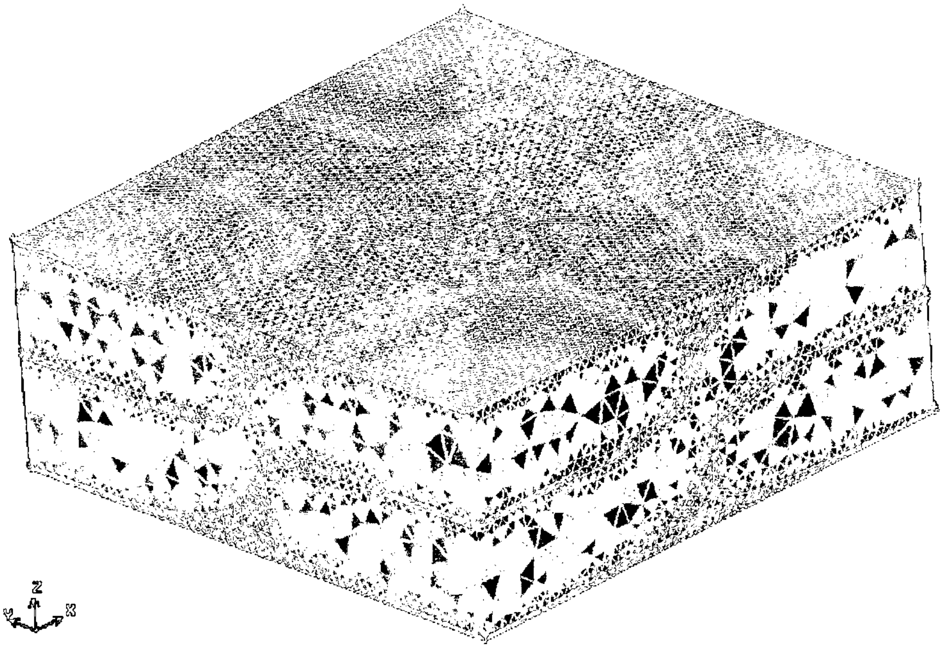

Figure 4.19: Woven reinforcement, stage 1, iteration 2: finite element mesh of the yarns and inter-yarn volume, defined over the repeating unit cell

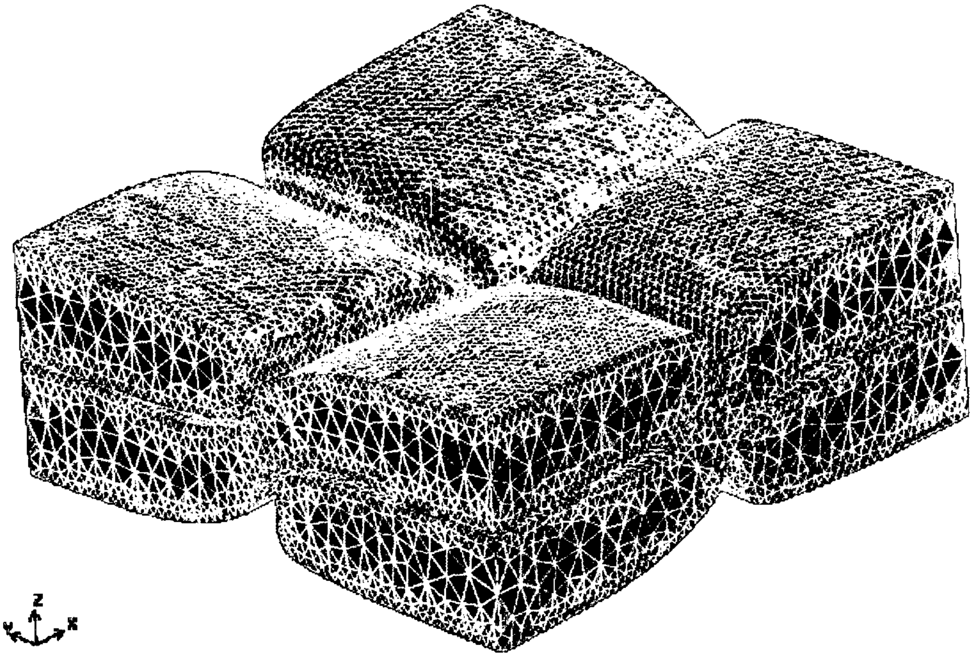

Figure 4.20: Woven reinforcement, stage 1, iteration 2: finite element mesh of the yarns, defined over the repeating unit cell

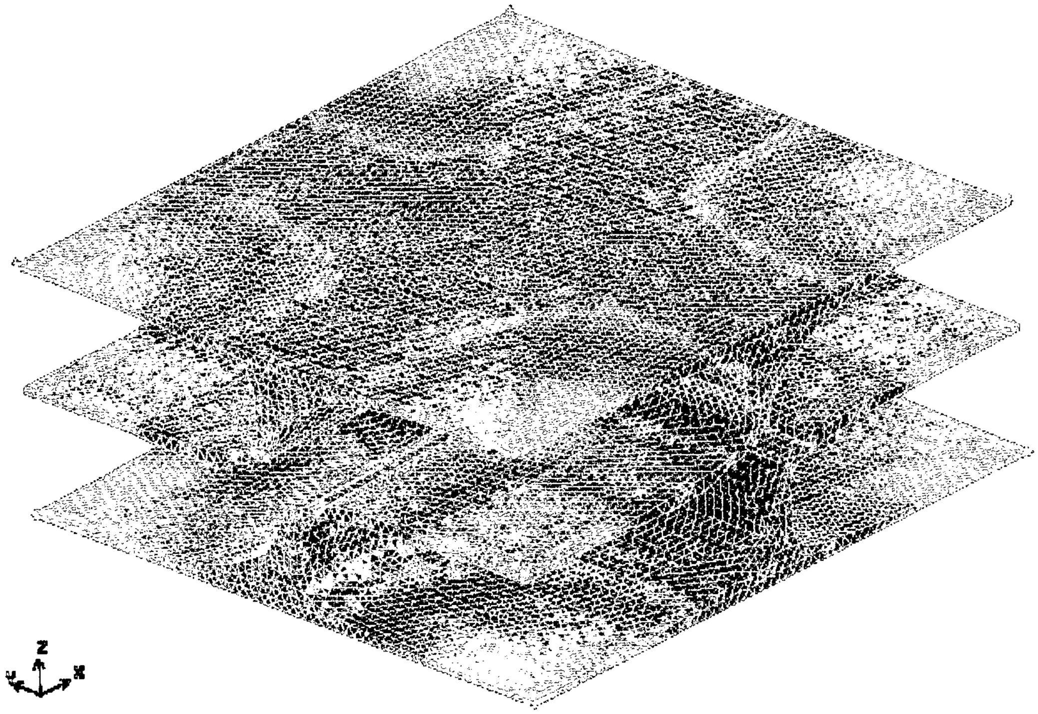

Figure 4.21: Woven reinforcement, stage 1, iteration 2: finite element mesh of the inter-yarn volume, defined over the repeating unit cell

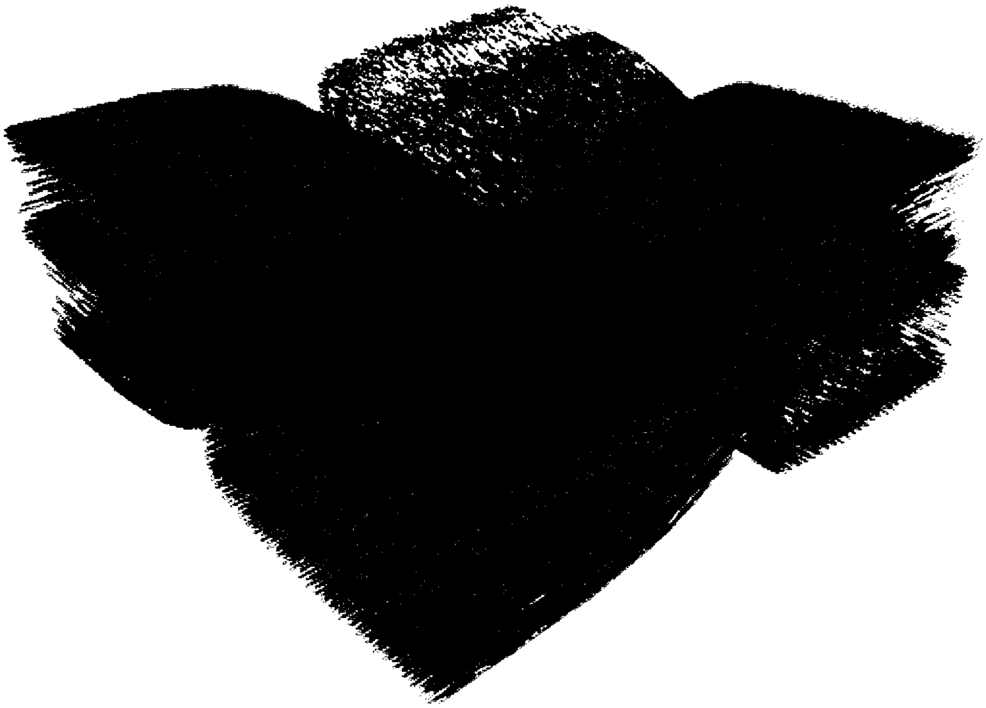

Figure 4.22: Woven reinforcement, stage 1, iteration 2: fibre orientations

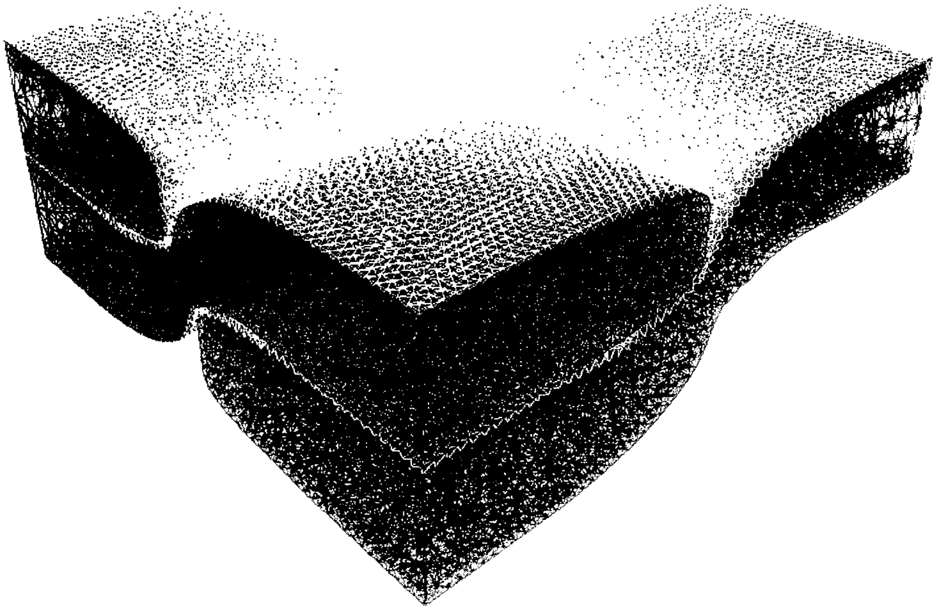

Figure 4.23: Woven reinforcement, stage 1, iteration 2: mesh with fibre orientations

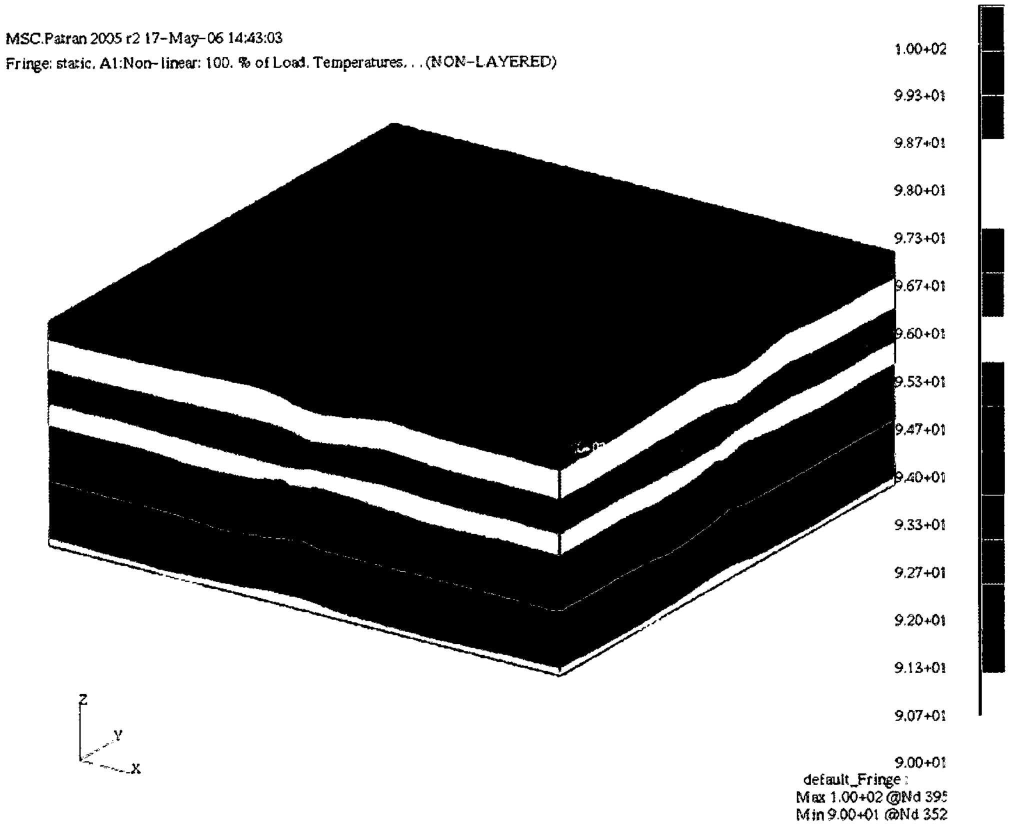

Figure 4.24: Woven reinforcement, stage 1, iteration 2: temperature distribution (°C)

Yarns in the models used in conducting heat transfer simulations were defined using 3 different cross-sections labeled S1, S2 and S3, Figure 4.25. The sections, which are normal to the yarn path, were not rotated around it; observation shows that this represents reality well in woven fabrics that are not subjected to in-plane shear. Sections S2 and S3 had the same 2 mm width as S1 but they were progressively thinner as listed in Table 4.8, and were characterized by different values of the power *n* as defined in Equation 4.5. Power *n* was a controlled parameter in section S1 and always took a value of 0.5, corresponding to an ellipse, in section S3; *n* took an intermediate value at section S2 as detailed in Table 4.8. Iteration 2 consisted of 6 simulations conducted for studying yarn crimp geometry. Controlled parameters were section heights S2 and S3. Steady-state heat transfer simulations were run with a constant yarn fibre volume fractions $V_{fy} = 0.75$ associated to all sections, and also with variable yarn fibre volume fractions $V_{fy} = 0.75$ at S1 and $V_{fy} = 0.90$ at S2 and S3, Figure 4.26. It should be noted that these values are feasible approximations based on the geometry. Fibre orientations were set using 4 groups per yarn as shown in Figure 4.27.

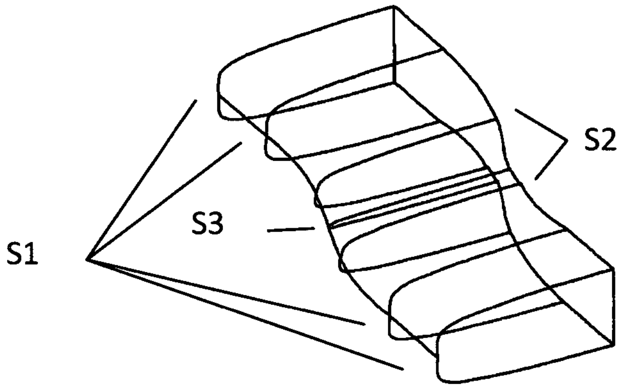

Figure 4.25: Woven reinforcement, stage 1, iteration 2: locations of sections S1, S2 and S3, cut along their mid-plane in the models and in this image

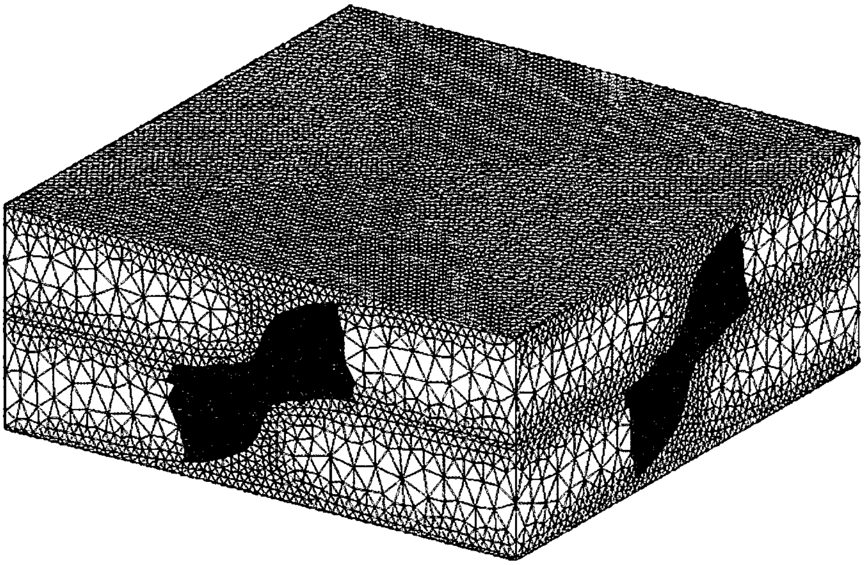

Figure 4.26: Woven reinforcement, stage 1, iteration 2: Variable V_{fy} case; red elements: V_{fy} = 0.90; yellow elements: V_{fy} = 0.75; white elements: inter-yarn volume

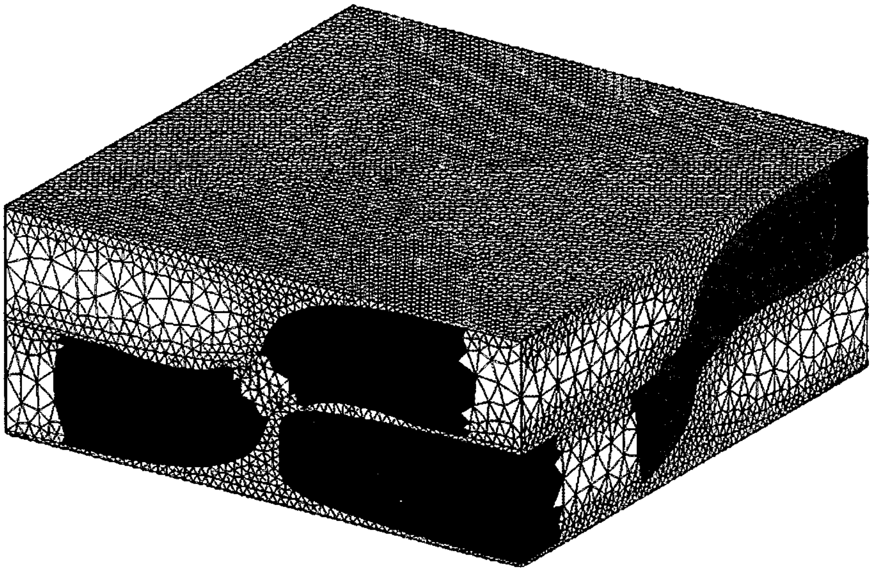

Figure 4.27: Woven reinforcement, stage 1, iteration 2: Each color corresponds to a specific fibre orientation

Table 4.8: Parameters for woven reinforcements, stage 1, iteration 2

Simulation	Section height (mm)			Through-thickness transverse thermal conductivity (W/mK)	
	S1	S2	S3	Constant V_f	Variable V_f
WR S1 I2-1	0.40	0.30	0.16	0.589	0.629
WR S1 I2-2	0.40	0.32	0.16	0.597	0.640
WR S1 I2-3	0.40	0.32	0.18	0.602	0.645
WR S1 I2-4	0.40	0.32	0.20	0.605	0.649
WR S1 I2-5	0.40	0.34	0.16	0.607	0.654
WR S1 I2-6	0.40	0.36	0.16	0.617	0.658

Values of the through-thickness transverse thermal conductivity were obtained using steady-state heat transfer simulations featuring boundary conditions and values similar to those reported previously for non-interlaced unit cells. Values of the axial fibre thermal conductivity, transverse fibre thermal conductivity and resin thermal conductivity representative of Hexcel AS4 fibres and epoxy resin were set at 6.83 W/mK, 1.19 W/mK and 0.25 W/mK respectively. Axial and transverse thermal conductivity values of the yarn were calculated using the rule of mixtures and inverse rule of mixtures [53].

Simulations performed in iteration 2 show that interlacing and crimp have a major effect on the through-thickness transverse thermal conductivity, as seen from comparison with results obtained for non-interlaced reinforcements. Beyond this, model WR S1 I2-2 was selected as the baseline geometry for the parametric study performed as iteration 3 and presented in the following section. This model was selected because its generation was relatively straightforward compared to models with fuller yarns such as WR S1 I2-4 and above; WR S1 I2-2 also provided needed latitude in altering its geometry in parametric studies whilst still being able to create models; this was used in iteration 3 presented in the next section.

From iteration 2, section heights at S2 and S3 were set at 80% and 40% of height of S1, respectively. It must be noted that the values are incompatible with the V_{fy} values used as stated above; therefore this first model is reasonably close to a woven equivalent of non-interlaced model NI S1 I3-4, but not completely realistic. Geometric issues in the models of unit cells of woven materials are addressed in stages 2 and 3 presented in sections 4.7 and 4.8.

4.6.3 Woven, Stage 1, Iteration 3

A parametric study was performed to quantify the effect of 6 geometric and constituent material parameters. Similarly to the case of simulations on non-interlaced materials reported in section 4.4, Parameter P1, the yarn aspect ratio, was expressed as a width-to-height ratio of the yarn cross-section with baseline value of 5:1. Parameter P2 was the hyperellipse yarn section shape power *n*, with baseline value of 0.3. Parameters P3 and P4 quantified the in-plane and through-thickness transverse inter-yarn gaps using ratios of the yarn width and height respectively; baseline values were 15:1 and 20:1. As P3 and P4 ratios increase the gaps between the yarns decrease and the overall V_f increases. As a result of changes in parameters the unit cell height and width as well as the fibre volume fraction differed between trials. Parameters P5 and P6 were the yarn transverse thermal conductivity and the resin thermal conductivity respectively. The yarn axial thermal conductivity was calculated from the ROM-A and constituent properties stated in section 4.6.2. A total of 17 parametric trials were conducted as shown in Table 4.9, along with through-thickness transverse thermal conductivity simulation results.

Figure 4.28 shows the following behaviour for the through-thickness transverse thermal conductivity of the composite:

- Parameter P1 yarn aspect ratio: k_T decreases slightly as the yarn aspect ratio (width-to-height) increases; this was also observed with non-interlaced reinforced unit cells. Woven materials with yarn aspect ratios greater than 6:1 could not be modelled due to major yarn interference.
- Parameter P2 yarn section shape power: k_T increases as the yarn section shape power n decrease, hence for more rectangular yarn sections. Small values of n lead to greater fibre volume fractions in the unit cell when the yarn fibre volume fraction is maintained constant, hence higher k_T. This was also observed with non-interlaced reinforced unit cells.
- Parameters P3 and P4 yarn spacing: k_T increases as the ratio of yarn width to inter-yarn gap increases for both the in-plane and transverse through-thickness directions. As the ratios increase yarn gaps get smaller and unit cell V_f increases, leading to higher k_T. This was also observed with non-interlaced reinforced unit cells.
- Parameters P5 and P6 yarn and resin conductivity: k_T increases as yarn and/or resin conductivity increases. An increase in k_{yt} has a greater effect than a similar increase in resin k for the selected parametric values. This was also observed with non-interlaced reinforced unit cells.

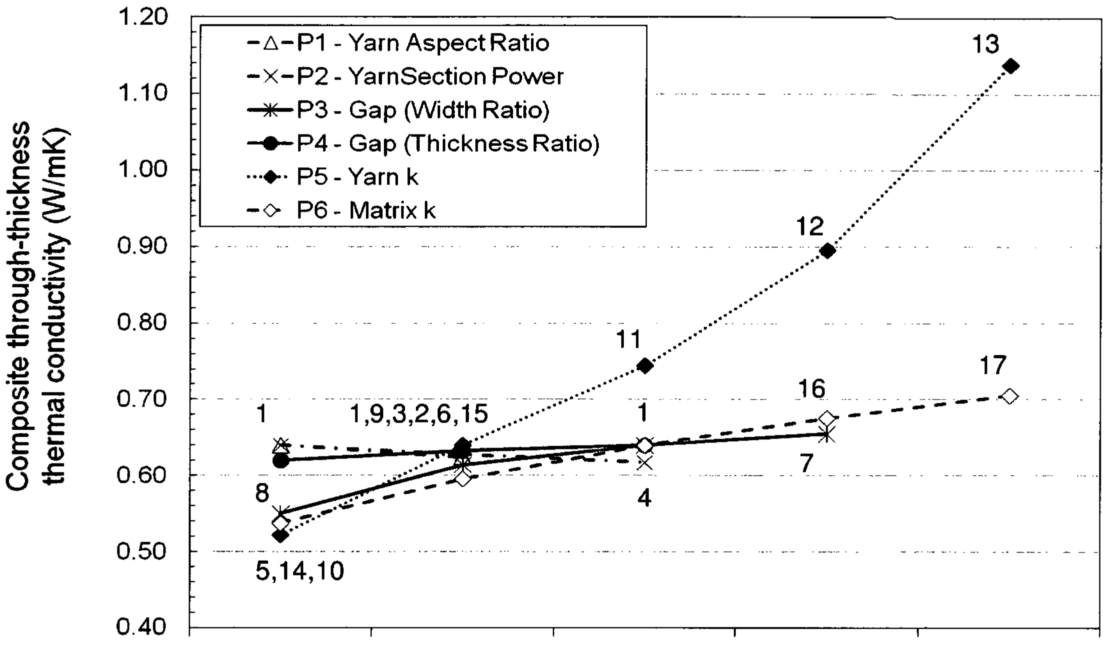

P1	5:1	6:1			
P2	0.3	0.4	0.5	0.4	0.5
P3	5:1	10:1	15:1	20:1	
P4	10:1	15:1	20:1		
P5	0.5	0.613	0.7	0.8	0.9
P6	0.15	0.20	0.25	0.30	0.35

Figure 4.28: Woven reinforcements, stage 1, iteration 3, effect of parameters P1 to P6; point labels are model numbers (WR S1 I3-X) with horizontal axis values to be read on line corresponding to relevant variable parameter

Table 4.9: Parametric study for woven reinforcements, stage 1, iteration 3

Simulation	**Parameters**									
	P1	**P2**	**P3**	**P4**	**P5**				**P6**	Effective composite through-thickness transverse conductivity [W/mK]
	Yarn aspect ratio	Yarn section shape power S1 / S2 / S3	Yarn spacing - ratio of width	Yarn spacing - ratio of thickness	Yarn transverse conductivity [W/mK]				Resin conductivity [W/mK]	
					V_f = 75%		V_f = 90%			
					Axial	Trans.	Axial	Trans.		
WR S1 I3-1	**5:1**	**0.3 / 0.4 / 0.5**	**15:1**	**20:1**	**5.185**	**0.613**	**6.172**	**0.865**	**0.25**	**0.640**
WR S1 I3-2	**6:1**	0.3 / 0.4 / 0.5	15:1	20:1	5.185	0.613	6.172	0.865	0.25	0.625
WR S1 I3-3	5:1	**0.4 / 0.45 / 0.5**	15:1	20:1	5.185	0.613	6.172	0.865	0.25	0.628
WR S1 I3-4	5:1	**0.5 / 0.5 / 0.5**	15:1	20:1	5.185	0.613	6.172	0.865	0.25	0.617
WR S1 I3-5	5:1	0.3 / 0.4 / 0.5	**5:1**	20:1	5.185	0.613	6.172	0.865	0.25	0.550
WR S1 I3-6	5:1	0.3 / 0.4 / 0.5	**10:1**	20:1	5.185	0.613	6.172	0.865	0.25	0.614
WR S1 I3-7	5:1	0.3 / 0.4 / 0.5	**20:1**	20:1	5.185	0.613	6.172	0.865	0.25	0.655
WR S1 I3-8	5:1	0.3 / 0.4 / 0.5	15:1	**10:1**	5.185	0.613	6.172	0.865	0.25	0.620
WR S1 I3-9	5:1	0.3 / 0.4 / 0.5	15:1	**15:1**	5.185	0.613	6.172	0.865	0.25	0.633
WR S1 I3-10	5:1	0.3 / 0.4 / 0.5	15:1	20:1	**3.290**	**0.500**	**3.898**	**0.625**	0.25	0.522
WR S1 I3-11	5:1	0.3 / 0.4 / 0.5	15:1	20:1	**7.593**	**0.700**	**9.061**	**1.094**	0.25	0.744
WR S1 I3-12	5:1	0.3 / 0.4 / 0.5	15:1	20:1	**5.185**	**0.613**	**15.393**	**1.423**	0.25	0.895
WR S1 I3-13	5:1	0.3 / 0.4 / 0.5	15:1	20:1	**5.185**	**0.613**	**35.063**	**1.877**	0.25	1.139
WR S1 I3-14	5:1	0.3 / 0.4 / 0.5	15:1	20:1	5.185	0.613	6.172	0.865	**0.15**	0.537
WR S1 I3-15	5:1	0.3 / 0.4 / 0.5	15:1	20:1	5.185	0.613	6.172	0.865	**0.20**	0.596
WR S1 I3-16	5:1	0.3 / 0.4 / 0.5	15:1	20:1	5.185	0.613	6.172	0.865	**0.30**	0.676
WR S1 I3-17	5:1	0.3 / 0.4 / 0.5	15:1	20:1	5.185	0.613	6.172	0.865	**0.35**	0.705

The effect of geometry on k_z as a function of unit cell V_f is shown in Figure 4.29 where values are graphed for simulations performed on models WR S1 I3-1 to WR S1 I3-9 featuring constant yarn and resin conductivity values. In a similar result to that presented for non-interlaced reinforcements, Figure 4.29 demonstrates that reinforcement geometry has an effect on k_T in addition to the constituent properties and unit cell V_f, suggesting there may be potential to adjust textile reinforcement geometry towards sought heat transfer properties.

Simulated k_z values obtained in stage 1, iteration 3 ranged from 0.433 to 1.139 W/mK. The baseline k_z value of 0.64 W/mK represents a 27% increase from 0.51 W/mK seen in the comparable case for non-interlaced reinforcements, section 4.4, as a result of weaving. The 0.64 W/mK k_z value can also be compared to k_T values measured on woven textile panels 7 through 9 from Table 3.4, ranging from 0.58 to 0.62 W/mK.

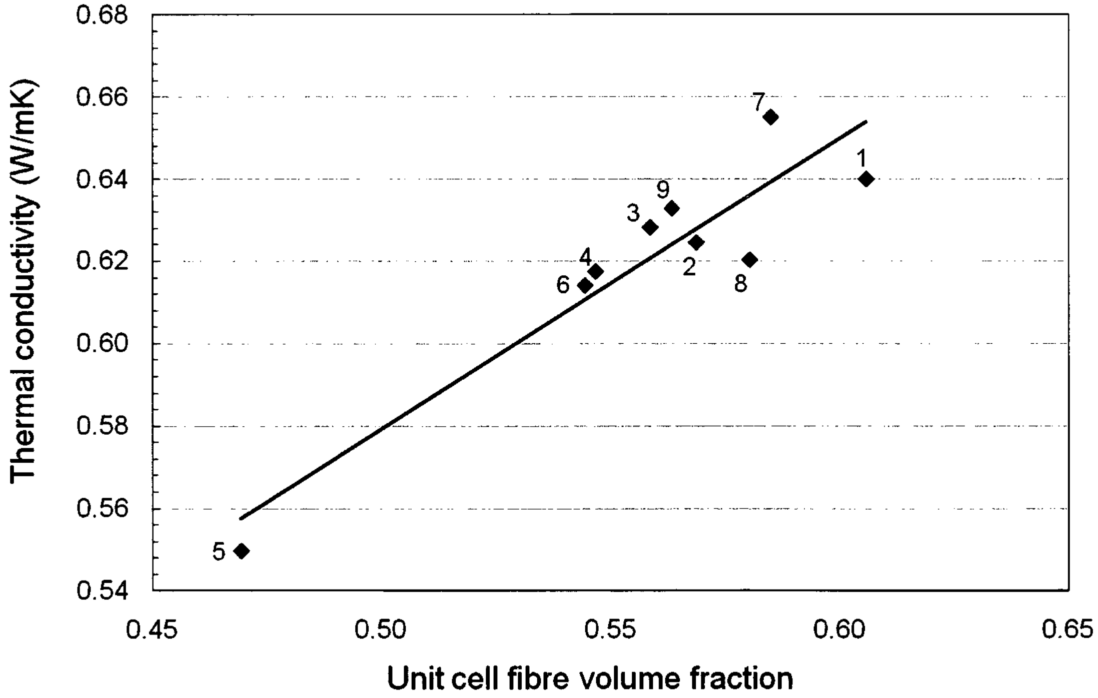

Figure 4.29: Woven reinforcements, stage 1, iteration 3, effect of fibre volume fraction

4.7 Woven Reinforcements Stage 2: Modelled from Measurements on Mat. 2

Geometric models developed as part of stage 1 allowed the quantification of the effect of interlacing on the through-thickness transverse thermal conductivity by comparison with results obtained with results from non-interlaced PMCs. However, as pointed above the geometry was not satisfactory from the perspective of modeling actual reinforcements; furthermore, the necessary drastic reduction in section area at crossover resulted in incompatibilities in yarn fibre volume fraction values V_{fy}.

In stage 2, thermal simulations were conducted for unit cell models of plain weave cross-ply $[0°/90°]_m$ and quasi-isotropic [0°/90°/+45°/-45°] laminates featuring one or two woven plies. Models of reinforcements were created from measurements made on a series of micrograph cross-sections of PMC samples made from material 2, Hexcel's HexPly F263 plain weave C/E prepreg. Average values of the section width, section height, crossover separation distance and total thickness for an 8-ply laminate were 1.901±0.192 mm, 0.136±0.003 mm, 2.260±0.175 mm and 1.493±0.042 mm respectively; a more realistic value of 14 was obtained for the ratio of yarn section width to height. It should be noted that variability in these measurements is not insignificant. Vertical inter-yarn gaps were not measured, although they are required in FE meshes as used in this work. Section 4.7.1 describes the geometric models; simulation results appear in section 4.7.2.

4.7.1 Woven Reinforcements Stage 2: Geometry

Stage 2 unit cell models of woven reinforcements were generated in TexGen v2 by specifying 40 points on a sinusoidal curve and using them as initial points in creating Bezier central path curves. Symmetry was used in the models as described in previous sections. All yarns in each models featured the same constant section. The sections were not defined using known profiles such as lenticular or elliptic. Instead, nominal unit cell fibre volume fraction was maximized by enforcing that the vertical inter-yarn gaps separating two yarns at any crossover remained constant at every point of the crossovers. This is illustrated in Figures 4.30 and 4.31. Figure 4.30 shows the definition of a section for a yarn A from the central path of a yarn B that interlaces it. The vertical gap extending between the red and yellow lines in Figure 4.30, that is between on one side, the vertical central mid-plane of a yarn A, and on the other side, the section of a yarn B that interlaces with yarn A, remains constant. Figure 4.31 shows yarn sections, as red lines, highlighted away from the yarn vertical mid-plane; gap height keeps the same value over the entire crossover surface. As a result, in the forthcoming models the yarn paths, yarn section height and gap height are set, and they determine the yarn width – values are provided below.

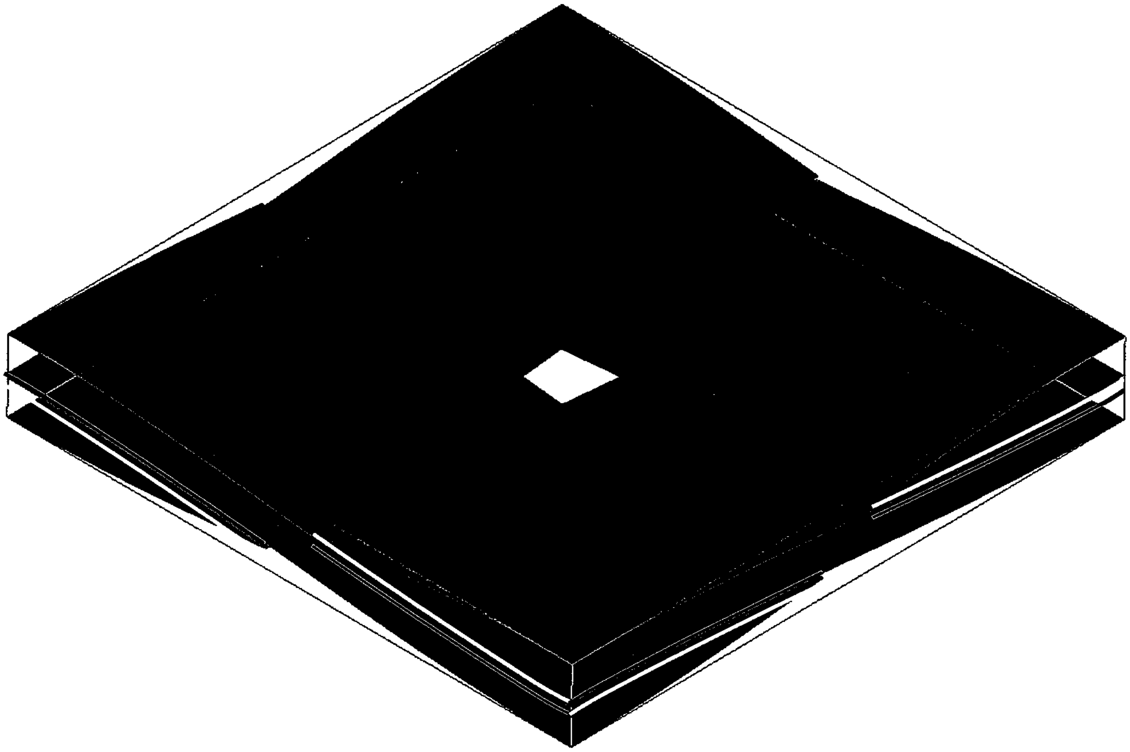

Figure 4.30: Vertical inter-yarn gaps in woven unit cell model

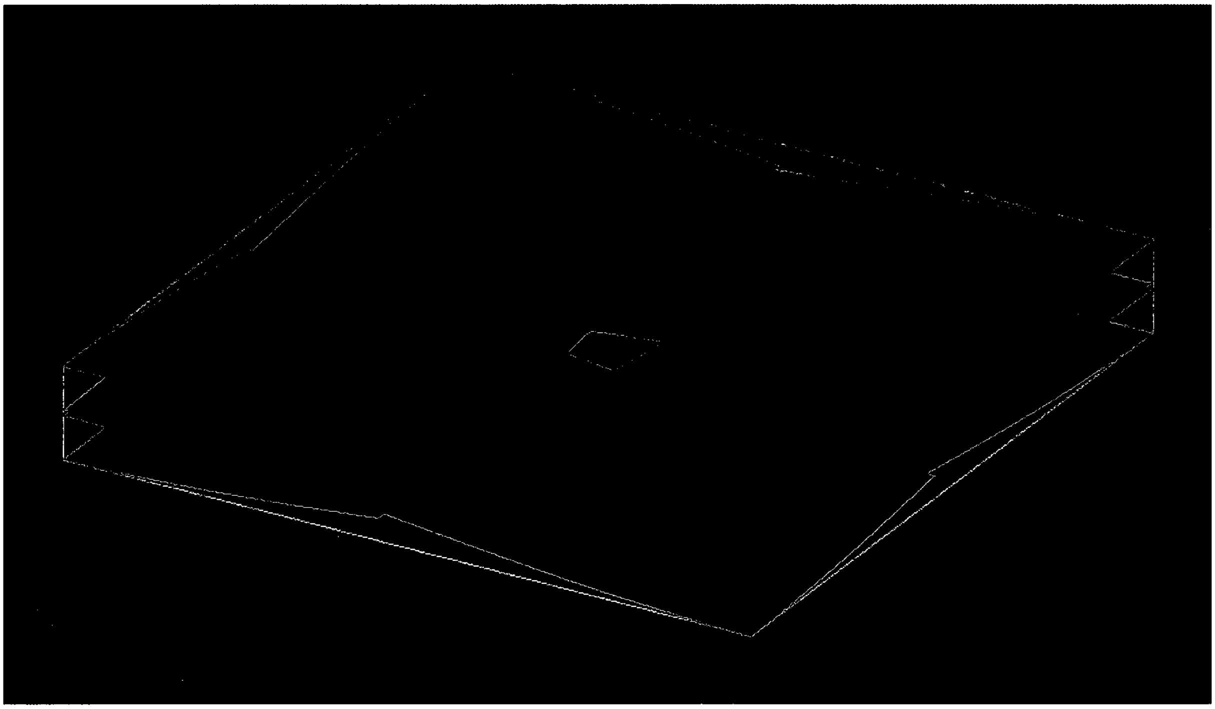

Figure 4.31: Vertical inter-yarn gaps in woven unit cell model, away from yarn mid-plane

Figure 4.32 illustrates the cases of bidirectional plies with geometries as described above, superimposed along perfectly aligned and perfectly staggered configurations. Using the above measured section height in each configuration leads to thicknesses 2.168 mm and 1.626 mm respectively for 8-layer modeled laminates. Both values are superior to the measured laminate thickness of 1.493±0.042 mm reported above. This highlights the prevalence of nesting in real reinforcement stacks and points to a limitation of models based on generic geometries. In this work the issue was investigated by creating models where yarn section heights were reduced to accommodate measured laminate thicknesses, as well as models where laminate thicknesses were increased to accommodate measured yarn section heights. The models are discussed below.

Figure 4.33 shows yarn section, as green lines, in the vertical mid-plane of the unit cell. The yarn sections occupy only a small fraction of the unit cell section, the remainder being filled by resin.

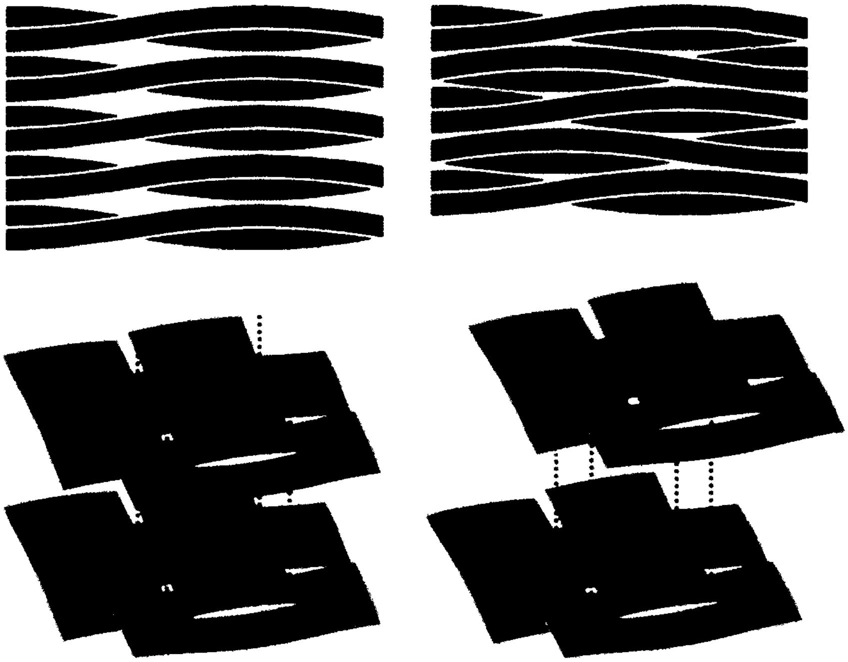

Figure 4.32: Superimposed bidirectional layers in woven unit cell model, superimposed in perfectly aligned (left) and perfectly staggered (right) patterns

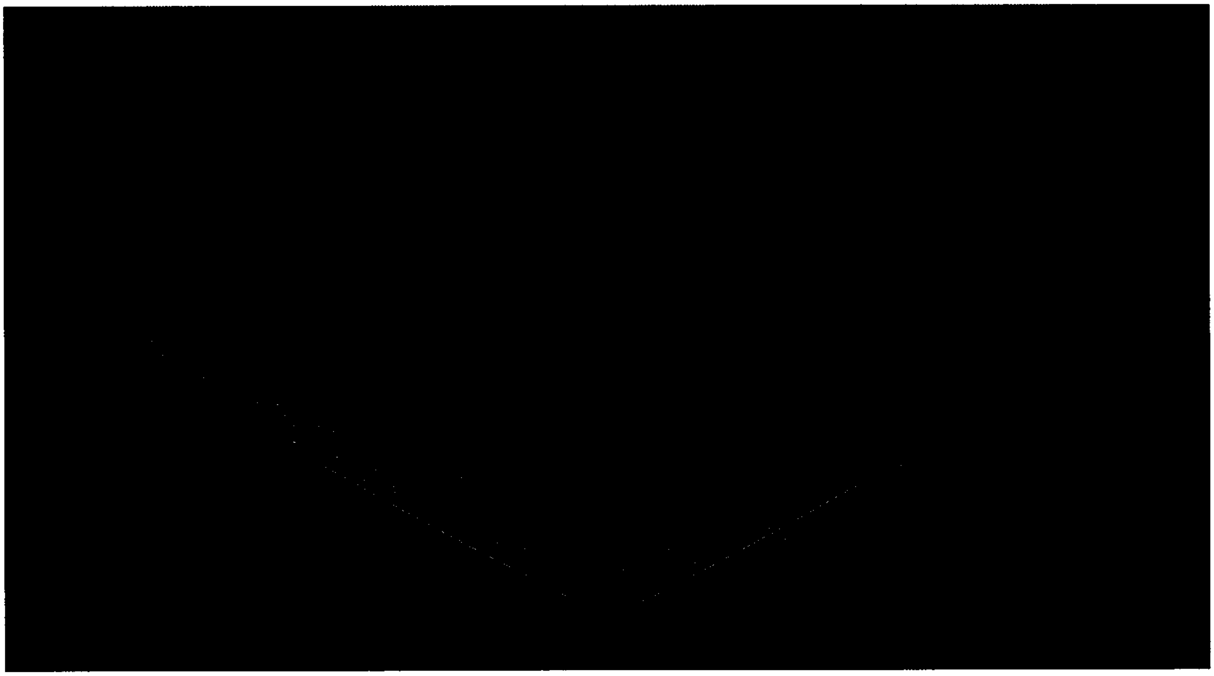

Figure 4.33: Yarn sections in central vertical plane of unit cell

These relatively large resin volumes in unit cell models representing a complete single layer of woven reinforcement result from the generic shape given to the yarns and parallelepiped shape given to the unit cells; they do not exist in reality. Similar volumes will be found near the topmost and lowermost surfaces of unit cells representing perfectly staggered layers of reinforcement in cases where these unit cells cover the full thickness of the laminate. Given their elongated in-plane shape these volumes can potentially have an especially strong effect on the transverse through-thickness thermal conductivity, and therefore result in inaccurate modeling. Attempts were made to correct this by creating models where single layers of reinforcements within stacks were cut through their horizontal mid-plane. These models are discussed below.

Models created at this stage of the work aimed at replicating the laminating sequences used with material 2 in the experimental section. One laminating sequence listed in Table 3.4 is $[(0/90)/(45/-45)/(45/-45)/(0/90)]_s$. It should be noted that crossover distances along x and y have no periodicity for the (0/90) and (45/-45) layers; therefore, generic geometric models of laminates featuring this laminating sequence are effected by the two issues listed above: nesting, which is necessarily present in actual material, cannot be modeled fully; furthermore, as a result of the aforementioned lack of periodicity it is not possible to stagger layers with different orientations, resulting in large resin volumes. Images of such models, which are discussed below, appear in Figure 4.34 to 4.38. Figure 4.34 shows successive bidirectional plain woven layers being superimposed; the layers have orientations (0/90) (layer 1, top left), (45/-45) (layer 2, top right), (45/-45) (layer 3, lower left) and (0/90) (layer 4, lower right). Layer 2 and 3 can be laid closer vertically, replicating nesting to some extent, because of their similar orientations. Greater vertical distances must separate layers 1 and 2, and layers 3 and 4 respectively.

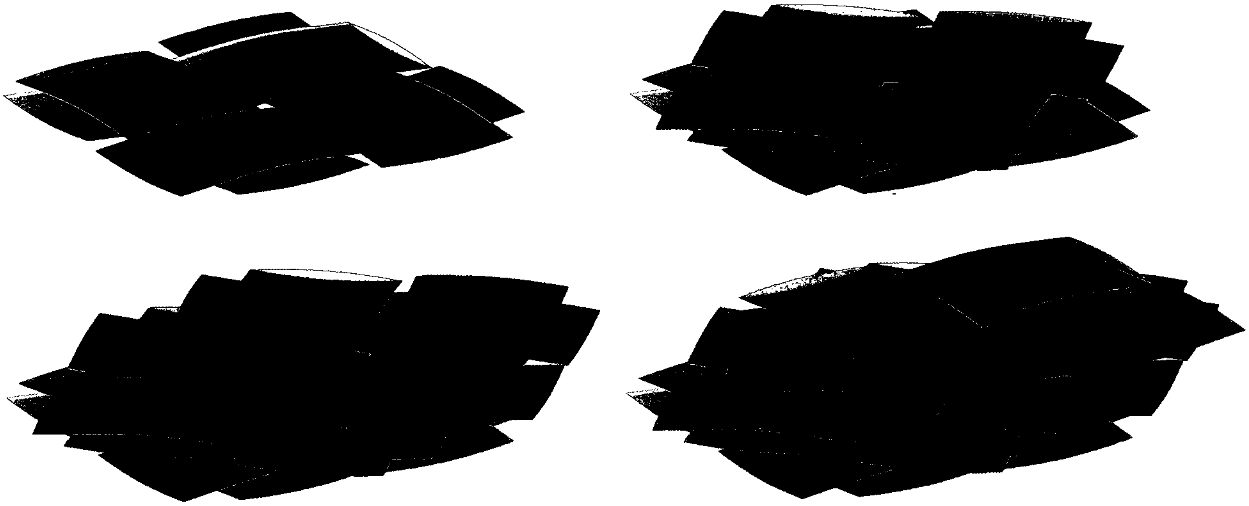

Figure 4.34: Superimposition of 4 plain woven reinforcement layers: Layer 1: (0/90), top left; Layer 2: (45/-45); Layer 3: (45/-45), perfectly staggered with layer 2, lower left; Layer 4: (0/90), lower right

The larger vertical distances separating both layers 1 and 2, and layers 3 and 4, compared to layers 2 and 3, are visible in the 3D view and section of Figures 4.35 and 4.36.

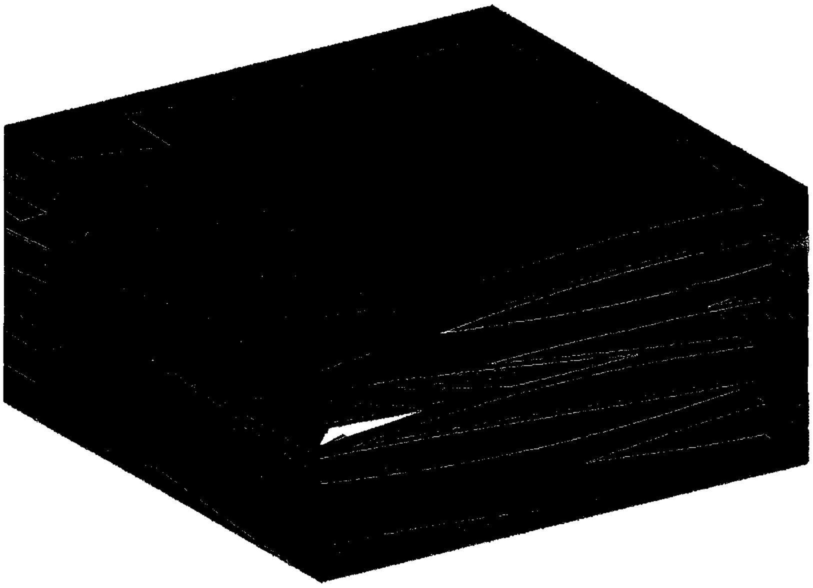

Figure 4.35: 3D view of geometric model of [(0/90)/(45/-45)/(45/-45)/(0/90)] laminate

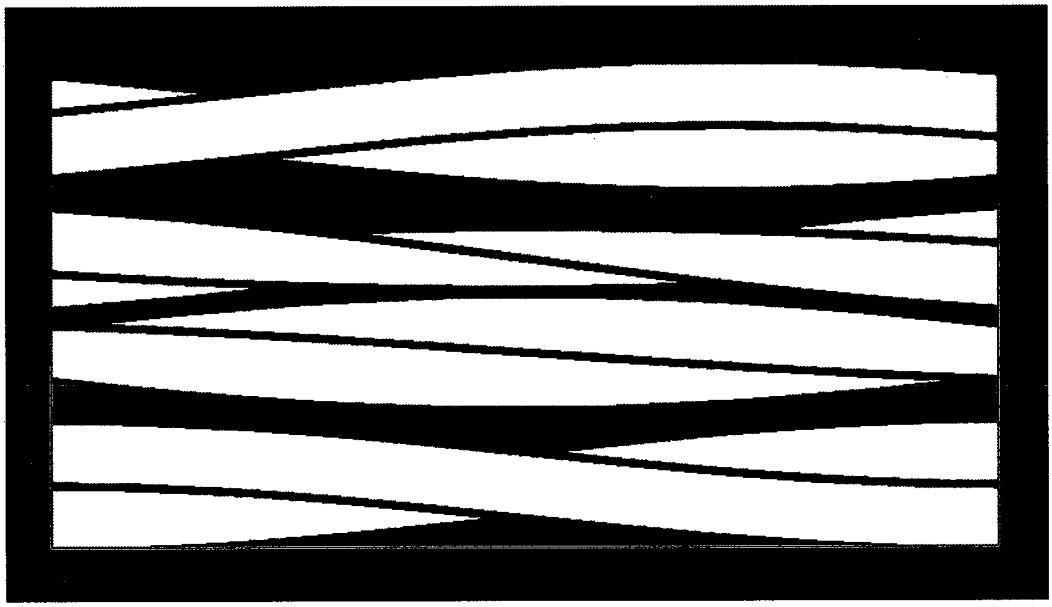

Figure 4.36: Section of geometric model of [(0/90)/(45/-45)/(45/-45)/(0/90)] laminate

The finite element mesh and resulting element orientations for the model with the above laminating sequence appear in Figures 4.37 and 4.38.

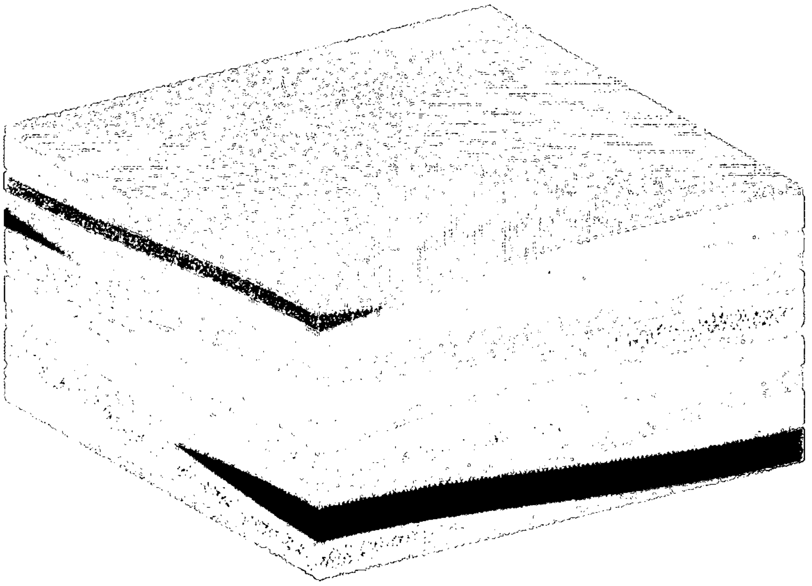

Figure 4.37: Mesh, model of [(0/90)/(45/-45)/(45/-45)/(0/90)] laminate

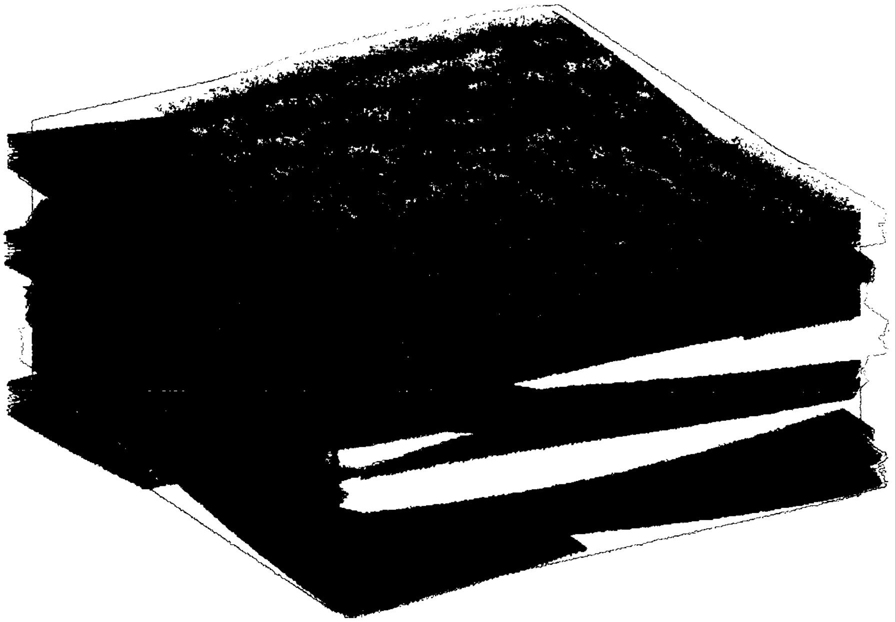

Figure 4.38: Element orientations, model of [(0/90)/(45/-45)/(45/-45)/(0/90)] laminate

A total of 11 geometric models were created in stage 2 of modeling work on woven reinforcements. In all models the in-plane distances between crossovers and between yarns were both equal to 2.26 cm, corresponding to unit cell size in all cases including models featuring (45/-45) layers. All vertical inter-yarn gaps were kept at 0.020 mm, both in models where yarn section height was modeled as measured or adapted to measured laminate thickness. Yarn section width was 2.075 mm in all cases, corresponding well with measured values of 1.901±0.192 mm. The axial and transverse thermal conductivities of the yarns and the thermal conductivity of the resin were 7.088 W/mK, 0.689 W/mK and 0.20 W/mK respectively; the yarn values were calculated from the ROM-A and from Clayton's model, Equations 2.1 and 2.2 respectively. Yarn fibre volume fraction was 0.84 in all cases. Tetrahedral element size quoted to Gambit™ for mesh generation was 0.020 mm.

Images of models WR S2 1 to WR S2 11 appear in Figures 4.39 to 4.41. Model WR S2 1 featured 1 (0/90) layer with yarn section heights modeled as measured at 0.136 mm. Unit cell thickness was 0.311 mm. The nominal and actual unit cell fibre volume fractions were 50.3% and 42.3% respectively. Values of the in-plane and transverse through-thickness thermal conductivities were obtained. Model WR S2 2 featured 2 perfectly staggered (0/90) layers with yarn section heights modeled as measured at 0.136 mm. The vertical distance separating the layer mid-planes was 0.220 mm, and the total unit cell thickness was 0.531 mm. The nominal and actual unit cell fibre volume fractions were 56.6% and 47.5% respectively. Values of the in-plane and transverse through-thickness thermal conductivities were obtained. Model WR S2 3 featured 3 perfectly staggered (0/90) layers with yarn section heights modeled as measured at 0.136 mm. The vertical distance separating the layer mid-planes was 0.220 mm; total unit cell thickness was 0.751 mm. The nominal and actual unit cell fibre volume fractions were 59.7% and 50.2% respectively. Values of the in-plane and transverse through-thickness thermal conductivities were obtained.

Model WR S2 4 featured 1 (0/90) layer with yarn section heights reduced to 0.093 mm to adapt total laminate thickness. Unit cell thickness was 0.227 mm. The nominal and actual unit cell fibre volume fractions were 45.9% and 38.6% respectively. Values of the in-plane and transverse through-thickness thermal conductivities were obtained. Model WR S2 5 featured 2 perfectly staggered (0/90) layers with yarn section heights reduced to 0.093 mm to adapt total laminate thickness. The vertical distance separating the layer mid-planes was 0.160 mm, and the total unit cell thickness was 0.387 mm. The nominal and actual unit cell fibre volume fractions were 52.0% and 43.7% respectively. Values of the in-plane and transverse through-thickness thermal conductivities were obtained.

Model WR S2 6 featured 1 (0/90) layer and 1 (45/-45) layer with yarn section heights modeled as measured at 0.136 mm. Because of their different orientations the vertical distance separating the layer mid-planes was equal to the single layer thickness including gaps at 0.311 mm. The nominal and actual unit cell fibre volume fractions were 47.3% and 39.7% respectively. Values of the in-plane and transverse through-thickness thermal conductivities were obtained. Model WR S2 7 featured 1 (0/90) layer, 2 perfectly staggered (45/-45) layers and 1 (0/90) layer with yarn section heights modeled as measured at 0.136 mm. As stated above, the two central layers were closer because of their orientation; vertical distance separating the layer mid-planes between those was 0.220 whilst it was 0.311 mm between layers 1 and 2, and layers 3 and 4. Unit cell thickness was 1.153 mm. The nominal and actual unit cell fibre volume fractions were 53.1% and 44.6% respectively. Values of the in-plane and transverse through-thickness thermal conductivities were obtained.

Model WR S2 8 featured 1 (0/90) layer and 1 (45/-45) layer with yarn section heights reduced to 0.093 mm to adapt total laminate thickness. Because of their different orientations the vertical distance separating the layer mid-planes was equal to the single layer thickness including gaps at 0.227 mm. The nominal and actual unit cell fibre volume fractions were 43.1% and 36.2% respectively. Values of the in-plane and transverse through-thickness thermal conductivities were obtained. Model WR S2 9 featured 1 (0/90) layer, 2 perfectly staggered (45/-45) layers and 1 (0/90) layer with yarn section heights reduced to 0.093 mm to adapt total laminate thickness. Remarks similar to those made for model WR S2 9 apply; unit cell thickness was 0.840 mm. The nominal and actual unit cell fibre volume fractions were 48.5% and 40.8% respectively. Values of the in-plane and transverse through-thickness thermal conductivities were obtained.

It should be noted that unit cells in models WR S2 6 to 9 are not periodic. The constant inter-yarn distances and layer orientations preclude building periodic unit cells in these cases.

Model WR S2 10 featured 2 perfectly staggered (0/90) layers with yarn section heights modeled as measured at 0.136 mm. The occurrence of resin volumes in the unit cell was alleviated by cutting each layer along its horizontal mid-plane; therefore unit cell thickness corresponded to that of a single layer. The nominal and actual unit cell fibre volume fractions were 72.7% and 61.1% respectively. A value of the transverse through-thickness thermal conductivity was obtained. Model WR S2 11 featured 3 perfectly staggered (0/90) layers with yarn section heights modeled as measured at 0.136 mm. The occurrence of resin volumes in the unit cell was alleviated by cutting the lower and upper layers along their respective horizontal mid-planes; therefore unit cell thickness corresponded to that of 2 layers. The nominal and actual unit cell fibre volume fractions were 72.7% and 61.1% respectively. A value of the transverse through-thickness thermal conductivity was obtained.

It should be noted that in the latter 2 models featuring layers cut along their horizontal mid-plane, isotropic yarn properties had to be assigned because of a software issue. The value of the transverse yarn thermal conductivity was used in all cases.

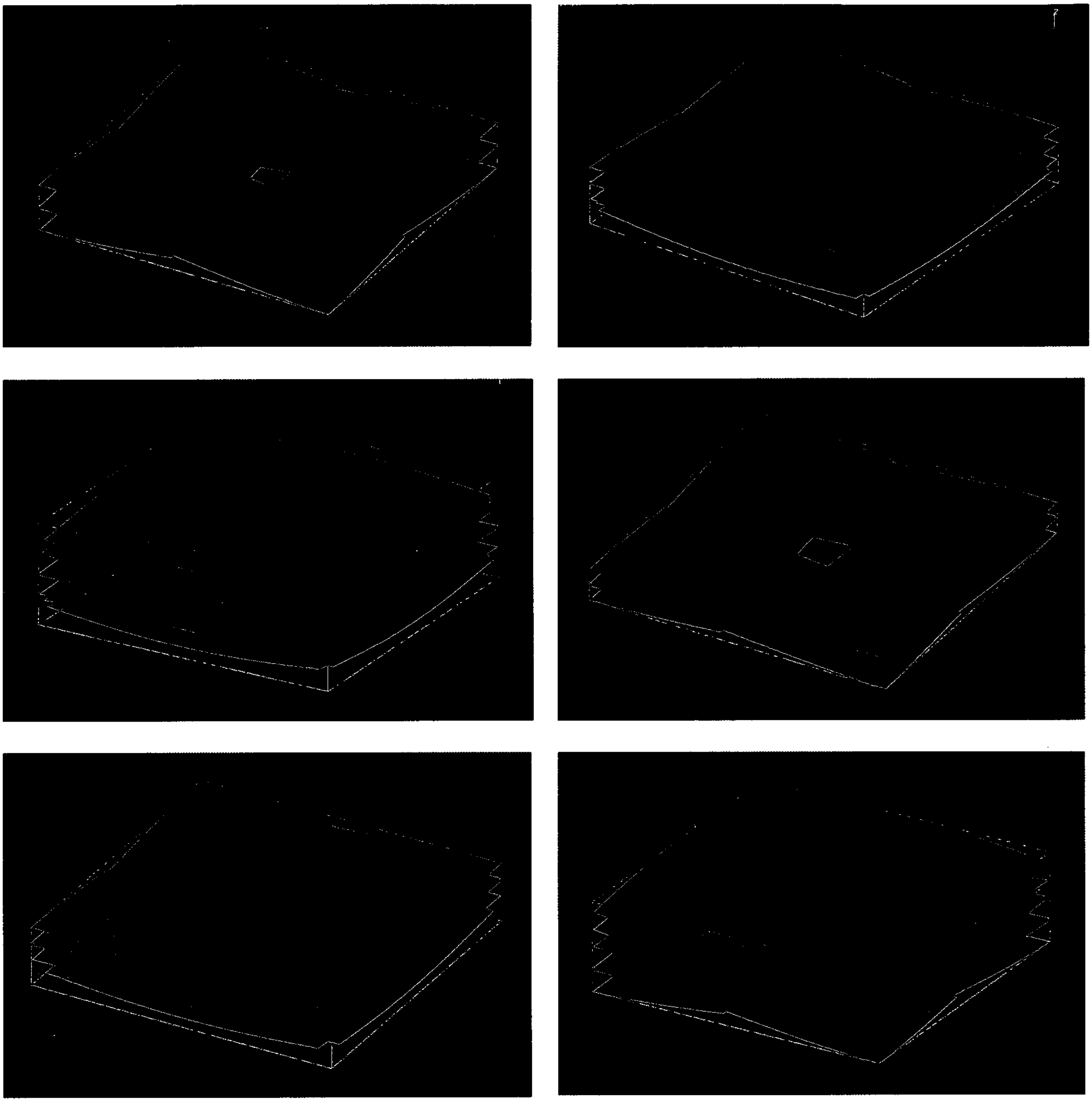

Figure 4.39: 3D view of geometric models WR S2 1 (top left), WR S2 2 (top right), WR S2 3 (centre left), WR S2 4 (centre right), WR S2 5 (lower left), WR S2 6 (lower right)

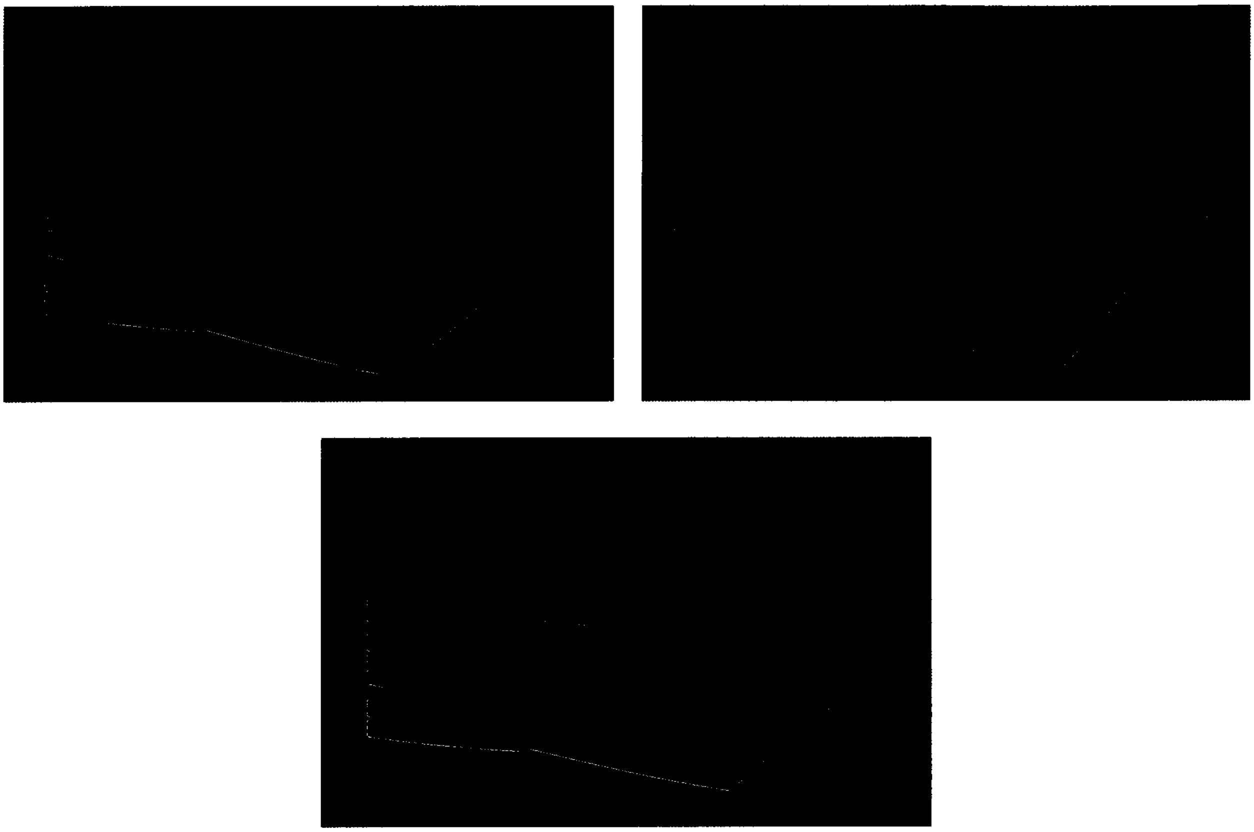

Figure 4.40: 3D view of geometric models WR S2 7 (top left), WR S2 8 (top right), WR S2 9 (lower left)

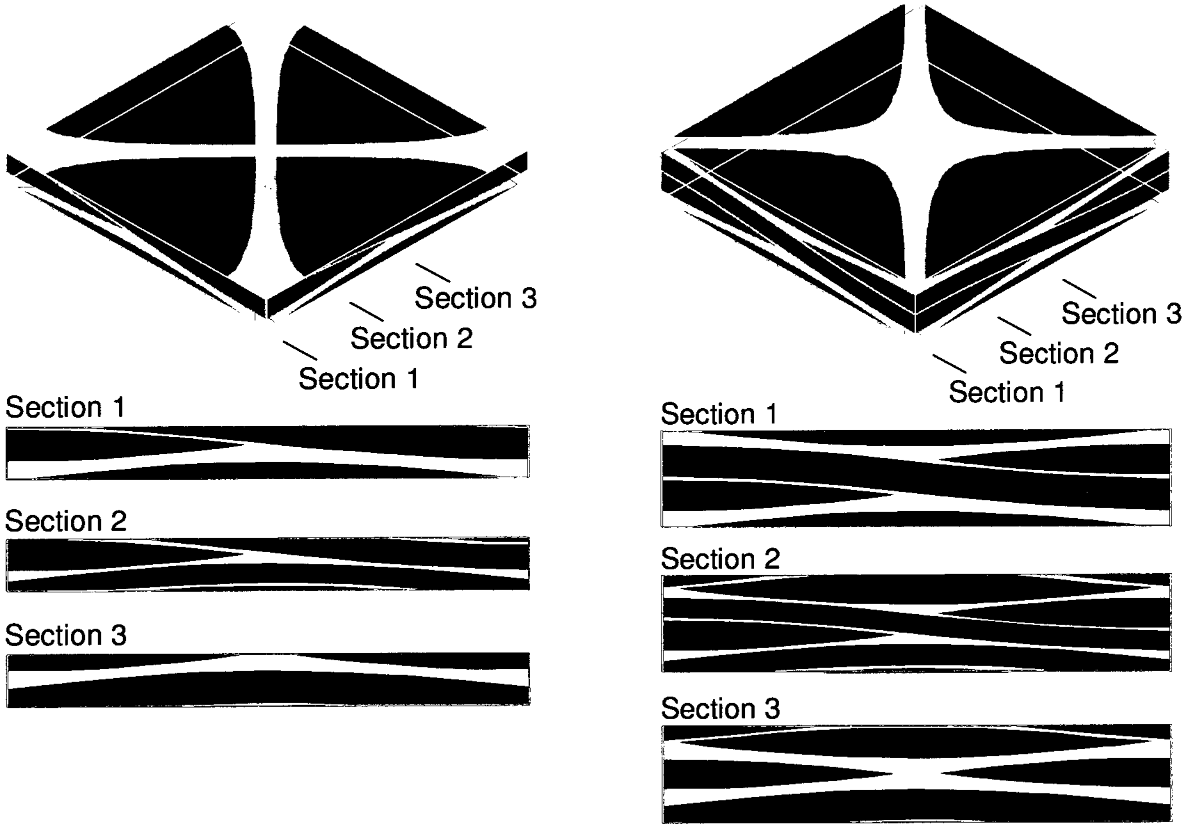

Figure 4.41: 3D and section views of geometric models WR S2 10 (left) and WR S2 11(right)

4.7.2 Woven Reinforcements Stage 2: Results

Predicted thermal conductivity data for stage 2 appear in Table 4.10. In-plane and transverse conductivities get progressively larger in models WR S2 1, WR S2 2 and WR S2 3. This reflects the progressive reduction of the relative importance of the resin volumes, and indicates that correct values representing a thicker laminate would still be larger than those reached with model WR S2 3. Similarly, conductivity values are larger for model WR S2 5 than for model WR S2 4 for the same reason. Conductivities for models WR S2 4 and WR S2 5 were lower than for their WR S2 1 and WR S2 2 equivalents as the yarn section height was reduced but gap height was not.

Table 4.10: Results for woven reinforcements, stage 2

Simulation	Parameters							
	Laminating sequence	Mid-plane cut outer layers	Unit cell thickness (mm)	Yarn section height (mm)	Nominal fibre volume fraction	Actual fibre volume fraction	Unit cell thermal conductivity [W/mK]	
							In-plane	Transverse
WR S2 1	[(0/90)]	no	0.311	0.136	50.3%	42.3%	2.033	0.345
WR S2 2	$[(0/90)]_2$	no	0.531	0.136	56.6%	47.5%	2.308	0.371
WR S2 3	$[(0/90)]_3$	no	0.751	0.136	59.7%	50.2%	2.426	0.386
WR S2 4	[(0/90)]	no	0.227	0.093	45.9%	38.6%	1.891	0.322
WR S2 5	$[(0/90)]_2$	no	0.387	0.093	52.0%	43.7%	2.191	0.341
WR S2 6	[(0/90)/(45/-45)]	no	0.622	0.136	47.3%	39.7%	1.916	0.325
WR S2 7	[(0/90)/(45/-45)/ (45/-45)/(0/90)]	no	1.153	0.136	53.1%	44.6%	2.164	0.347
WR S2 8	[(0/90)/(45/-45)]	no	0.454	0.093	43.1%	36.2%	1.855	0.305
SW S2 9	[(0/90)/(45/-45)/ (45/-45)/(0/90)]	no	0.840	0.093	48.5%	40.8%	2.136	0.324
WR S2 10	$[(0/90)]_2$	yes	0.311	0.136	72.7%	72.7%	-	0.484
WR S2 11	$[(0/90)]_3$	yes	0.467	0.136	61.1%	61.1%	-	0.493

The above points clearly to the importance of resin volumes and resin gaps in FE-based models. The results for model WR S2 6 are relatively close to those of model WR S2 1, which is expected as their fibre volume fraction is also close, and the relative presence of gaps is similar. The reason behind the slightly different values of *Vf* and transverse conductivities have to do with the lack of periodicity of the 45/-45 layer in the unit cell; had the boundaries been cut differently, larger values of *Vf* and *kz* would have been obtained. This result points to the variability inherent to such simulations; experimental measurements performed at the same scale would in all likelihood show similar variability as the reinforcement is not purely periodic. Results for model WR S2 7 are larger than those of model WR S2 6, and they are between those obtained from models WR S2 1 and WR S2 2; this was expected, again from the relative presence of resin volumes and gaps in the different unit cells. Values for models WR S2 8 and WR S2 9 are lower than those obtained for models WR S2 6 and WR S2 7, because of the thinner yarns combined with vertical inter-yarn gaps having the same thickness. The relatively low k_z = 0.345 W/mK obtained from model WR S2 1 can be traced to the resin volumes in the domain and low composite V_f. Models WR S2 10 and WR S2 11 were created to address this, although software issues prevented the specification of yarn orientations in these 2 models. Transverse yarn properties were used and the in-plane thermal conductivities of unit cells were not calculated. Values obtained for the transverse through-thickness thermal conductivity were significantly larger at k_z = 0.484 W/mK and 0.493 W/mK. They show good consistency, and they highlight once again the strong effect of resin volumes. In comparison to experimental values they remain low; this can be traced to resin-rich zones between individual layers that remain too large despite of correct V_f and V_{fy} values.

5 Discussion

The thermal conductivity of carbon fibres varies widely. Values between 8 W/mK and 11 W/mK are reported for room-temperature axial conductivity of PAN-based fibres such as those used in this work; the effect of temperature is limited. Very limited information is available in terms of transverse fibre conductivity, which is generally extracted from axial data with various models which introduce additional variability. Finding data to comparable to specific laminates such as the ones studied in this thesis is improbable.

More than 750 directional thermal conductivity measurements were collected for materials made from 2 different carbon fibres, AS4 and T300, various lamination sequences, 2 manufacturing methods and 3 separate material configurations: unidirectional prepreg tape, non-woven textile and woven textile reinforcement. Variability levels are quantified; good repeatability was obtained in most cases. For composites, variability up to ±12.9% was observed in experimental values obtained for each given property and material; it was lower than ±5% in most cases and lower than ±2% in more than half of cases. Differences between values obtained for similar laminates (1 and 2, 7 and 8 or 10 and 11) or k_z values for laminates made of the same material could be explained by differences in panel thickness only in some cases. Variability was present but overall repeatability was generally good. The author found no commercially available equipment capable of measuring directional in-plane and transverse thermal conductivity using specimens removed from the same laminate. Measurements of directional conductivity from the modified configuration of the THISYS device succeeded as shown by excellent agreement of k_{90} and k_z values for both laminates 1 and 2, intermediate values of k_0 and k_{90} obtained for laminates 5 and 6, credible orthotropy ratios, and by the fact that the effect of reinforcement structure was observed for laminates 7 and 8. Alternative commercially available measurement systems would require the manufacture of very costly and time consuming specimens making the effort impractical.

A range of diverse predictive models were applied to predict k_z and k_{ci} for the range of reinforcement architecture complexity provided by materials 1, 2 and 3. In the case of UD tape prepregs such as material 1 the lamination sequence does not affect k_z. The through-thickness conductivity can be measured and if an available value of axial fibre conductivity can be confidently applied the rule of mixtures and the lamination theory can be used to predict in-plane directional conductivity values of laminates within reasonable variability margins. This is not equally true in the case of textile reinforcements as found in materials 2 and 3 where reinforcement structure affects conductivity. CLT was successfully used to predict k_{ci} of prepreg tape laminates. Used in combination with CLT, ROM and models used for the prediction of thermal conductivity in aligned assemblies of fibres, such as Clayton's and Nielsen's model, can be used to back calculate yarn properties.

FE simulations were capable of detecting variations in thermal conductivity due to subtle changes in geometry. For material 3, non-woven unidirectional and cross-ply unit cell simulations results demonstrate that k_z is not sensitive to reinforcement geometry or lamination sequence based on the minimal variability. There is a similar limited variability in k_z measured experimentally. These observations are supported by the widespread success of published models for the prediction of k_z, regardless of complexity [8-10, 29]. It should be noted that reinforcement geometry has a much greater impact on other properties such as permeability [71]. As would be expected, lamination sequence has a major effect on k_{ci} for non-woven reinforcements. Non-woven models simulated k_z values ranged from 0.46 to 0.52 W/mK compared to the average experimental value of 0.48 W/mK. For k_z predictions, it is clear that modeling of the structure is needed; but what is most important is the representation of the yarn gaps. In these models the geometry is simplified and accurate results are still achievable. Also, it is clear that modeling multilayer is not needed. The non-woven predicted k_{ci} values for unidirectional laminates ranged from 5.25 to 5.38 W/mK along the direction of the yarns and 0.49 to 0.50 across the yarns, compared to 4.86 and 0.36 W/mK, respectively. The non-woven simulated k_{ci} value for a cross-ply laminate was 3.25 W/mK compared to average experimental measurements of 2.79 W/mK.

Woven unit cell models of material 2 were created with realistic reinforcement geometric parameters obtained from experimental measurements of micrographs. More accurate models were developed by cutting the upper and lower faces at mid-yarn thereby increasing V_f. Woven unit cell simulation results indicate that the cut models were the most accurate predictors of k_z. No in-plane results for the cut models are available. The non-cut models identified the effect of the number of plies, degree of nesting, and lamination sequence on V_f for both k_{ci} and k_z predictions. Woven models simulated k_z values of 0.32 to 0.49 W/mK compared to experimental measurements of 0.60 W/mK. For this particular case, a series model predicts 0.63 W/mK.

Generic woven textile models are able to detect trends but cannot predict accurate directional thermal conductivity values for high V_f materials. For the case of the woven geometry presented, simply accounting for the through-thickness inter-yarn gaps yields an accurate prediction. The model of Ning and Chou [29] is also very simplified and does account for these gaps but will work only with accurate reinforcement measurements. More advanced models such as Dasgupta's [7] also work given accurate geometries, but creating the models is time consuming. The micrographs of materials 2 and 3 in section 3.2.4 feature irregular, non-idealized geometry that cannot be accurately modeled with a single unit cell. Reaching high V_f in a unit cell model of a woven composite whilst keeping yarn fibre volume fraction V_{fy} at a reasonable value requires intricate nesting patterns, as it does in real materials. Yarns paths cannot be described by simple mathematical functions and regular cross-section shapes, as is the case with published unit cell models. In a nested laminate unit cell, geometry varies from point to point in the material, inducing variability in local thermal conductivity.

The NRC-IAR conductive heating program has benefitted considerably from this thesis work. The literature review provided further insight into the problem of textile reinforcement meso-scale modelling as well as the state of carbon fibre thermal conductivity data available. The Hukseflux THASYS and THISYS unit in the directional configuration permit the accurate and highly repeatable measurement of directional thermal conductivity. The collection of thermal conductivity measurements provides a basis of thermal modelling properties for the three most commonly used aerospace C/E PMC structures. The successful use of classical lamination theory for modelling tape prepregs was presented. Using FE was straightforward and reliable in predicting the directional thermal conductivities of non-woven textile reinforced composites. FE limitations and insensitivity of thermal conductivity to certain changes in geometric parameters suggest that simpler predictive models could be used to predict directional thermal conductivities in composites with more complex textile reinforced architectures. Finite element methods may still be the preferred modelling solution. With accurate k_{cd} measurements on laminates, FE models are capable of detecting relative change or trends in k_{cd} due to subtle changes in reinforcement configuration. In order to improve geometric models, scripts could be written to develop a wide range of models with a set of varying parameters. Post-statistical analysis would determine the properties of an average unit cell which could then be used in a macro scale model. Micro CT may also play a part in the development of more accurate geometries in the future.

REFERENCES

1. D. Raizenne, S. Hind and J. Poupore, *Proc. 6th Joint Canada-Japan Workshop for Composites*, Canadian Association for Composite Structures and Materials (2006).
2. L. Piraux, B. Nysten, A. Haquenne, J.P. Issi, M.S. Dresselhaus, and M. Endo, *Solid State Commun.*, 50, 697 (1984).
3. B. Nysten, L. Piraux, and J.P. Issi, *J. Phys. D: Appl. Phys.*, 18, 1307 (1985).
4. J. Heremans and C.P. Beetz Jr., *Phys. Rev. B.*, 32, 1981 (1985).
5. E.P. Scott and J.V. Beck, *J. Compos. Mater.*, 26, 132 (1992).
6. J.D. Thornburg and C.D. Pears, *ASME Paper 65*-WA/HT-4 (1965).
7. A. Dasgupta and R.K. Agarwal, *J. Compos. Mater.*, 26, 2736 (1992).
8. A. Dasgupta, R.K. Agarwal, and S.M. Bhandarkar, *Compos. Sci. Technol.*, 56, 209 (1996).
9. D. Bigaud, J.M. Goyheneche, and P. Hamelin, *Compos. Part A: Appl. S.*, 32, 1443 (2001).
10. Y. Gowayed and J.C. Hwang, *Compos. Eng.*, 5, 1177 (1995).
11. http://www.cytec.com
12. W. Johnson and W. Watt, *Nature*, 215, 384 (1967).
13. R. Moreton, W. Watt and W. Johnson, *Nature*, 213, 690 (1967).
14. H. Lee and R. Taylor, *Carbon*, 13, 521 (1975).
15. L. Piraux, B. Nysten, A. Haquenne and J.P. Issi, *Solid State Commun.*, 50, 697 (1984).
16. B. Nysten, L. Piraux and J.P. Issi, *J. Phys. D: Appl. Phys*, 1 8, 1307 (1985).
17. J. Heremans and C.P. Beetz, Jr., *Physical Review B*, 32, 1981 (1985).
18. J. Heremans, I. Rahim and M.S. Dresselhaus, *Physical Review B*, 32, 6742 (1985).
19. B. Nysten, J.P. Issi, R. Barton, Jr., D.R. Boyington and J.G. Lavin, *Physical Review B*, 44, 2142 (1991).
20. N.C. Gallego, D.D. Edie, B. Nysten, J.P. Issi, J.W. Treleaven and G.V. Deshpand, *Carbon*, 38, 1003 (2000).
21. N.C. Gallego and D.D. Edie, *Composites: Part A*, 32, 1031 (2001).
22. J.G. Lavin, D.R. Boyington, J. Lahijani, B. Nysten and J.P. Issi, *Carbon*, 32, 1045 (1994).

23. B.W. James, G.H. Wostenholm, G.S. Keen and S.D. Mclvor, *J. Phys. D: Appl. Phys.*, 20, 261 (1987).

24. J. Heremans, C.P. Beetz, Jr., I. Rahim and M.S. Dresselhaus, *Therm. Cond.*, 331 (1988).

25. J.H. Barkyoumb, D.J. Land and J.N. Kidder, Jr., *Mat. Res. Soc. Proc.*, 305, 117 (1993).

26. X. Zhang, S. Fujiwara and M. Fujii, *International Journal of Thermophysics*, 21, 965 (2000).

27. D. Rochais, H. Le Hou¨edec, F. Enguehard, J. Jumel and F. Lepoutre, *J. Phys. D: Appl. Phys.*, 38, 1498 (2005).

28. T. Yamane, S. Katayama, M. Todoki and I. Hatta, *J. Wide Band. Mater.*, 7 , 294 (2000).

29. Q.G. Ning and T.W. Chou, *J. Compos. Mater.*, 29 , 2280 (1995).

30. J.W. Klett and D.D. Edie, *Carbon*, 33 , 1485 (1995).

31. J.R. Gaier, Y. Yodervandenberg, S. Berkebile, H. Stueben and F. Balagadde, *Carbon*, 41 , 2187 (2003).

32. C. C. Chamis, *Proc. 39th Annual Conference, Reinforced Plastics/Composites Institute*, Society of Plastics Industry Inc., Session 11-D: 1-16 (1984).

33. J.J. Pigliacampi, *Engineered Materials Handbook, Vol. 1: Composites*, ASM International, Metals Park, Ohio, 54 (1984).

34. T. Ishikawa, *Heat Transfer – Jap. Res.*, 9 , 41 (1980).

35. A. Salazar and A. Sánchez-Lavega, *Int. J. Thermophys.*, 19 , 625 (1998).

36. M.W. Pilling, B. Yates, M.A. Black and P. Tattersall, *J. Mater. Sci.*, 14 , 1326 (1979).

37. B.W. James, G.H. Wostenholm, G.S. Keen and S.D. McIvor, *J. Phys. D: Appl. Phys.*, 20 , 261 (1987).

38. http://www.cytec.com/

39. http://www.grafil.com/

40. http://www.toraycfa.com/

41. D.J. Radcliffe and H.M. Rosenberg, *Cryogenics*, 22 , 245 (1982).

42. Rayleigh, Lord, *PhilMag*, 34, 481 (1892).

43. G.S. Springer and S.W. Tsai, *J. Compos. Mater.*, 1 , 166. (1967).

44. G.E. Zinsmeister and K.S. Purohit, *J. Composite Materials*, 4, 278 (1970).
45. E. Behrens, *J. Compos. Mater.*, 2 , 2 (1968).
46. J. Donea, *J. Compos. Mater.*, 6 , 262 (1972).
47. W.A. Clayton, *AIAA Paper* 71-380 (1971).
48. L.E. Nielsen, *Ind. Eng. Chem. Fund.*, 13, 17 (1974).
49. R.C. Progelhof, J.L. Throne and R.R. Ruetsch, *Polym. Eng. Sci.*, 16 , 615 (1976).
50. R. Pal, *Compos. Part A-Appl. S.,* 39 , 718 (2008).
51. R.H. Knibbs and J.B. Morris, *Composites*, 5, 209 (1974).
52. M. W. Pilling, B. Yates, M. A. Black, and P. Tattersall, *Journal of Materials Science*, 14, 1326 (1979).
53. S.W. Tsai and H.T. Hahn, *Introduction to Composite Materials*. Technomic Publishing, Pennsylvania, USA (1980).
54. Composite Materials Handbook, MIL-HDBK-17E
55. J.T. Mottram and R. Taylor, *Comp. Sci. Technol.*, 29 , 211 (1987).
56. J.P. Holman, *Heat Transfer*, McGraw Hill, New York, 1997.
57. G.E. Zinmeister and K.S. Purohit, *J. Compos. Mater.*, 4, 278 (1970).
58. THA01 Thin heater Apparatus - USER MANUAL, version 050, Hukseflux Thermal Sensors, http://www.hukseflux.com, The Netherlands.
59. ASTM C1114 - 06 Standard Test Method for Steady-State Thermal Transmission Properties by Means of the Thin-Heater Apparatus, 2006.
60. ASTM D5470 - 06 Standard Test Method for Thermal Transmission Properties of Thermally Conductive Electrical Insulation Materials, 2006.
61. THISYS Apparatus thermal conductivity measurement of thin samples - THISYS manual, version 0512, Hukseflux Thermal Sensors, http://www.hukseflux.com, The Netherlands.
62. M. Zou, B. Yu, D and Zhang, Y. Ma, *J. of Heat Trans.*, 125, 980 (2003).
63. D. Raizenne, S. Hind and J. Poupore, *Proc. 6th Joint Canada-Japan Workshop for Composites*, Canadian Association for Composite Structures and Materials (2006).
64. S. Hind and F. Robitaille, *Proc. 9th International Conference on Textile Composites*, TEXCOMP-9 (2008)

65. S. Hind, D. Raizenne and F. Robitaille, *Proc. 8th International Conference on Textile Composites*, TEXCOMP-8 (2006)

66. http://texgen.sourceforge.net

67. http://www.fluent.com

68. http://www.patran.mscsoftware.com

69. http://www.mscnastran.com

70. M. Duval, "Investigation and Modelling of the Heat Transfer Process in Carbon Fibre/Epoxy Composite Tools" MASc, Mechanical and Aerospace Engineering, Carleton University, Ottawa, 2005.

71. F. Robitaille, "Concurrent Predictions of Flow, Thermal and Structural Properties for Unidirectional and Bidirectional Non-Woven Textile Composites," *submitted to Comp A*, 2008.

Appendix A – isotropic material conductivity and specimen average thickness data

Material	Thickness (mm) for THA and THI	THASYS Dimensions (mm)	Thermal k (W/mK)	THISYS (Mod) Dimensions (mm)	Thermal k (W/mK)
Teflon	6.223	110 x 70	0.406	110x22	0.188
	6.223		0.405	with foam	0.190
	6.223		0.405		0.189
	6.223		0.406		0.187
	6.223		0.406		0.187
	6.223		0.407		0.184
			0.406		0.188
Teflon	6.223	110 x 70	0.406	110x22	0.421
	6.223		0.406	no foam	0.431
	6.223		0.406		0.457
	6.223		0.406		0.464
	6.223		0.406		0.465
	6.223		0.406		0.469
	6.223		0.406		0.469
Polycarbonate 1	3.211	110 x 70	0.202	110x22	0.117
	3.211		0.202	with foam	0.135
	3.211		0.202		0.141
	3.211		0.202		0.134
	3.211		0.202		0.138
	3.211		0.203		0.132
	3.211		0.203		0.137
	3.211		0.203		0.136
			0.202		0.134
Polycarbonate 1	3.211	110 x 70	0.203	110x22	0.441
	3.211		0.203	no foam	0.439
	3.211		0.203		0.435
	3.211		0.203		0.431
	3.211		0.203		0.430
	3.211		0.203		0.462
Polycarbonate 2	5.809	110 x 70	0.189	110x22	0.113
	5.809		0.189	with foam	0.115
	5.809		0.189		0.117
	5.809		0.189		0.106
	5.809		0.189		0.122
	5.809		0.189		0.119
	5.809		0.189		0.118
			0.189		0.116

Silicone	1.525	110 x 70	0.224	110x22	0.118
	1.525		0.224	with foam	0.117
	1.525		0.224		0.117
	1.525		0.224		0.141
	1.525		0.224		0.124
			0.224		0.123
Copper Epoxy	3.350	110 x 70	0.773	110x22	0.259
	3.350		0.774	with foam	0.253
	3.350		0.774		0.253
	3.350		0.774		0.253
			0.774		0.255
HDPE	6.250	110 x 70	0.527	110x22	0.214
	6.250		0.527	with foam	0.213
	6.250		0.527		0.212
			0.527		0.213
Glass 1	4.770	110 x 70	0.991	110x22	0.339
	4.770		0.991	with foam	0.341
	4.770		0.991		0.343
			0.991		0.341
Glass 2	2.380	110 x 70	0.976	110x22	0.326
	2.380		0.977	with foam	0.327
	2.380		0.977		0.317
			0.977		0.323
Stainless Steel	6.556	110 x 70	10.010	110x22	2.918
	6.556		10.025	with foam	2.882
	6.556		10.076		2.901
			10.037		2.900

Appendix B – material data sheets

1. unidirectional prepreg tape AS4/3501-6 from Hexcel
2. plain weave prepreg HexPly F263 from Hexcel
3. unidirectional woven fabric style 1152 from Fabric Development impregnated with Mia-epoxy 100 resin and hardener 95
4. unidirectional prepreg tape Hexply 6376 from Hexcel

3501-6 Epoxy Matrix

High Strength, Damage-Resistant, Structural Epoxy Matrix

Product Data

Description

3501-6 is an amine cured epoxy resin system supplied with unidirectional or woven carbon or glass fibers. Typical reinforcement is continuous AS4 carbon filaments. 3501-6 was developed to operate in a temperature environment of up to 350°F (177°C). AS4/3501-6 is recommended for general purpose structural applications.

Features

- Service Temperature up to 350°F (177°C)
- Damage-Resistant System
- 350°F (177°C) Cure

Neat Resin Properties

Density	1.265 gm/cc
T_g dry 6 hr 350°F (177°C) cure	410°F (210°C)
T_g wet 6 hr 350°F (177°C) cure	304°F (151°C)
Tensile strength	6.6 ksi
Tensile modulus	0.615 msi
Tensile elongation	1.10%
Shear strength	7.0 ksi
Shear elongation to failure	1.95%
Flexural modulus	484 ksi
Poisson's ratio	36.50%
Strain energy release rate, G_{1C}	0.733 in-lb/in^2
Gel time @ 350°F (177°C)	4–10 minutes
Minimum viscosity	4.0 Poise
Coefficient of thermal expansion (CTE)	
RT–163°F (RT–73°C)	21.1 x 10^{6}/°F
160–250°F (71–121°C)	24.4 x 10^{6}/°F
250–350°F (121–177°C)	33.3 x 10^{6}/°F

3501-6 Epoxy Matrix *Product Data*

Physical Properties

		AS4	A185CSW	A193P	A280-5H	A370-8H
Prepreg	% Resin content	32–45	32–45	32–45	32–45	32–45
	Areal weight GSM	150	185	193	280	370
	% Volatiles	1.5 max	1.5 max	1.5 max	1.5 max	1.5 max
	% Flow	12-32	12-32	12-32	12-32	12-32
	Gel time @ 350°F (177°C)	6–12	6–12	6–12	6–12	6–12
Laminate	Cured thickness per ply (in)	5.2 mils	7.5 mils	7.7 mils	10.0 mils	14.0 mils
	Fiber volume	62%	58%	58%	58%	58%

Mechanical Properties

Property	Temp °F (°C)	Condition	AS4	A185CSW	A193P	A280-5H	A370-8H
0° Tensile strength, ksi	RT	Dry	310.0	120.0	110.0	120.0	120.0
0° Tensile modulus, msi	RT	Dry	20.5	10.0	10.0	10.0	10.0
0° Compression strength, ksi	RT	Dry	250.0	120.0	125.0	130.0	125.0
0° Flexural strength, ksi	RT	Dry	260.0	10.0	9.0	9.0	9.0
0° Flexural strength, ksi	350 (177)	Dry	185.0	-	-	150.0	130.0
0° Flexural modulus, msi	RT	Dry	18.5	-	-	-	-
0° Flexural modulus, msi	350 (177)	Dry	18.0	-	-	10.0	9.0
Short beam shear, psi	RT	Dry	18,500	-	-	-	-
Short beam shear, psi	350 (177)	Dry	9,500	12,000	12,000	12,000	12,000

Cure Cycle

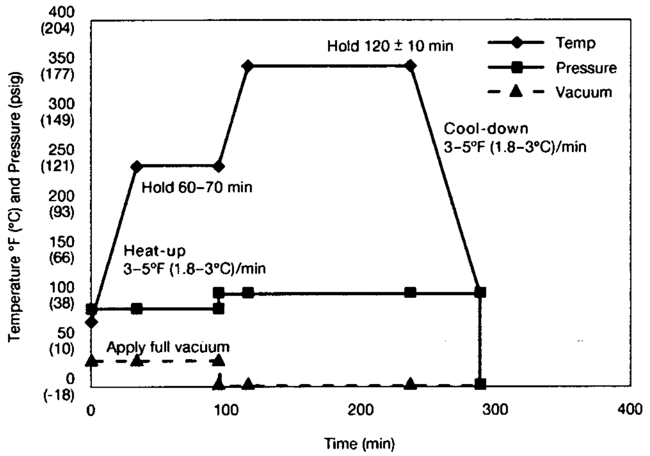

Cure Procedure

Autoclave

1. Apply full vacuum and 85 psig pressure.
2. Heat at 3-5°F (1.8-3°C)/minute to 240°F (116°C).
3. Hold at 240°F (116°C) for 60-70 minutes.
4. Raise pressure to 100 psig; vent vacuum.
5. Raise temperature to 350°F (177°C) at 3-5°F (1.8-3°C)/minute.
6. Hold at 350°F (177°C) for 120 ± 10 minutes.
7. Cool at 2-5°F (1.2-3°C) to 100°F (38°C) and vent pressure.

Note: Straight-up cure cycle may be used.

3501-6 Epoxy Matrix *Product Data*

Handling and Safety Precautions

Hexcel recommends that customers observe established precautions for handling resins and fine fibrous materials. Operators working with this product should wear clean, impervious gloves to reduce the possibility of skin contact and to prevent contamination of the material.

Material Safety Data Sheets (MSDS) have been prepared for all Hexcel products and are available to company safety officers on request from your nearest Hexcel Sales Office.

Storage

3501-6 prepreg should be sealed in a polyethylene bag and refrigerated, preferably below 32°F (0°C). Following removal from refrigerated source, allow the prepreg to reach room temperature before opening the polyethylene bag to prevent moisture condensation.

Shelf Life

12 months at 0°F (−18°C)

4 months at 40°F (4°C)

10 days at 70°F (21°C)

Shipping

Prepreg is generally shipped in a sealed polyethylene bag in refrigerated transportation or in containers with dry ice.

Disposal of Scrap

Disposal of this material should be in a landfill in accordance with state and federal regulations.

Important

Hexcel Corporation makes no warranty, whether expressed or implied, including warranties of merchantability or of fitness for a particular purpose. Under no circumstances shall Hexcel Corporation be liable for incidental, consequential, or other damages arising out of a claim from alleged negligence, breach of warranty, strict liability or any other theory, through the use or handling of this product or the inability to use the product. The sole liability of Hexcel Corporation for any claims arising out of the manufacture, use, or sale of its products shall be for the replacement of the quantity of this product which has proven to not substantially comply with the data presented in this bulletin. Users should make their own assessment of the suitability of any product for the purposes required. The above supercedes any provision in your company's forms, letters, or other documents.

Printed on recycled paper

(4 98)

HexPly® F263

Resin Systems for Advanced Composites

Product Data

Description

HexPly® F263 is a structural, heat resistant epoxy resin formulated for excellent translation of high modulus carbon fiber properties in typical aerospace applications. HexPly® F263 is a high temperature, aerospace grade, epoxy resin for HMG with a 350°F (177°C) core.

Features

Uncured

- Good Tack and Drape to Assist Layup and Assembly
- Adaptable for Use on Various Fiber and Weave Combinations
- Moderate Viscosity During Cure
- Resin System Lends Itself to a Simple Cure Cycle
- Long Shelf Life

Cured

- High Strength Retention: -65°F to 350°F (-54° to 177°C)
- Excellent Translation of Carbon Fiber Properties
- Self-Extinguishing When Tested per F.A.R. 25.853

Neat Resin Properties

Specific gravity	1.267
T_g wet	271°F (133°C)
T_g dry	370°F (188°C)
Equilibrium moisture absorption	4.8%
Linear coefficient of thermal expansion	2.9 x 10^{-5} in/in/°F (1.6 x 10^{-5} cm/cm/°C)
Tensile strength	10.9 ksi (75 MPa)
Tensile modulus	0.62 msi (4.27 GPa)
Tensile strain	2.4%
Fracture toughness, K_{1C}	0.55 ksi $\sqrt{in}$ (0.60 MPa $\sqrt{m}$)
Strain energy release rate, G_{1C}	0.43 in-lb/in^2 (0.075 kJ/m^2)
Gel time @ 350°F (177°C)	2–9 min

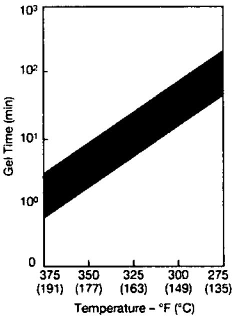

Gel Time vs Temperature

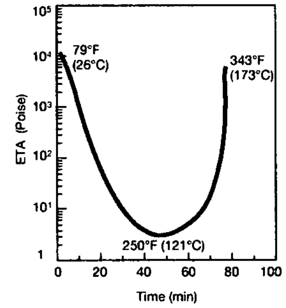

Rheometrics Curve of F263
3.3°F (2°C)/min, 50% Strain, 10 rad/sec, RDS-7700, 50 mm Plates

HEXCEL

HexPly® F263 *Product Data*

Availability

Form	Hexcel Designation	Fiber	Fiber Areal Wt. g/m^2	Weave	Count Warp x Fill	Available Widths Standard Width, in (cm)
Carbon Fabric	W3T282-42"-F263 W3C282-42"-F263	T300 Celion	194	Plain	12.5 x 12.5	42" (106.7)
	F3T584-42"-F263 F3C584-42"-F263	T300 Celion	370	8 Harness Satin	24 x 24	42" (106.7)
Glass Fabrics	120-38"-F263	450-1/2	115	Crowfoot MIL-C-9084 TYIII	60 x 58	38", 44", 50", 60" (96.5, 111.8, 127, 152.4)
	1581-38"-F263	150-1/2	303	8 Harness Satin MIL-C-9084 TYVIIIA	57 x 54	38", 44", 50", 60", 72" (96.5, 111.8, 127, 152.4, 182.9)
	7781-38"-F263	75-1/0	303	8 Harness Satin MIL-C-9084 TYVIIIA	57 x 54	38", 44", 50", 60", 72" (96.5, 111.8, 127, 152.4, 182.9)
Carbon Tapes	T_095-12"-F263	Various	95	n/a	n/a	12", 3"-24" (30.5, 7.6-61)
	T_145-12"-F263	Various	145			
	T_190-12"-F263	Various	190			

Note: Alternatively, carbon and glass fabric weaves may be used with the HexPly® F263 Resin System. Also, HexPly® F263 carbon tapes may be produced with various carbon fiber types and tow sizes. In designating carbon tape, the second digit represents tow size and the third digit represents fiber source. Consult your nearest Hexcel Sales Representative for additional information.

Physical Properties

	Property	Carbon Fabrics		Carbon Tapes			Glass Fabrics	
Prepreg	Material description	W3T282 or W3C282	F3T584 or F3C584	95 g/m^2	145 g/m^2	190 g/m^2	120	7781
	% Flow @ 350°F, 50 psi (177°C, 345 kPa)	9–22	9–22	11–24	11–24	11–24	15–30	10–30
	% Resin content (dry)	38–42	35–39	35–39	35–39	35–39	42–48	36–40
Laminate	Cured thickness per ply – in (cm)	0.0072 (0.018)	0.0135 (0.034)	0.0039 (0.010)	0.0059 (0.015)	0.0078 (0.020)	0.0045 (0.011)	0.010 (0.025)
	% Fiber volume	61	62	55	55	55	38	45

Mechanical Properties (Autoclave Cure)

Property	Temp	Carbon Fabrics		Carbon Tapes			Glass Fabrics	
	°F (°C)	W3T282	W3T584	T3T095	T3T145	T3T190	120	7781
Tensile strength, ksi (MPa)	75 (24)	82.6 (570)	88.4 (610)	180.8 (1247)	197.5 (1362)	196.3 (1353)	53.4 (368)	66.9 (461)
Tensile modulus, msi (GPa)	75 (24)	8.81 (60.7)	9.24 (63.7)	19.55 (134.8)	19.19 (132.3)	19.12 (131.8)	3.47 (23.9)	4.30 (29.7)
Tensile strain	75 (24)	9,762	10,024	9,267	10,345	10,142		
Tensile strength, ksi (MPa)	350 (177)	78.5 (541)	84.0 (579)		187.6 (1260)		38.1 (263)	55.8 (385)
Tensile modulus, msi (GPa)	350 (177)	8.37 (57.7)	8.78 (60.5)		18.23 (125.7)		2.94 (20.3)	3.46 (23.9)
Compression strength, ksi (MPa)	75 (24)	94.0 (648)	96.6 (666)	206.0 (1420)	193.3 (1333)	175.8 (1212)	68.7 (474)	71.2 (491)
Compression modulus, msi (GPa)	75 (24)						3.41 (23.5)	4.36 (30.1)
Compression strength, ksi (MPa)	160 (71)	83.4 (575)	84.9 (585)	182.7 (1260)	167.4 (1154)	171.8 (1185)		
Compression strength, ksi (MPa)	350 (177)						50.0 (345)	51.2 (353)
Compression modulus, msi (GPa)	350 (177)						3.11 (21.4)	3.83 (26.4)
Short beam shear, ksi (MPa)	–65 (–54)	10.50 (72)	9.46 (65)	18.92 (130)	17.99 (124)	17.76 (122)		
Short beam shear, ksi (MPa)	75 (24)	10.72 (74)	10.40 (72)	16.06 (111)	16.16 (111)	15.92 (110)		
Short beam shear, ksi (MPa)	270 (132)	8.05 (56)	6.99 (48)	10.87 (75)	10.48 (72)	10.96 (76)		
Short beam shear, ksi (MPa)	350 (177)	6.73 (46)	6.88 (47)		9.82 (68)			
Interlaminar shear, ksi (MPa)	75 (24)						2.99 (21)	3.37 (23)
Interlaminar shear, ksi (MPa)	350 (177)						2.24 (15)	2.61 (18)

All mechanical property values are based on the calculated fiber volume found on the previous table.

Reported property values are averages to which no statistical assurance should be associated. While Hexcel believes that the data contained herein are factual, the data are not to be taken as a warranty or representation for which Hexcel assumes legal responsibility. They are offered solely for your consideration, investigation, and verification.

Cure Cycle

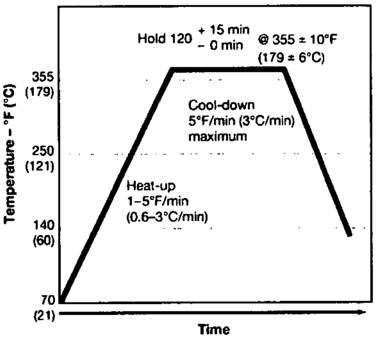

Cure Procedure

A. Apply vacuum of 22 inches (74 kPa) Hg minimum.

B. Apply 85 + 15 – 0 psig (586 + 103 – 0 kPa) pressure for laminates.

C. Apply 45 + 15 – 0 psig(310 + 103 – 0 kPa) pressure for sandwich.*

D. Vent vacuum bag to atmosphere when pressure reaches 20 psi (138 kPa).

E. During cool-down when the part temperature falls below 140°F (60°C), pressure can be relieved and the test panel removed from the autoclave and debagged.

* Typical for HRH 10–1/8-3.0 honeycomb.

Storage

HexPly® F263 prepreg should be sealed in a polyethylene bag and refrigerated, preferably below 32°F (0°C). Following removal from refrigerated storage, allow the prepreg to reach room temperature before opening the polyethylene bag to avoid moisture condensation. Shelf life: 6 months @ 0°F (–18°C), 3 months @ 40°F (4°C).

Shipping

Prepreg fabric and tape are generally shipped in sealed polyethylene bags in insulated containers packed with dry ice.

Disposal of Scrap

Disposal of this material should be in a secure landfill in accordance with state and federal regulations.

Handling and Safety Precautions

Hexcel recommends that customers observe established precautions for handling epoxy resins and fine fibrous materials. Operators working with this product should wear clean, impervious gloves to reduce the possibility of skin contact and to prevent contamination of the material.

Airborne graphite as a result of sawing, grinding, etc., can present electrical shorting hazards; refer to NASA Technical Memorandum 78652. Material Safety Data Sheets (MSDS) have been prepared for all Hexcel products and are available to company safety officers on request from your nearest Hexcel Sales Office.

Important

For more Information

Hexcel is a leading worldwide supplier of composite materials to aerospace and other demanding industries. Our comprehensive product range includes:

- Carbon Fiber
- RTM Materials
- Honeycomb Cores
- Continuous Fiber Reinforced Thermoplastics
- Carbon, Glass, Aramid and Hybrid Prepregs
- Structural Film Adhesives
- Honeycomb Sandwich Panels
- Special Process Honeycombs
- Reinforced Fabrics

For US quotes, orders and product information call toll-free 1-800-688-7734. For other worldwide sales office telephone numbers and a full address list please click here: **http://www.hexcel.com/contact/salesoffices**.

October 2005

MIA Poxy 100 resin (http://miapoxy.com/)

The MIAPOXY system has at its base a well-formulated epoxy resin called 100. Using this base, you will be able to create many different combinations to suit your requirements. The resin is clear with a slight bluish haze and is low viscosity. You can use two different hardener systems with it, giving you several options for cure time and ambient temperature. The resin has been formulated for ease of use and fast wet-out capabilities. It will work perfectly with fiberglass, wood, metal, honeycomb core, PVC foams, and many other standard materials found in composite structures. The resin can be used as an adhesive, although we recommend you consult our complete line of adhesive products for maximum performance.

MIA hardener 95 (http://miapoxy.com/)

This is the "slow" hardener in the MIAPOXY line. It is recommended for beginners, or simply for people who need more time to work with the product. At room temperature (77° F), it will give you 30–35 minutes of "pot life" or "gel time." This gives you enough time to properly wet out your surface or complete any type of large bonding or gap-filling operation. This longer pot life also allows you to use any type of bubble remover tool, such as an aluminum roller, to make sure your laminate is void free. It, too, is a 4-to-1 mix and light amber in color. It is not intended for use in cold temperatures as the slow reaction could be stopped by the cold. It is, however, very well suited to warm tropical-type climates. Please note that the hotter the ambient temperature, the less time you will have to work with the product.

GEL TIME (4 fl. oz.): 38 minutes at 77° F Mixed Viscosity: 800 cPs
Cure Time: 24 hours at 77° F or 6 hours at 150° F
Compressive Strength: 26,000 psi
Flexural Strength: 39,000 psi
Tensile Strength: 36,000 psi

6376

175℃ curing epoxy matrix

Product Data

Description

6376 is a high performance tough matrix formulated for the fabrication of primary aircraft structures. It offers high impact resistance and damage tolerance for a wide range of high temperature applications.

Benefits and Features

- Excellent toughness and damage tolerance
- Simple straight-up cure cycle
- Controlled matrix flow for ease of processing
- Effective translation of fibre properties
- Good hot/wet properties up to 150℃

Resin Matrix Properties

Rheology

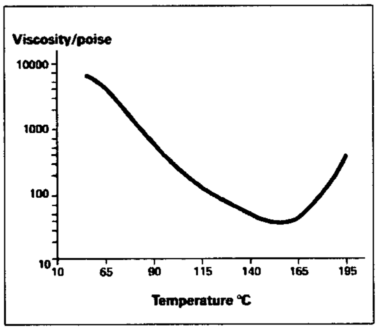

Gel Time

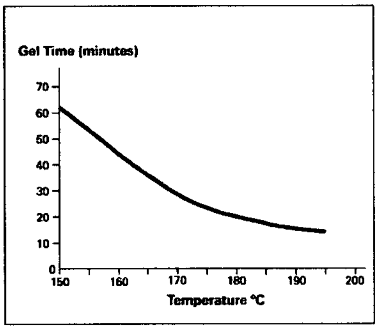

HEXCEL Composites

6376 *Product Data*

Cured Matrix Properties (cured at 175°C)

		Method
Tensile strength	105 MPa	ISO R527 type 1
Tensile modulus	3.60 GPa	ISO R527 type 1
Tensile strain	3.1%	ISO R527 type 1
Flexural strength	144 MPa	ISO 178
Flexural modulus	4.4 GPa	ISO 178
Toughness G_{IC}	432 J/m^2	Tested in accordance with EGF Task Group on Polymers and Composites protocol.
Cured density	1.31 g/cm^3	

Prepreg Curing Conditions

2 hours at 175°C and 700kN/m^2 (7 bar) pressure.

Heat up rate 2°C to 5°C.

Components up to 30 mm thick can be cured without a dwell in the schedule provided that the heat-up rate is not more than 3°C/minute. There is no deterioration in performance after 3 times the recommended cure schedule (verified by interlaminar shear strength tests).

Prepreg Storage Life

- Tack Life @ 23°C 10 days (still processable for up to 21 days).
- Guaranteed Shelf Life @ -18°C 6 months (minimum)

- Storage conditions.
  6376 prepregs should be stored as received in a cool dry place or in a refrigerator. After removal from refrigerator storage, prepreg should be allowed to reach room temperature before opening the polythene bag, thus preventing condensation. (A full reel in its packaging can take up to 48 hours).

Precautions for Use

The usual precautions when handling uncured synthetic resins and fine fibrous materials should be observed, and a Safety Data Sheet is available for this product. The use of clean disposable inert gloves provides protection for the operator and avoids contamination of material and components.

Publication FTA051 (February '97)

Appendix C - experimental thermal conductivity and specimen thickness data

Panel 1

	Specimen	Thickness (mm)	Measurement Direction	Thermal Conductivity (W/mK)								
				#1	#2	#3	#4	#5	#6	#7	Average	Std. Dev.
THASYS (Transverse)	1a/1b	1.472/1.453	transverse	0.810	0.810	0.810					0.810	0.000
	1c/1b	1.469/1.453	transverse	0.804	0.805	0.804					0.804	0.001
	2a/2b	1.487/1.561	transverse	0.714	0.716	0.717					0.716	0.002
	2c/2b	1.603/1.561	transverse	0.694	0.694	0.696					0.695	0.001
	3a/3b	1.583/1.616	transverse	0.687	0.686	0.686					0.686	0.001
	3a/3c	1.583/1.668	transverse	0.670	0.670	0.671					0.670	0.001
										overall	0.730	0.058
THISYS (In-Plane Bulk)	1a	1.472	avg. in-plane	3.191	3.155	3.159					3.168	0.020
	1b	1.453	avg. in-plane	3.215	3.165	3.170					3.183	0.028
	1c	1.469	avg. in-plane	3.136	3.140	3.140					3.139	0.002
										overall	3.163	0.026
	2a	1.487	avg. in-plane	3.296	3.296	3.294					3.295	0.001
	2b	1.561	avg. in-plane	3.076	3.069	3.043					3.063	0.017
	2c	1.603	avg. in-plane	2.938	2.955	2.963					2.952	0.013
										overall	3.103	0.152
	3a	1.583	avg. in-plane	3.013	2.984	2.991					2.996	0.015
	3b	1.616	avg. in-plane	2.940	2.934	2.911					2.928	0.015
	3c	1.668	avg. in-plane	2.897	2.876	2.874					2.882	0.013
										overall	2.936	0.051
Modified (In-Plane Directional)	1d_1	1.436	0°	6.403	6.661	5.823	5.922	6.163	6.311	6.449	6.247	0.298
	1d_2	1.416	0°	6.442	6.492	6.615	6.686	6.835			6.614	0.157
										overall	6.400	0.305
	2d_1	1.452	90°	0.689	0.777	0.848	0.897	0.844	0.813	0.830		
				0.834	0.600	0.590	0.643	0.745	0.781	0.798		
				0.837	0.798	0.714	0.689	0.678	0.668	0.671	0.750	0.089
	2d_2	1.482	90°	0.537	0.551	0.593	0.569	0.625	0.636	0.699		
				0.721	0.756	0.745	0.717	0.505	0.547	0.547	0.625	0.089
										overall	0.700	0.107

3d_1	1.420	45°	2.761	2.747	2.722	2.729		2.740	0.018
3d_2	1.400	45°	2.701	2.750	2.743	2.800		2.749	0.041
							overall	2.744	0.029

Panel 2

	Specimen			Thermal Conductivity (W/mK)							
		Thickness (mm)	Measurement Direction	#1	#2	#3	#4	#5	#6	Average	Std. Dev.
THASYS (Transverse)	1a/1b	1.457/1.432	transverse	0.763	0.763	0.764				0.763	0.001
	1c/1b	1.465/1.432	transverse	0.804	0.803	0.803				0.803	0.001
	2a/2b	1.425/1.460	transverse	0.821	0.822	0.824				0.822	0.002
	3a/3b	1.414/1.440	transverse	0.857	0.857	0.857				0.857	0.000
									overall	0.812	0.035
THISYS (In-Plane Bulk)	1a	1.457	avg. in-plane	3.121	3.075	3.077				3.091	0.026
	1b	1.432	avg. in-plane	3.269	3.229	3.230				3.243	0.023
	1c	1.465	avg. in-plane	3.166	3.111	3.114	3.108			3.125	0.028
									overall	3.150	0.069
	2a	1.425	avg. in-plane	3.395	3.386	3.367				3.383	0.014
	2b	1.460	avg. in-plane	3.369	3.365	3.360				3.365	0.005
									overall	3.374	0.014
	3a	1.414	avg. in-plane	3.326	3.327	3.312				3.322	0.008
	3b	1.440	avg. in-plane	3.361	3.325	3.322				3.336	0.022
									overall	3.329	0.017
Modified (In-Plane Directional)	1c_1	1.436	0°	2.016	2.167	2.323	2.226			2.183	0.129
	1c_2	1.416	0°	2.054	2.073	2.094	2.123			2.086	0.030
									overall	2.135	0.101
	2b_1	1.452	90°	0.252	0.270	0.035	0.334	0.334	0.336	0.260	0.116
	2b_2	1.482	90°	0.278	0.261	0.268	0.246	0.242		0.259	0.015
	2b_3	1.448	90°	0.286	0.283	0.316	0.335	0.342		0.312	0.027
									overall	0.276	0.073
	3b_1	1.420	45°	0.950	0.943	0.949	0.944			0.947	0.004
	3b_2	1.400	45°	1.012	1.014	1.012	1.010			1.012	0.002
									overall	0.979	0.035

Panel 3

	Specimen	Thickness (mm)	Measurement Direction	Thermal Conductivity (W/mK)					
				#1	#2	#3	#4	Average	Std. Dev.
THASYS (Transverse)	1a/1b	2.199/2.119	transverse	0.726	0.728	0.729		0.728	0.002
	2a/2b	2.098/2.070	transverse	0.772	0.773	0.772		0.772	0.001
	3a/3b	2.032/2.155	transverse	0.725	0.726	0.726		0.726	0.001
							overall	0.742	0.023
THISYS (In-Plane Bulk)	1a	2.199	avg. in-plane	2.849	2.853	2.859		2.854	0.005
	1b	2.119	avg. in-plane	2.965	2.960	2.936		2.954	0.016
							overall	2.904	0.056
	2a	2.098	avg. in-plane	3.034	3.029	3.029		3.031	0.003
	2b	2.070	avg. in-plane	3.093	3.087	3.091		3.090	0.003
							overall	3.061	0.033
	3a	2.032	avg. in-plane	3.090	3.086	3.083		3.086	0.004
	3b	2.155	avg. in-plane	2.902	2.910	2.908		2.907	0.004
							overall	2.997	0.098
Modified (In-Plane Directional)	0_1	2.199	0°	3.847	3.850	3.885	3.900	3.871	0.026
	0_2	2.119	0°	3.878	3.878	3.871	3.882	3.877	0.005
							overall	3.874	0.018
	90_1	2.098	90°	3.765	3.659	3.652	3.652	3.682	0.055
	90_2	2.07	90°	3.793	3.783	3.783		3.786	0.006
							overall	3.727	0.068
	45_1	2.032	45°	3.917	3.903	3.903	3.903	3.907	0.007
	45_2	2.155	45°	3.868	3.857	3.864	3.871	3.865	0.006
							overall	3.886	0.023

Panel 4

	Specimen	Thickness (mm)	Measurement Direction	Thermal Conductivity (W/mK)					
				#1	#2	#3	#4	Average	Std. Dev.
THASYS (Transverse)	1a/1b	1.539/1.521	transverse	0.749	0.749	0.750		0.749	0.001
	1c/1b	1.515/1.521	transverse	0.759	0.758	0.759		0.759	0.001
	2a/2b	1.518/1.506	transverse	0.745	0.746	0.747		0.746	0.001
	3a/3b	1.553/1.571	transverse	0.722	0.722	0.722		0.722	0.000
							overall	0.744	0.014
THISYS (In-Plane Bulk)	1a	1.539	avg. in-plane	3.153	3.133	3.184		3.157	0.026
	1b	1.521	avg. in-plane	3.203	3.197	3.191		3.197	0.006
							overall	3.177	0.028
	2a	1.518	avg. in-plane	3.226	3.226	3.192		3.215	0.020
	2b	1.506	avg. in-plane	3.215	3.220	3.220		3.218	0.003
							overall	3.217	0.013
	3a	1.553	avg. in-plane	3.132	3.126	3.117		3.125	0.008
	3b	1.571	avg. in-plane	3.130	3.142	3.140		3.137	0.006
							overall	3.131	0.009
Modified (In-Plane Directional)	1d_1	1.565	0°	4.621	4.628	4.670	4.649	4.642	0.022
	1d_2	1.552	0°	4.699	4.769	4.787	4.900	4.789	0.083
							overall	4.715	0.097
	2d_2	1.553	90°	2.888	2.917	2.895	2.895	2.899	0.013
	2b_3	1.575	90°	2.711	2.711	2.715	2.708	2.711	0.003
							overall	2.805	0.101
	3d_1	1.593	45°	3.440	3.429	3.489	3.496	3.464	0.034
	3d_2	1.587	45°	3.574	3.574	3.581	3.585	3.579	0.005
							overall	3.521	0.065

Panel 5

	Specimen			Thermal Conductivity (W/mK)					
		Thickness (mm)	Measurement Direction	#1	#2	#3	#4	Average	Std. Dev.
THASYS (Transverse)	1a/1b	2.022/2.003	transverse	0.765	0.765	0.767		0.766	0.001
	1c/1b	2.017/2.003	transverse	0.769	0.770	0.770		0.770	0.001
	2a/2b	2.035/2.041	transverse	0.728	0.730	0.730		0.729	0.001
	2c/2b	2.063/2.041	transverse	0.739	0.738	0.738		0.738	0.001
	3a/3b	2.066/2.073	transverse	0.725	0.727	0.727		0.726	0.001
	3a/3c	2.066/2.104	transverse	0.708	0.711	0.711		0.710	0.002
							overall	0.740	0.022
THISYS (In-Plane Bulk)	1a	2.022	avg. in-plane	3.143	3.167	3.179		3.163	0.018
	1b	2.003	avg. in-plane	3.180	3.188	3.183		3.184	0.004
	1c	2.017	avg. in-plane	3.101	3.137	3.138		3.125	0.021
							overall	3.157	0.029
	2a	2.035	avg. in-plane	3.106	3.136	3.136		3.126	0.017
	2b	2.041	avg. in-plane	3.119	3.154	3.164		3.146	0.024
	2c	2.063	avg. in-plane	3.072	3.081	3.083		3.079	0.006
							overall	3.117	0.033
	3a	2.066	avg. in-plane	3.079	3.085	3.081		3.082	0.003
	3b	2.073	avg. in-plane	3.024	3.039	3.039		3.034	0.009
	3c	2.104	avg. in-plane	2.961	2.964	2.964		2.963	0.002
							overall	3.026	0.052
Modified (In-Plane Directional)	1d_1	2.078	0°	3.663	3.702	3.376	3.387	3.532	0.175
	1d_2	2.078	0°	3.578	3.592	3.627	3.585	3.596	0.022
	1d_3	2.078	0°	3.408	3.390	3.394	3.348	3.385	0.026
							overall	3.504	0.131
	2d_1	2.069	90°	3.649	3.627	3.557	3.553	3.597	0.049
	2d_2	2.069	90°	3.500	3.542	3.528		3.523	0.021
							overall	3.565	0.054
	3d_1	2.102	45°	3.578	3.581	3.659	3.705	3.631	0.062
	3d_2	2.102	45°	3.511	3.504	3.578	3.592	3.546	0.045
	3d_3	2.102	45°	3.603	3.535	3.447	3.461	3.512	0.072
							overall	3.563	0.076

Panel 6

	Specimen	Thickness (mm)	Measurement Direction	Thermal Conductivity (W/mK) #1	#2	#3	Average	Std. Dev.
THASYS (Transverse)	1a/1b	1.566/1.566	transverse	0.707	0.707	0.706	0.707	0.001
	2a/2b	1.604/1.602	transverse	0.697	0.698	0.698	0.698	0.001
	3a/3b	1.607/1.537	transverse	0.722	0.723	0.723	0.723	0.001
						overall	0.709	0.011
THISYS (In-Plane Bulk)	1a	1.566	avg. in-plane	3.017	3.007	3.003	3.009	0.007
	1b	1.566	avg. in-plane	3.043	3.055	3.052	3.050	0.006
						overall	3.030	0.023
	2a	1.604	avg. in-plane	3.056	3.054	3.053	3.054	0.002
	2b	1.602	avg. in-plane	3.050	3.040	3.020	3.037	0.015
						overall	3.046	0.014
	3a	1.607	avg. in-plane	3.017	3.012	3.014	3.014	0.003
	3b	1.537	avg. in-plane	3.175	3.160	3.151	3.162	0.012
						overall	3.088	0.081
Modified (In-Plane Directional)	1d_1	1.583	0°	5.409	5.459	5.463	5.444	0.030
	1d_2	1.583	0°	5.424	5.417	5.438	5.426	0.011
						overall	5.435	0.022
	2d_1	1.549	90°	1.580	1.548	1.541	1.556	0.021
	2d_2	1.549	90°	1.845	1.831	1.838	1.838	0.007
						overall	1.697	0.155
	3d_1	1.501	45°	3.504	3.514	3.532	3.517	0.014
	3d_2	1.501	45°	3.493	3.500	3.511	3.501	0.009
						overall	3.509	0.014

Panel 7

	Specimen	Thickness (mm)	Measurement Direction	Thermal Conductivity (W/mK)					
				#1	#2	#3	#4	Average	Std. Dev.
THASYS (Transverse)	1a/1b	2.022/2.003	transverse	0.765	0.765	0.767		0.766	0.001
	1c/1b	2.017/2.003	transverse	0.769	0.770	0.770		0.770	0.001
	2a/2b	2.035/2.041	transverse	0.728	0.730	0.730		0.729	0.001
	2c/2b	2.063/2.041	transverse	0.739	0.738	0.738		0.738	0.001
	3a/3b	2.066/2.073	transverse	0.725	0.727	0.727		0.726	0.001
	3a/3c	2.066/2.104	transverse	0.708	0.711	0.711		0.710	0.002
							overall	0.740	0.022
THISYS (In-Plane Bulk)	1a	2.022	avg. in-plane	3.143	3.167	3.179		3.163	0.018
	1b	2.003	avg. in-plane	3.180	3.188	3.183		3.184	0.004
	1c	2.017	avg. in-plane	3.101	3.137	3.138		3.125	0.021
							overall	3.157	0.029
	2a	2.035	avg. in-plane	3.106	3.136	3.136		3.126	0.017
	2b	2.041	avg. in-plane	3.119	3.154	3.164		3.146	0.024
	2c	2.063	avg. in-plane	3.072	3.081	3.083		3.079	0.006
							overall	3.117	0.033
	3a	2.066	avg. in-plane	3.079	3.085	3.081		3.082	0.003
	3b	2.073	avg. in-plane	3.024	3.039	3.039		3.034	0.009
	3c	2.104	avg. in-plane	2.961	2.964	2.964		2.963	0.002
							overall	3.026	0.052
Modified (In-Plane Directional)	1d_1	2.078	0°	3.663	3.702	3.376	3.387	3.532	0.175
	1d_2	2.078	0°	3.578	3.592	3.627	3.585	3.596	0.022
	1d_3	2.078	0°	3.408	3.390	3.394	3.348	3.385	0.026
							overall	3.504	0.131
	2d_1	2.069	90°	3.649	3.627	3.557	3.553	3.597	0.049
	2d_2	2.069	90°	3.500	3.542	3.528		3.523	0.021
							overall	3.565	0.054
	3d_1	2.102	45°	3.578	3.581	3.659	3.705	3.631	0.062
	3d_2	2.102	45°	3.511	3.504	3.578	3.592	3.546	0.045
	3d_3	2.102	45°	3.603	3.535	3.447	3.461	3.512	0.072
							overall	3.563	0.076

Panel 8

	Specimen	Thickness (mm)	Measurement Direction	Thermal Conductivity (W/mK)								
				#1	#2	#3	#4	#5	#6	#7	Average	Std. Dev.
THASYS (Transverse)	1a/1b	1.494/1.494	transverse	0.606	0.607	0.607	0.608				0.607	0.001
	2a/2b	1.501/1.494	transverse	0.600	0.600	0.600					0.600	0.000
	3a/3b	1.499/1.494	transverse	0.605	0.604	0.605					0.605	0.001
										overall	0.604	0.003
THISYS (In-Plane Bulk)	1a	1.494	avg. in-plane	2.557	2.643	2.532					2.577	0.058
	1b	1.494	avg. in-plane	2.552	2.537	2.537					2.542	0.009
										overall	2.560	0.042
	2a	1.501	avg. in-plane	2.543	2.534	2.540					2.539	0.005
	2b	1.494	avg. in-plane	2.585	2.567	2.555					2.569	0.015
										overall	2.554	0.019
	3a	1.499	avg. in-plane	2.565	2.555	2.542					2.554	0.012
	3b	1.494	avg. in-plane	2.604	2.599	2.593					2.599	0.006
										overall	2.576	0.026
Modified (In-Plane Directional)	0_1	1.500	0°	2.994	3.040	3.040					3.025	0.027
	0_2	1.510	0°	3.076	3.047	3.051	3.040				3.054	0.016
	0_3	1.500	0°	3.054	3.005	3.012	3.033				3.026	0.022
										overall	3.036	0.024
	90_1	1.500	90°	2.991	2.885	2.888	2.871				2.909	0.055
	90_2	1.500	90°	2.906	2.924	2.878	2.821				2.882	0.045
	90_3	1.490	90°	2.906	2.913	2.952	2.980	2.895	2.895	2.892	2.919	0.034
										overall	2.906	0.043
	45_1	1.593	45°	2.729	2.719	2.704					2.717	0.013
	45_2	1.495	45°	2.750	2.782	2.825					2.786	0.038
	45_3	1.490	45°	3.040	3.008	3.228	3.235				3.128	0.121
										overall	2.902	0.209

Panel 9

	Specimen	Thickness (mm)	Measurement Direction	Thermal Conductivity (W/mK)					
				#1	#2	#3	#4	Average	Std. Dev.
THASYS (Transverse)	1a/1b	1.593/1.582	transverse	0.564	0.565	0.565		0.565	0.001
	1c/1b	1.555/1.582	transverse	0.575	0.574	0.575		0.575	0.001
	2a/2b	1.545/1.579	transverse	0.586	0.587	0.587		0.587	0.001
	2c/2b	1.586/1.579	transverse	0.585	0.586	0.587		0.586	0.001
	3a/3b	1.616/1.581	transverse	0.573	0.573	0.573		0.573	0.000
	3c/3d	1.645/1.614	transverse	0.565	0.564	0.564		0.564	0.001
							overall	0.575	0.009
THISYS (In-Plane Bulk)	1a	1.593	avg. in-plane	2.440	2.424	2.381		2.415	0.031
	1b	1.582	avg. in-plane	2.432	2.400	2.395		2.409	0.020
	1c	1.555	avg. in-plane	2.480	2.457	2.410		2.449	0.036
							overall	2.424	0.032
	2a	1.545	avg. in-plane	2.492	2.455	2.452		2.466	0.022
	2b	1.579	avg. in-plane	2.421	2.402	2.392		2.405	0.015
	2c	1.586	avg. in-plane	2.382	2.381	2.381		2.381	0.001
							overall	2.418	0.040
	3a	1.616	avg. in-plane	2.400	2.381	2.350		2.377	0.025
	3b	1.581	avg. in-plane	2.385	2.377	2.372		2.378	0.007
	3c	1.645	avg. in-plane	2.341	2.334	2.336		2.337	0.004
	3d	1.614	avg. in-plane	2.419	2.400	2.350		2.390	0.036
							overall	2.370	0.028
Modified (In-Plane Directional)	1c_1	1.555	0°	2.740	2.856	2.849	2.871	2.829	0.060
	1c_2	1.555	0°	2.764	2.733	2.722	2.757	2.744	0.020
	1c_3	1.555	0°	2.743	2.818	2.892	3.016	2.867	0.116
							overall	2.813	0.088
	2d_1	1.552	90°	2.757	2.793	2.789	2.818	2.789	0.025
	2d_2	1.552	90°	2.832	2.782	2.789	2.779	2.796	0.025
							overall	2.792	0.023
	3e_1	1.636	45°	2.655	2.704	2.701	2.757	2.704	0.042
	3e_2	1.636	45°	2.782	2.761	2.782	2.768	2.773	0.011
							overall	2.739	0.046

Panel 10

Specimen	Thickness (mm)	Measurement Direction	Thermal Conductivity (W/mK)						
			#1	#2	#3	#4	#5	Average	Std. Dev.
THASYS (Transverse)									
1a/1b	2.204/2.220	transverse	0.450	0.451	0.452	0.452	0.452	0.451	0.001
THISYS (In-Plane Bulk)									
1a	2.204	0°	2.040	2.039	2.036			2.038	0.002
Modified (In-Plane Directional)									
0_1	2.172	avg. in-plane	4.571	4.847	4.837	4.844		4.775	0.136

Panel 11

Specimen	Thickness (mm)	Measurement Direction	Thermal Conductivity (W/mK)							
			#1	#2	#3	#4	#5	#6	Average	Std. Dev.
THASYS (Transverse)										
1a/1b	2.220/2.215	transverse	0.454	0.455	0.458	0.458	0.459	0.459		
			0.458	0.459	0.459	0.459			0.458	0.002
THISYS (In-Plane Bulk)										
1a	2.220	avg. in-plane	2.086	2.057	2.056				2.066	0.017
1b	2.215	avg. in-plane	2.042	2.042	2.041				2.042	0.001
								overall	2.054	0.017
Modified (In-Plane Directional)										
0_1	2.212	0°	4.865	4.914	4.953				4.911	0.044
90_1	2.196	90°	0.371	0.360	0.360	0.360			0.363	0.006
45_1	2.177	45°	1.661	1.636	1.700				1.666	0.032

Panel 12

	Specimen	Thickness (mm)	Measurement Direction	Thermal Conductivity (W/mK)							
				#1	#2	#3	#4	#5	#6	Average	Std. Dev.
THASYS (Transverse)	1a/1b	1.550/1.542	transverse	0.448	0.450	0.451	0.451	0.451	0.451		
				0.451	0.451						
									overall	0.451	0.001
THISYS (In-Plane Bulk)	1a	1.550	avg. in-plane	2.262	2.254	2.257				2.258	0.004
	1b	1.542	avg. in-plane	2.282	2.267	2.266				2.272	0.009
									overall	2.265	0.010
Modified (In-Plane Directional)	0_1	1.472	0°	2.616	2.630	2.634				2.627	0.009
	0_2	1.502	0°	2.581	2.616	2.616				2.604	0.020
									overall	2.616	0.019
	90_1	1.478	90°	2.418	2.581	2.574	2.570			2.536	0.079
	90_2	1.466	90°	2.651	2.977	2.987	2.973			2.897	0.164
									overall	2.716	0.227
	45_1	1.406	45°	3.093	3.182	3.189				3.155	0.054
	45_2	1.422	45°	2.775	2.952	2.991				2.906	0.115
									overall	3.030	0.158

Panel 13

	Specimen	Thickness (mm)	Measurement Direction	Thermal Conductivity (W/mK)							
				#1	#2	#3	#4	#5	#6	Average	Std. Dev.
THASYS (Transverse)	1a/1b	2.053/2.070	transverse	0.454	0.455	0.458	0.458	0.459	0.459		
				0.458	0.459	0.459	0.459				
									overall	0.458	0.002
THISYS (In-Plane Bulk)	1a	2.053	avg. in-plane	2.426	2.422	2.422				2.423	0.002
	1b	2.070	avg. in-plane	2.427	2.425	2.427				2.426	0.001
									overall	2.425	0.002
Modified (In-Plane Directional)	0_1	2.054	0°	3.535	3.521	3.518				3.525	0.009
	0_2	2.036	0°	3.553	3.539	3.528				3.540	0.013
									overall	3.532	0.013
	90_1	2.084	90°	2.029	1.994	1.987				2.003	0.023
	90_2	2.088	90°	2.068	2.050	2.036				2.051	0.016
									overall	2.027	0.032
	45_1	2.038	45°	2.879	2.743	2.729				2.784	0.083
	45_2	2.048	45°	2.796	2.775	2.768				2.780	0.015
									overall	2.782	0.053

Panel 14

	Specimen	Thickness (mm)	Measurement Direction	Thermal Conductivity (W/mK)							
				#1	#2	#3	#4	#5	#6	Average	Std. Dev.
THASYS (Transverse)	1a/1b	2.080/2.063	transverse	0.506	0.507	0.507	0.507	0.507	0.507		
				0.507	0.507						
									overall	0.507	0.000
THISYS (In-Plane Bulk)	1a	2.080	avg. in-plane	2.406	2.427	2.406				2.413	0.012
	1b	2.063	avg. in-plane	2.437	2.435	2.434				2.435	0.002
									overall	2.424	0.014
Modified (In-Plane Directional)	0_1	2.130	0°	2.750	2.736	2.711				2.732	0.020
	0_2	2.130	0°	2.439	2.443	2.453	2.475			2.453	0.016
									overall	2.572	0.150
	90_1	2.170	90°	2.782	2.768	2.775	2.768			2.773	0.007
	90_2	2.160	90°	2.860	2.842	2.828	2.821			2.838	0.017
									overall	2.806	0.037
	45_1	2.110	45°	2.757	2.768	2.786				2.770	0.015
									overall	2.770	0.015